RECONFIGURABLE DEFECTED MICROSTRIP PHASE SHIFTER FOR PHASED ARRAY ANTENNAS

by

Can Ding

Dissertation submitted in fulfilment of the requirements

for the degree of

DOCTOR OF PHILOSOPHY

Department of Engineering
Faculty of Science and Engineering
Macquarie University
Sydney, Australia

July 19 2016

ABSTRACT

Beamforming and its most common variant, phased arrays, offer a number of advantages for wireless communications and radar systems. These include increased range and capacity, immunity against interference, and system flexibility. However, due to the associated high cost, both digital and analogue beamforming systems are primarily employed in defence and space applications where cost is not necessarily an obstacle. This thesis is motivated by a strong need from civilian applications where low-cost beamforming systems are required.

In a beamforming system, a phase shifter is one of the most critical devices. Usually, a large number of phase shifters are employed, however they are very costly. Therefore, reducing the cost of phase shifters is an effective way to decrease the total cost of a beamforming system. And so, a phase shifter that is low in cost, compact, has an easy control method, and which can be constructed using a simple fabrication process is in high demand.

In this thesis, firstly, some basics of phased arrays and different types of phase shifters used in phased arrays are reviewed. Then, a novel type of phase-shifting unit called as reconfigurable defected microstrip structure (RDMS) is proposed. The RDMS is printed on a microstrip line due to its low cost, low complexity, and for its incomparable popularity in antenna and microwave designs. A series of phase shifters employing RDMS are discussed and intergrated in phased arrays, to demonstrate their practicability in beamforming systems. Subsequently, a modified RDMS (MRDMS) phase-shifting unit is introduced, which is smaller in size but has comparable or even better performance. Based on the MRDMS unit, a complete phase shifter design scheme consisting of three steps is presented, and

each step is elaborated with theory, simulation, and experiment. A significant improvement in performance and a reduction in cost are achieved and illustrated by comparing the performance of the phase shifters employing RDMS and MRDMS units to each other. Finally, the proposed RDMS- and MRDMS-based phase shifters are used to construct a phased array antenna and a reconfigurable PRS antenna, which proves them to be excellent candidates to provide phase shifts in antenna systems. Future work will focus on the realization of large-scale phased array antennas using the proposed phase shifters.

STATEMENT OF CANDIDATE

I certify that the work in this thesis has not previously been submitted for a degree nor has it been submitted as part of the requirements for a degree to any other university or institution other than Macquarie University.

I also certify that the thesis is an original piece of research and it has been written by me.

In addition, I certify that all information sources and literature used are indicated in the thesis.

. . . .

Can Ding

ACKNOWLEDGMENTS

I would like to express my profound gratitude to my supervisor, Prof. Y. Jay Guo and my senior colleague and friend, Dr. Pei-Yuan Qin. They offered me enormous, valuable help in all respects, not only in the research, but also in my daily life in Australia. Without them, I will never get to this stage. I can still remember the illuminating and encouraging discussions with them that lead to this accomplishment. I will never forget the days they helped struggling me to polish my papers.

I would also like to acknowledge my supervisors Prof. Eryk Dutkiewicz in Macquarie University, Australia, and Prof. Yintang Yang in Xidian University, China for their support, advice, and encouragement throughout this work.

Further more, I would like to thank the following people who helped me with some technical issues of the work presented in this dissertation. The first acknowledgement goes to Dr. Trevor Bird who offered advices and helped to revise a paper. Then I have to thank Dr. Nan Yang and Dr. Zhuo Chen for their suggestions in academic paper writing and oral presentation. I would like to extend my gratitude to Ms. Mei Shen and Mr. Robert Shaw for their help in the simulation and fabrication of RF lumped elements.

Special thanks goes to my cousin Mrs. Lyndsey Jean Chen-Yang who had cultivated me into a responsible and independent person.

Many thanks to my friends Dr. Qimin You and Dr. Luyang Ji for the days we shared a office. Those days were delightful, encouraging, and full of memories.

Finally, I am forever indebted to my parents for their infinite support, encouragement and love.

To My Parents

Contents

List of Figures

List of Tables

Chapter 1

Introduction

1.1 Motivation and Research Focus

Beamforming technology provides a promising solution to increase the spatial reuse, improve the transmission reliability, extend the transmission range, and save the power consumption in wireless communications and ad hoc networks [1–5]. This is due to its ability to change radiation patterns to receive signals from a specific direction, and reduce the distortion of noises from other directions. However, this advantage comes with dramatically increased cost and size, which substantially limits their application.

A beamforming system consists of a Beam Forming Network (BFN) and an antenna array. Beamforming is realized by using the BFN to adjust the magnitude and phase of signals received by the array elements. It is the BFN that dominates the cost of the entire beamforming system. The gain and phase applied to signals derived from each element may be thought of as a single complex quantity referred to as a weighting applied to the signals. The BFN has several predefined combinations of weighting factors which correspond to different sets of beams. After the estimation of signal arrival direction, the BFN selects one beam so that the antenna array has the maximum gain at that direction to have the highest signal collecting efficiency.

Beamforming can be divided into fixed beamforming and adaptive beamforming. Adaptive beamforming provides a high degree of configuring the radiation pattern. By applying a variety of signal processing algorithms, adaptive array antennas can adjust their weights in order to maximize the resulting Signal to Interference and Noise Ratio (SINR). The main lobe of an array can be directed towards a target, and nulls can be additionally placed in the direction of interfering sources to suppress their interference. But adaptive BFNs for large-scale arrays need massive amplifiers and phase shifters, resulting in unacceptably high prices for many applications.

Fixed beamforming can provide most of the benefits of smart antennas at a fraction of cost and design complexity. The BFN has several predefined combinations of weighting factors corresponding to different sets of beams. However, they do not guarantee maximum gain. If the desired direction is not on one of the predetermined beam directions, the transceiver will suffer from gain reduction. Moreover, switched beam antennas are not able to fully eliminate interference outside the main lobe due to the absence of control of the side lobes. Although fixed beamformings are more economical than smart antennas, they can still be expensive.

Beamforming systems, either fixed or adaptive, can be achieved in either in digital or analog ways. Analogue Beamforming (ABF) means that, the received signals from each antenna of array are combined at the RF carrier frequency level. The analogue beamformer feeds up to the centralized receiver channels, down-converting the signal to an intermediate frequency (IF). The following Analogue-to-Digital Converter (ADC) then digitizes the IF. In Digital Beamforming (DBF), there are many digital receivers, one own receiver at each of the radiating elements of the antenna. This baseband processing requires dedicated RF chain (which is expensive) per each antenna. The down-converting to IF-frequency and digitizing the signals is realized at each individual antenna element.

The most economic implementation form of beamforming is the passive phased array. In a passive phased array, there is no element for amplitude control. Only phase shifters are used at each element to provide required phase shift for beam scanning. This eliminates the need for amplifiers and attenuators, and simplifies the control circuit, resulting in a significantly lower costs. Passive phased arrays are used extensively in radar systems to seek and track targets. Nowadays, high gains are required to form a clear image. To achieve a high gain, a very large phased array is required, and therefore also a great amount of phase shifters. The high price of phase shifters contributes to a large proportion of the overall cost of the beamforming system.

Traditional phase shifters used in phased arrays are ferrite and diode phase shifters. Ferrite phase shifters are low cost and low loss, but they are relatively bulky and heavy, and require significant switching power. Diode phase shifters have fast switching times, low weights, and are low cost, but have high insertion losses. There are also new phase-shifting technologies employing Radio Frequency Microelectromechanical Systems (RF MEMS) and liquid crystal. Phase shifter designs are becoming increasingly complicate, but the cost remains a problem.

In this thesis, we aim to develop a new type of phase shifter that can provide a low-cost phase-shifting solution for phased array / beamforming applications. As well as the cost, size, and performance of the phase shifter, the control circuit will also be considered. This work provides a comprehensive description of the introduction, analysis, optimization, and validation of a phase-shifting unit based on simple microstrip lines.

1.2 Thesis Contribution

The key contribution of this thesis is to provide a novel low-cost phase-shifting solution, which substantially reduces the cost of phase-shifting in beamforming systems. To be specific, the contributions are summarized as follows:

1. A novel reconfigurable defected microstrip structure (RDMS) has been proposed to provide controllable phase shift;
2. The working mechanism of the RDMS has been studied, including how the phase shift is produced and where the insertion loss (IL) comes from.
3. We have analyzed the connections between physical dimensions and performance index by conducting a large amount of simulations on a Full-Wave simulation software platform.
4. A multiplied phase-shifting ability and lower IL have been achieved by cascading the RDMS.
5. Stepwise phase shifters have been designed, fabricated, and measured based on the cascaded RDMS, which validated the phase-shifting ability of the RDMS.
6. A modified RDMS (MRDMS) is introduced. It is smaller and more cost-effective.
7. The insight of MRDMS working mechanism is provided, and used to explain the fact that, the performance of the RDMS remains comparable level with the the size and cost reduction.
8. We have also presented a complete design scheme and optimization methodology of stepwise phase shifters based on MRDMS. Each step has been elaborated with theory, simulations, and experiments.
9. Stepwise phase shifters based on the MRDMS have been fabricated and tested. They have been proved to be excellent candidates for beamforming systems, due to the fact that they are compact, low cost, easy to fabricate, easy to integrate with

microstrip systems, and are able to provide flexible phase shifts with a simple Direct Current (DC) control.

10. The RDMS and MRDMS-based phase shifters have been used to construct the feed network of a phased array antenna as an implementation in a basic beamforming system. The obtained arrays with RDMS and MRDMS are tested to demonstrate their potential to be used in beamforming systems.

11. The MRDMS-based phase shifters have also been used in the feed network of a reconfigurable phased-array-fed partially reflective surface (PRS) antenna that can switch its beam to nine directions with high gain.

1.3 Thesis Outline

The remainder of this thesis is organized as follows. We first present some background information in Chapter 2, including phased arrays, phase shifters, and some lumped elements used in this work. In Chapter 3, the RDMS is introduced and analyzed, followed by the analysis of phase shifter designs. Then, the modified RDMS (MRDMS) is discussed, and a complete design methodology is presented in Chapter 4. Chapter 5 describes the phase shifters' applications in antenna systems. Finally, the thesis is concluded in Chapter 6.

1.4 List of Publications

Journal Papers

[P1] **Can. Ding**, Y. Jay Guo, Pei-Yuan Qin, and Yintang Yang, "A Compact Phase Shifter Employing Reconfigurable Defected Microstrip Structure (RDMS) for Phased Array Antennas," *IEEE Trans. Antennas Propag.*, Vol. 63, no. 05, Mar. 2015.

[P2] Dongfang Guan, **Can Ding**, Zuping Qian, Ying Song Zhang, and Wenquan Cao, "A SIW Based Large-Scale Corporate-Feed Array Antenna", *IEEE Trans. Antennas Propag.*, Vol. 63, no. 07, pp. 2969–2976, Jul. 2015.

[P3] **Can Ding**, Y. Jay Guo, Pei-Yuan Qin, Trevor S. Bird, and Yintang Yang, "A Defected Microstrip Structure (DMS)-Based Phase Shifter and Its Application to Beamforming Antennas", *IEEE Trans. Antennas Propag.*, vol. 62, no. 2, pp. 641 - 651, Feb. 2014.

[P4] Pei-Yuan Qin, Y. Jay Guo, and **Can Ding**, "A Beam Switching Quasi-Yagi Dipole Antenna", *IEEE Trans. Antennas Propag.*, vol. 61, no. 10, pp. 4891 - 4899, Oct. 2013.

[P5] Pei-Yuan Qin, Y. Jay Guo, and **Can Ding**, "A Dual-Band Polarization Reconfigurable Antenna for WLAN Systems", *IEEE Trans. Antennas Propag.*, vol. 61, no. 11, pp. 5706 - 5713, Oct. 2013.

Conference Papers

[P1] **Can. Ding**, Y. Jay Guo, Pei-Yuan Qin, Eryk Dutkiewicz, and Yintang Yang, "A Phased Array Antenna Employing Reconfigurable Defected Microstrip Structure (RDMS)," *Antennas and Propagation and USNC/URSI National Radio Science Meeting, 2015 IEEE International Symposium on*, pp. 2469–2470, Jul. 2015.

[P2] **Can. Ding**, Y. Jay Guo, Pei-Yuan Qin, and Yintang Yang, "A compact phase-shifting unit for phased array antennas," *European Radar Conference (EuRAD), 2014 11th*, pp. 443 - 446, Oct. 2014.

[P3] **Can. Ding**, Y. Jay Guo, Pei-Yuan Qin, and Yintang Yang, "A reconfigurable defected microstrip structure for applications in phase shifter," *Antennas and Propagation (EuCAP), 2014 8th European Conference on*, pp. 2342 - 2346, Apr. 2014.

[**P4**] **Can. Ding**, Y. Jay Guo, Pei-Yuan Qin, Luyang Ji, and Yintang Yang, "A compact phase shift unit for analogue beamforming," *Antenna Technology: "Small Antennas, Novel EM Structures and Materials, and Applications" (iWAT), 2014 International Workshop on*, pp. 93 - 95, Mar. 2014.

[**P5**] Y. Jay Guo, Pei-Yuan Qin, and **Can Ding**, "Low-cost beamforming employing reconfigurable antennas," *Antenna Technology: "Small Antennas, Novel EM Structures and Materials, and Applications" (iWAT), 2014 International Workshop on*, pp. 155 - 158, Mar. 2014.

[**P6**] **Can Ding**, Y. Jay Guo, Pei-Yuan Qin, Trevor S. Bird. and Yintang Yang, "A Novel Phase Shifter Based on Reconfigurable Defected Microstrip Structure (RDMS) for Beam-Steering Antennas," *Antennas and Propagation (ISAP), 2013 Proceedings of the International Symposium on*, vol. 02, pp. 993 996, Oct. 2013.

[**P7**] Pei-Yuan Qin, **Can Ding**, and Y. Jay Guo, "A High-Gain Beam-Steering Quasi-Yagi Antenna," *Antennas and Propagation (ISAP), 2012 International Symposium on*, vol. 02, pp. 122 125, Nov. 2012.

Chapter 2

Preliminary

In this chapter, we present an overview of key technologies related to the thesis topic, including the phased arrays and phase shifters. Firstly, the background and basic theory of phased array antennas are discussed. Then, phase shifters frequently used in phased array antennas are reviewed, and their design considerations are discussed. Subsequently, lumped elements including the PIN diode and printing capacitor that are specifically used in this work are introduced and analyzed.

2.1 Phased Array Antenna

Phased array antennas were firstly developed in the 1950s [6–11] and gained popularity in satellite communications, radar systems, and other military applications [12–15]. Phased array antennas consist of multiple stationary antenna elements, which are fed coherently and use phase shifters or time-delay lines to control the signals at each element to scan the beam to a desired direction. They are attractive due to their flat structure and a capability of rapid and accurate beam scanning with high gain. In addition, beam patterns can be shaped, or multiple beams can be realized by controlling both the magnitudes and phases of the signals applied to each element. Another advantage is that very high power can be generated from the numerous radiators distributed across the aperture. A disadvantage of the phased array antenna is that the cost is very high due to the RF chain or BFN used to feed the antenna elements. The following section covers some basics of phased array antennas [12, 13, 16, 17], including array scanning theory and some design considerations.

2.1.1 Array Scanning Theory

Usually, identical radiators are used in an array and the radiation pattern is the product of two functions, the array factor and element factor. The total field of an array is determined by five controls. These are: the geometric configuration of the array, the relative displacement between the array elements, the excitation amplitudes on array elements, the excitation phases on array elements, and the radiation pattern of individual array elements. The first four controls determine the array factor and the last one is instantiated in the element factor. We will use only the array factor, which is the main issue concerned in this thesis, to describe the array scanning characteristics.

An array with $2N$ equally spaced elements is shown in Fig. 2.1. Since all elements are identical, they have similar current distribution I_0 when excited. However, due to the different amplitude and phase excitation, the actual current distribution on the element n is $I_n = A_n e^{-jZ_n} I_0$. For this linear array, the array factor $F_a(\theta, \phi)$ can be expressed by

$$F_a(\theta, \phi) = \sum_{n=-N}^{n=N} \frac{I_n}{I_0} e^{jnkdcos\theta} = \sum_{-N}^{N} A_n e^{jnkdcos\theta} e^{(-jZ_n)}, \tag{2.1}$$

where $k = 2\pi/\lambda$ and λ is the wavelength.

Particularly, when the signals at each element are equal in both the magnitude and phase, the array factor can be reduced to

$$F_a(\theta, \phi) = \sum_{n=-N}^{n=N} e^{jnkdcos\theta}. \tag{2.2}$$

In this case, the array factor is equal to a sum of phasers of unity magnitude with a

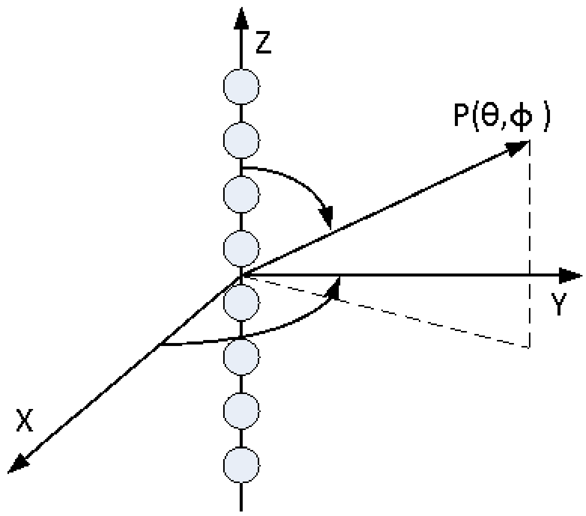

Figure 2.1: Linear array with equally spaced elements along z-axis.

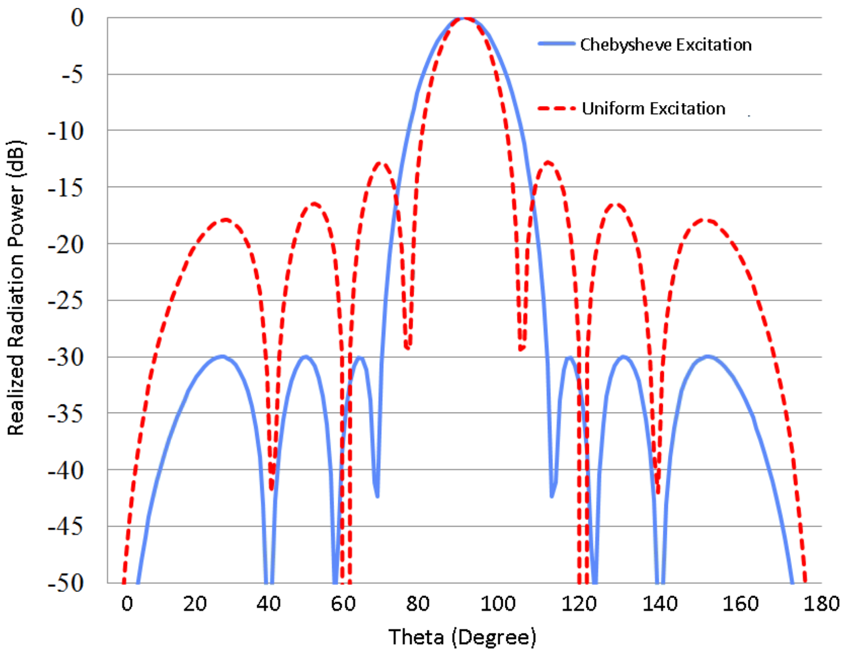

Figure 2.2: Radiation pattern of a 8-element linear array with uniform amplitude excitation and Chebyshev amplitude excitation.

progressive multiple of the basic angle ψ

$$\psi = \frac{2\pi d}{\lambda} cos\theta. \tag{2.3}$$

Usually, it is assumed that the length of the array is very large compared to a wavelength

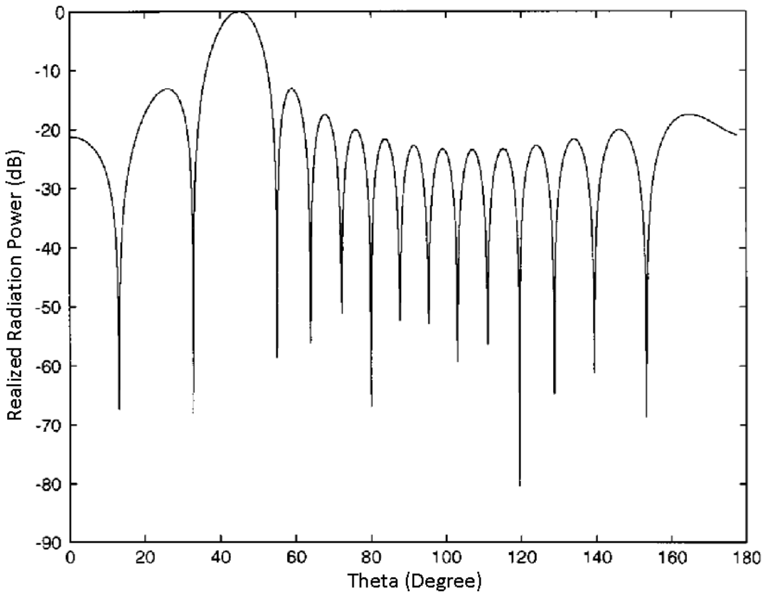

Figure 2.3: Radiation pattern of a 15-element equally spaced linear array with steered main beam.

and the element spacing is less than a wavelength. Under this condition, the array pattern gives a narrow beam at boreside with several sidelobes. The sidelobe level (SLL) can be reduced by tapering the magnitude of the currents across the array [17–22]. For example, Fig. 2.2 depicts the radiation pattern of an 8-element array with uniform amplitude excitation and Chebyshev amplitude excitation. The elements are equally spaced by a distance of half-wavelength. By using Chebyshev amplitude excitation, the SLL can be reduced by 15 dB.

By changing the phases of the excitations at each element, the array shown in Fig. 2.1 can have a steered main beam. Assuming that the element currents have equal amplitudes and uniform progressive phase shift $I_n = I_0 e^{(-jna_z)}$, the array factor described in Equation 2.1 becomes

$$F_a(\theta, \phi) = \sum_{n=-N}^{n=N} e^{jn(kdcos\theta - a_z)}. \quad (2.4)$$

Thus, the uniform progressive phase shift a_z changes the main beam position from boreside

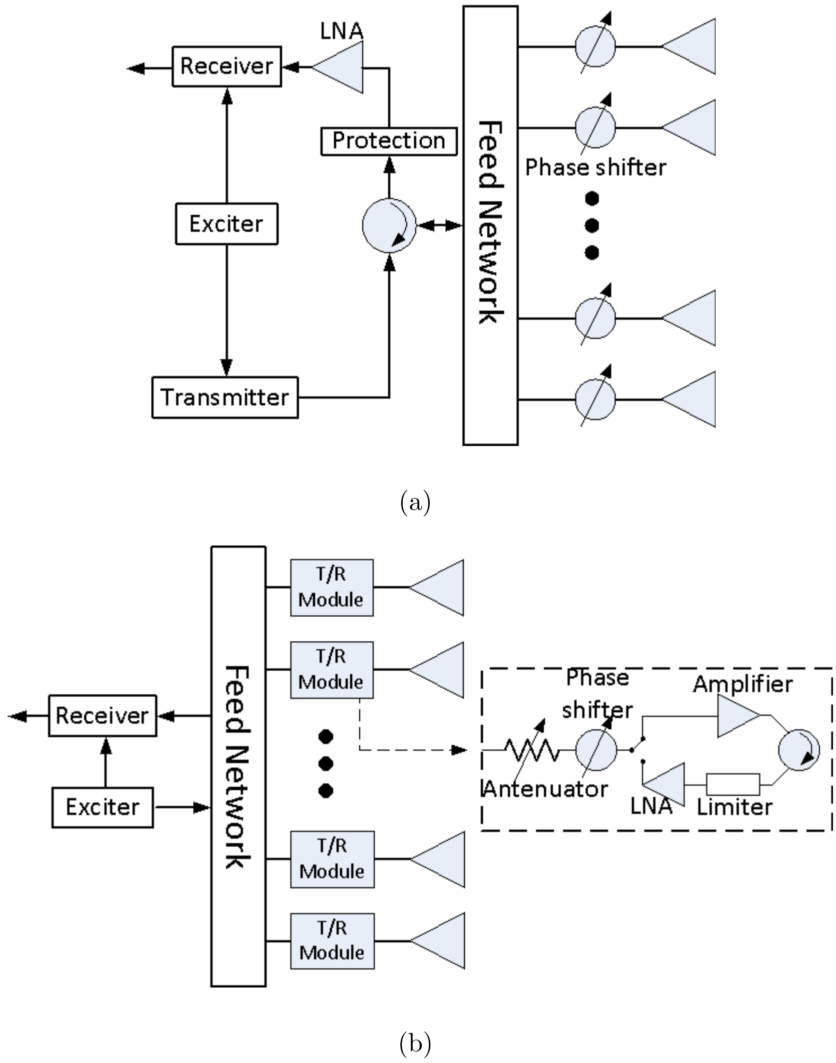

Figure 2.4: Architectures of (a) passive and (b) active phased array.

to another angle in space θ_0, where

$$\theta_0 = arccos\left[\frac{a_z}{2\pi}\frac{\lambda}{d}\right]. \tag{2.5}$$

Fig. 2.3 shows an example of a 15-element linear array with the main beam steered 45° away from the boreside.

2.1.2 Phased Array Architecture

There are generally two types of phased arrays, passive and active phased array, and their structures are illustrated in Fig. 2.4(a) and 2.4(b), respectively. Passive array, as shown in Fig. 2.4(a), uses a central transmitter and receiver. A circulator is used to direct the energy received by the antenna to the receiver. A limiter can be placed before a low noise amplifier (LNA) to avoid damage to the LNA. The energy reflected by the limiter will then be directed into the transmitter [23]. Phase shifters are employed before each element to provide phase shifts. But there is no amplitude control components in passive arrays. The design challenge is to minimize losses in the feed network which is composed of power dividers and phase shifters, to increase the system sensitivity and efficiency. Passive arrays are a less expensive alternative compared to active arrays for electronic beam scanning since only phase shifters are required. However, due to the eliminated amplitude controls, the SLL could be high. To achieve a lower SLL, a separate receive feed network with appropriate amplitude weighting methods can be used.

In active arrays as shown in Fig. 2.4(b), the power amplifiers (PAs), LNAs, phase shifters, attenuators, and limiter are integrated in transmitting and receiving modules (TRM), which are connected to each array element, offering both the magnitude and phase controls. Details of the TRM can be found in [23]. Losses in the feed network are tolerable due to the presence of amplifiers. Nevertheless, active arrays require a great number of amplifiers and other related devices. The improvements in sensitivity and reliability are obtained with significantly increased complexity and cost.

2.1.3 Design Consideration

Grating Lobes

In a phased array, a second main beam called grating lobe will appear if the space d between the elements is too large compared to a wavelength. This happens when the following condition is satisfied:

$$kdcos\theta' - a_z = \pm 2\pi. \tag{2.6}$$

The grating lobe will appear at the angle θ', where

$$\theta' = arccos(cos\theta_0 \pm \frac{\lambda}{d}). \tag{2.7}$$

To avoid a grating lobe, the spacing d must meet the following condition:

$$\frac{d}{\lambda} < \frac{1}{1 + |cos\theta_0|}. \tag{2.8}$$

For example, if the phased array is designed to scan close to endfire ($\theta_0 = 0 \; or \; \pi$), the space between elements must be less than $\lambda/2$ to prevent a grating lobe. There are also other solutions proposed to suppress grating lobes [24–27] in some special cases.

Bragg Lobes

Bragg lobes are retro-directive reflections that may be received by a detecting radar at an angle off boreside when Bragg condition is fulfilled:

$$d = \frac{n\lambda_r}{2sin\theta_r}, \tag{2.9}$$

where d is the spacing between antenna elements and θ_r is the angle of the detecting radar. This should be prevented for military applications to grantee stealth. To minimize the antenna's radar cross section, the first Bragg lobe ($n = 1$) must be 90^o off boreside, which means $d \leq \lambda_r/2$.

Random Errors

Array elements in a phased array have random errors in amplitude and phase. The random errors decrease the peak gain of the antenna, introduce beam-pointing error, and increase SLL. Fortunately, adjusting phase-shifter control settings with limits can minimize the negative effects resulted from the errors. Studies have been made to characterize the effects statistically in [8, 9, 28–36]. By following the analysis in [8], a phased array is assumed to have an amplitude error of δ_n and a phase error of ϕ_n at the nth element. This means the actual excitation at the nth element is $(1+\delta_n)I_n e^{(j\phi_n)}$, where I_n is the correct excitation current. The random amplitude error δ_n has zero mean and variance $\bar{\delta^2}$. The resultant changes in SLL, directivity, and beam pointing angle are derived and shown as follows.

For an array of N isotopical elements, the increased SLL due to the random errors is given in by

$$\bar{\sigma^2} = \frac{\bar{\phi^2} + \bar{\delta^2}}{N\eta_T}, \tag{2.10}$$

where η_T is the array taper efficiency equal to one for for uniform distributions and less than one for tapered apertures. It is thus deduced that the SLL can be reduced by increasing the size of the array.

The reduction in array directivity is given approximately by [36] as

$$\frac{D}{D_i} = \frac{1}{1 + \bar{\delta^2} + \bar{\phi^2}}, \tag{2.11}$$

where D and D_i are the directivities of the array with and without errors. The directivity decline is only a function of error variance but has nothing to do with array size.

As studied in [30], the variance of beam pointing deviation is given by

$$\bar{\Delta^2} = \frac{12}{N^3}\bar{\phi^2}. \tag{2.12}$$

According to the equation, the distortion of beam pointing angle is insignificant for a large scale array.

2.1.4 Feed Network

There are generally two types of techniques to feed a phased array, i.e., constrained and unconstrained (space-fed) [37–40]. In a constrained feed, the energy is distributed via transmission lines and power dividers to the array elements. Constrained feed can be further characterized as parallel [22, 41–45] and serial feeds [46–52]. In a parallel feed as shown in Fig. 2.5(a), there are power dividers to split the power from the source to the array element. Usually, 2^{n-1} power dividers are employed to feed a phased array that has 2^n elements. The power dividers are usually same for uniform excited arrays but unequal power dividers are required for tapered amplitude excitations. Serial feeds are composed of cascaded power dividing junctions (coupler) in serial, as shown in Fig. 2.5(b). In a serial feed, when the energy flows across a coupler, part of that energy goes to the corresponding element and the rest of the energy continues to flow until it reaches the next coupler. While serial feeds have very low loss and excellent power division, but each coupler needs a separate design which increases complexity. Recently, some new series-parallel feed networks were also investigated to feed large arrays consisting of sub-arrays [53–55]. In serial-parallel-fed arrays, sub-arrays are serial-fed and array elements in a sub-array are fed in parallel.

Unconstrained feeds [56–59] can be considered to be somewhat between a parallel feed and a center-fed series feed. In an unconstrained feed, the energy is distributed in transmission medium. For example, in Fig. 2.5(c), the array is illuminated by a horn antenna. The energy is captured by receivers and then radiated out after some phase manipulation in TRMs. The unconstrained feed has the advantages of being lighter in weight and lower in cost. It should be noted that unconstrained feed networks tend to have relatively larger phase errors than constrained feed networks, thus the effects of phase errors should be taken into consideration in the array design.

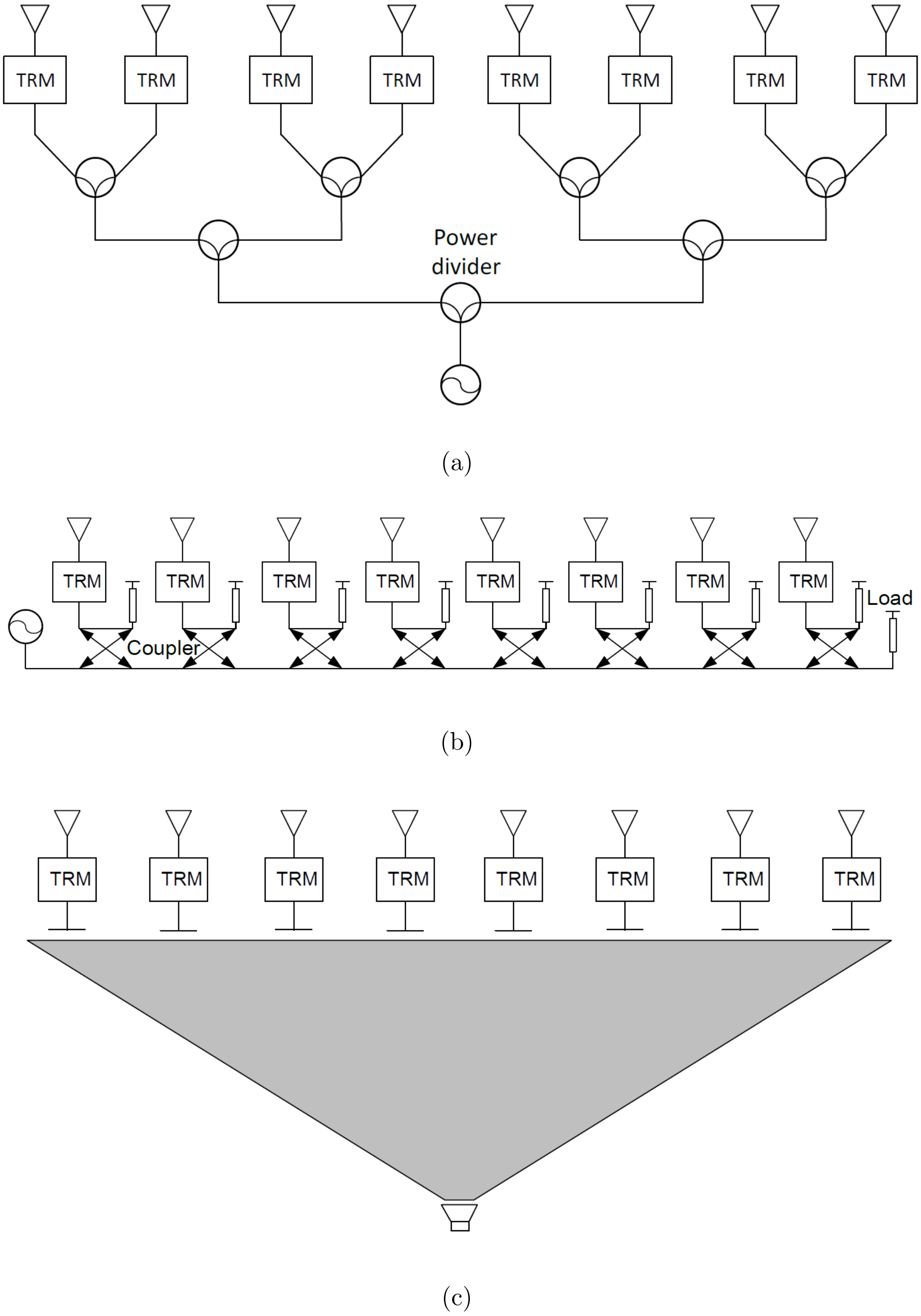

Figure 2.5: Phased array feed networks: Constrained (a) parallel and (b) serial feed networks; (c) Unconstrained feed network.

2.2 Phased Shifter

In phased arrays, the phase shifters are the essential device that allow the antenna beam to be steered in the desired direction without physically rotating the antenna. Beam steering is realized by allocating phase shifters to each radiating element. Usually, this requires many phase shifters in a large array. Therefore, an electronically controlled phase shifter that is small, low loss, and low cost is desirable. In this section, the major parameters used to define a phase shifter are introduced. Then, a summary of different types of passive planar phase shifters and their recent progresses are presented.

2.2.1 Major Parameters

A phase shifter is a two-port device that produces an adjustable change in the phase of the wave transmitted through it. The key propagation characteristics concerned in phase shifter designs are the propagation constant, phase shift, and time delay. The definitions of the parameters are given and relationships between them are presented as follow.

The propagation constant is the measure of change undergone by the source quantity as it propagates from one port to the other port. In a transmission line, the propagation constant is defined by the ratio of the amplitude at the source of the wave to the amplitude at some distance x, such that,

$$\frac{A_0}{A_x} = e^{\gamma x}, \tag{2.13}$$

where the real portion α and the imaginary portion βx are the attenuation and phase constants, respectively. The attenuation constant α determines the way a signal is reduced in the amplitude as it propagates, while the phase constant βx represents the phase shift of the voltage between the input port and at a distance x.

It takes some time for a wave to transmit from one point to another point of a transmission line, and that time is defined as time delay. The relationship between the phase shift and time delay is given as:

$$Time\,delay\,(seconds) = \frac{Phase\,shift(^\circ)}{360 \times frequency(Hz)}, \tag{2.14}$$

The amount of delay that a transmission line introduces per distance x is

$$Time\,delay\ = \frac{x}{V_p} = \frac{\beta x}{\omega}, \tag{2.15}$$

where V_p is the phase velocity.

Group delay is the average delay time that a specific narrow range of frequencies experiences when passing through a circuit. It is proportional to the rate of phase shift at each frequency of interest.

$$Group\,delay\,(seconds) = \frac{1}{360} \times \frac{\Delta\phi}{\Delta f}, \tag{2.16}$$

The aforementioned parameters reveal the transmission characteristics of a transmission line. A device that allows one or all the characteristics to change electronically can be seen as a phase shifter. Some more intuitionistic parameters are used to define the phase shifters, including frequency range, bandwidth (BW), total phase shift ($\Delta\phi$), accuracy, resolution, switching speed, and power handling.

2.2.2 Review of Different Types of Planar Phase Shifters

In this subsection, different types of widely used planar phase shifters are reviewed, including High-pass/Low-pass, Loaded-line, Switched-line, Reflective-type, Slow-wave, and Ferrite phase shifters. Their design theories are investigated followed by summaries of recent progresses on these phase shifters.

High-Pass/Low-Pass

The high-pass/low-pass phase shifter was firstly introduced in [60] and attracted lots of attentions since then. It has superior power and phase bandwidth capabilities when

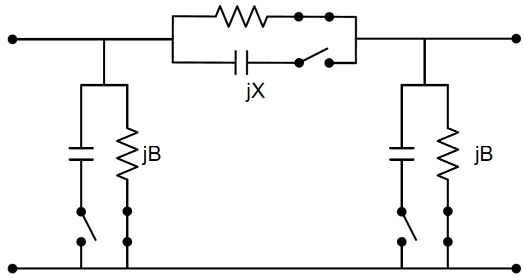

Figure 2.6: Topology of the high-pass/low-pass phase shifter.

compared with more conventional phase shifters using switched lines, reflection or loaded lines. Moreover, from simple bit topologies with PIN diode switches to more complicated designs, the high-low pass phase shifter has been found to be ideal on-chip architecture due to its small size, flat response over a wide frequency band and ability to cancel out phase effects induced by switches and routing schemes.

In principle, any variable reactance in series or parallel across a transmission line can be used to introduce phase shift. A high-pass/low-pass phase shifter has two configurations, the high-pass network and low-pass network, as shown in Fig. 2.6. When the phase shifter works in the high-pass state, a relative phase delay is realized. By toggling switches employed, the phase shifter is switched to the low-pass state, resulting in a phase advance [61]. If the circuit is matched, $X = 2B/(1+B^2)$ and the insertion phase is $tan^{-1}(2B/(B^2-1))$ [62]. Traditional transmission line models of the phase shifter in both the high- and low-pass states are π-networks. This topology can achieve a phase shift of 180° with about 20% bandwidth.

Recent works on high-pass/low-pass phase shifters have shown improvements from different aspects, including the reduced chip size [63], lower insertion loss [64, 65], and smaller phase error [66]. Size reduction of the phase shifter can be realized by lowering the number of capacitors and/or inductors required in the high-pass or/and low-pass networks. In [63], the phase shifter topology in the high-pass state is a t-network rather

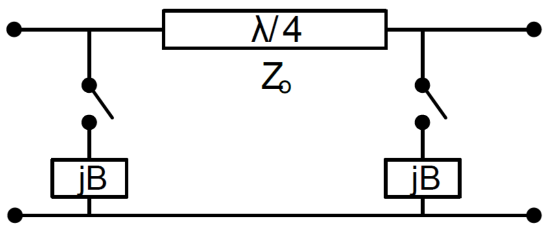

Figure 2.7: Topology of the loaded-line phase shifter.

than a π-network. The required number of the inductors is halved, which significantly reduces the chip size.

High-pass/low-pass phase shifters usually suffer from high insertion losses [67–69]. The largest component of the losses comes from the switches. Therefore, MEMS switches that have the lowest insertion loss among variable switches were used to obtain a low insertion loss [64]. Another method to reduce the insertion loss is to achieve better match by changing the phase shifter's topology [65].

The high-pass/low-pass phase shifters are very popular in SiGe integrated circuit (IC) design platforms targeting monolithic T/R module applications for phased array radar [68, 70]. However, the silicon-based monolithic design has inherent design limitations in achieving small phase errors. To reduce the phase errors, a comprehensive analysis of error sources in a monolithic high-pass/low-pass microwave phase shifters due to device size limitations, inductor parasitics, loading effects, and nonideal switches was presented in [66].

Loaded Line

Fig. 2.7 gives the schematic of a loaded line phase shifter. In this type of phase shifter, two reactive loads are shunted across a transmission line and spaced apart from each other by a quarter wavelength. The first susceptance (jB) is employed to provide phase shift, and the second susceptance (jB) is used to cancel the reflection introduced by the first susceptance. In designing this type of phase shifter, we aim to equate the ABCD matrix to a section of a transmission line with the length of θ_L and characteristic impedance of Z:

$$\begin{bmatrix} 1 & 0 \\ jB & 1 \end{bmatrix} \begin{bmatrix} 0 & jZ_0 \\ j/Z_0 & 0 \end{bmatrix} \begin{bmatrix} 1 & 0 \\ jB & 1 \end{bmatrix} = \begin{bmatrix} cos(\theta_L) & jZsin(\theta_L) \\ jsin(\theta_L)/Z & cos(\theta_L) \end{bmatrix} \tag{2.17}$$

By solving the equation, we can determine

$$Z = \frac{Z_0}{[1-(BZ_0)^2]^{1/2}} \tag{2.18}$$

and

$$\theta_L = \frac{1}{cos(-BZ_0)} \tag{2.19}$$

Using this topology, the phase velocity (V_p) can be increased or decreased if the susceptance (jB) is capacitive or inductive, respectively. Traditional loaded line phase shifters are narrow-band and generally used for achieving 22.5° to 45° phase shift [71].

Recent improvements of loaded line phase shifters are focused on the realizations of the employed reactive loads. Controllable capacitors and inductors are used as the loads, which brings more flexibility of the phase shifters. The most well-developed technology is MEMS-based varactor that has been shown to provide very low insertion loss [72–74]. Another noteworthy progress is the development of tunable inductors based on low-temperature co-fired ceramic (LTCC)-ferrite tape [75] that a low cost and high power handling capability.

Switched Line

Switch-line phase shifters are also popular because they are designer-friendly. As shown in Fig. 2.8, switches are used to toggle between transmission lines with different path lengths. This phase shifter can introduce a phase shift of

$$\Delta\phi = \beta(L_2 - L_1), \tag{2.20}$$

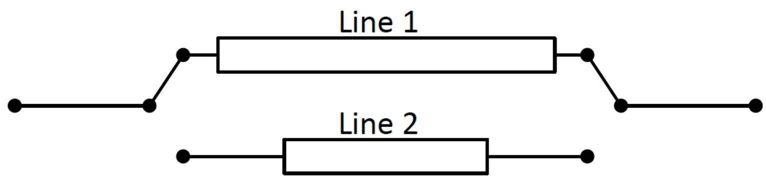

Figure 2.8: Topology of the switched-line phase shifter.

where β is the propagation constant of the transmission line. Note that β is in proportion to radian frequency ω, which means that the phase shifter is a true time-delay device providing a phase response proportional to frequency (ω). For this type of phase shifter, $\tau = -d\phi/d\omega$ is a constant over the bandwidth. A clear advantage of the constant time-delay is that the beam steering angle is independent of frequency. However, it is noted that the off path length and switch capacitance can conspire to create a through path in parallel with the on path, resulting in high insertion loss and abrupt phase change in the frequency band.

Switches are the key component in switched line type phase shifters. The employed switches can significantly affect the performance of the phase shifter. Different switches including PIN diodes [76], CMOS [77], and MEMS switches [78–81] have been used in phase shifters to achieve the excellent performance in various frequency bands in the last few years. Especially the RF-MEMS based phase shifters have advanced significantly with its high linearity, low loss, and excellent phase accuracy within a compact size. Except the switches, there are also works on proposing new transmission lines employed in this type of phase shifter. In [82], Left-hand/right-hand transmission lines have been used that can provide positive and negative dispersion in different working states.

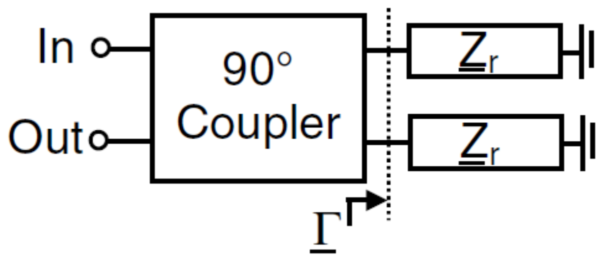

Figure 2.9: Topology of the reflective-type phase shifter.

Reflective

The most common type of analog phase shifters is the reflective-type phase shifter [83–92]. Fig. xx shows the architecture of a reflective-type phase shifter consisting of a branch-line coupler and two reflective loads with equal impedances Z_r. The input signal is divided into two parts and reflected at the reflective loads. Given that the reflective loads are purely reactive, no power is lost and all signal power is coupled into the output. One significant benefit of this type of phase shifter is that the input and output impedance matching is preserved. With the characteristic coupler impedance Z_0, the reflection coefficient observed between Z_r and coupler ports is given by

$$\Gamma = \frac{Z_r - Z_0}{Z_r + Z_0}. \tag{2.21}$$

By changing Z_r, the phase of this reflection coefficient can be varied. Given the maximum and minimum impedance of the reflective loads, the phase variation can be obtained as

$$\Delta\phi = 2[arctan(\frac{Z_{max}}{Z_0}) - arctan(\frac{Z_{min}}{Z_0})]. \tag{2.22}$$

Variable active inductances, capacitances, and LC networks can be applied as the reflective loads. The reflective-type phase shifter can be used to provide any desired phase shift. It can provides a bandwidth of up to an octave, mainly depending on the bandwidth of the coupler.

The reflective-type phase shifter was firstly proposed in [93] and then further developed with a variety of topologies and substrate using various hybrids and couplers [reflection phase shifter [87]. In designing this type of phase shifters, the coupler is the backbone. The most popular couplers used in this type of phase shifters are 90° hybrid couplers and lang couplers as shown in Fig. xx. Usually, the couplers have to be approximately a quarter wavelength long. However, a recent work [83] shows that a coupled structure that is less than one tenth of the of a wavelength is sufficient to build a high-performance reflection-type phase shifters. Another innovative progress on the couplers used in reflective-type phase shifters is a reconfigurable coupler based on MEMS that endows the phase shifter with a wide frequency range and a high power handling capability [91].

The reflective loading is the other significant component in this type of phase shifters. The variation range of the reflective loading determines the phase shift range and the insertion loss variation of the phase shifters. Variable active inductances and capacitances can be employed in the reflective loadings. Due to the advantages in terms of loss, size, and power consumption, varactors are employed in most cases. However, the phase shift range is limited to 180° by using only controllable capacitances. By resonating the capacitance of the varactor with a series inductor, the phase control range can be significantly increased, up to an ideal 360° phase shift change. In the last few years, several different loading topologies have been proposed, aiming to increase the phase shift range and lower the amplitude variation [84–86, 89, 92].

Slow Wave

Periodically loaded transmission lines are used to achieve band-pass, slow-wave circuits that have the phase velocity $V_p < c$ [94–98]. By tuning the loads, the phase velocity can be changed, resulting in phase shift. An infinite transmission line with periodically loaded lumped element shown in Fig. 2.10 is a slow-wave structure. The structure can be divided

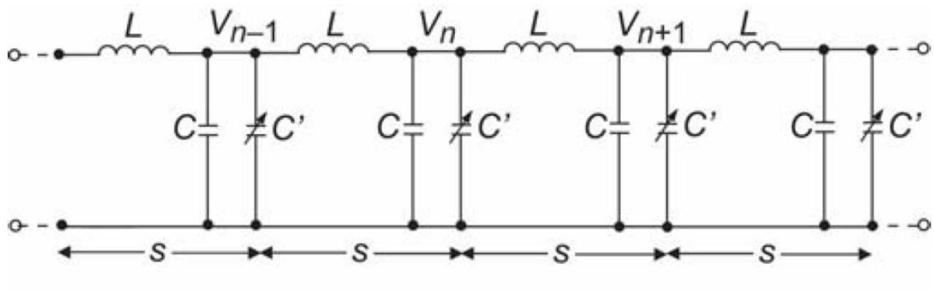

Figure 2.10: A slow wave structure realized by periodically loaded lumped elements.

into several uniform sections, with each section composed of L, C, and C_0. Assuming the separation distance of each unit cell is chosen as s, a wave travelling through this periodic structure will only experience a phase shift from unit cell to unit cell, such that V_n is delayed relative to V_{n-1} as

$$V_n = V_{n-1}e^{-j\theta_n} \tag{2.23}$$

By summing the currents leaving node n, we can get

$$V_n(j\omega C + j\omega C') + [V_n - V_{n-1}(-j/\omega L)] + [V_n - V_{n-1}(-j/\omega L)] = 0. \tag{2.24}$$

Substituting equation 2.23 into equation 2.24, it is shown that

$$cos(\theta_s) = \frac{1}{2}(2 - \omega^2 L(C + C')). \tag{2.25}$$

In a propagation mode, θ_s has to be real. Letting $cos(\theta_s) = \pm 1$, we note that the slow-wave structure has a lower cutoff frequency $\omega_L = 0$ and an upper cutoff frequency ω_H

$$\omega_H = \frac{2}{[L(C + C')]^{1/2}}. \tag{2.26}$$

Since $\theta_s = \beta s$, the introduced phase shift can be approximated by giving the extremes of the tuning range of C' and the number of the sections cascaded. Note that, slow-wave phase shifters are actually time delay devices and the phase shift is proportional to frequency.

Various slow-wave phase shifters have been studied with different methods to tune C' [99–106]. One of the most popular types is based on ferroelectric varactors [99–101] which achieves excellent results. One advantage of using the parallel plate ferroelectric varactors is that low tuning voltage is used. Another advantage is that circuits can be fabricated on convenient Si substrate. New technologies have been employed recently to design slow-wave phase shifters, including MEMS technology [102–104], liquid crystal [105], and quartz substrate [106]. These technologies have resulted in enhanced performance, however, costs are also increased.

Ferrite

The fundamental source of a material's magnetic property is the magnetic dipole moment. In non-magnetic materials, the net magnetic moment is negligible, due to the fact that the number of electrons with up and down spins is equal. In magnetic materials, one jargon type of material dominates, and can be aligned by an external DC magnetic bias field H to generate a large magnetic moment. The spin magnetic moment vector precesses about the H-field vector at a frequency of $\omega_m = 2\pi f_m$. Precession polarization depends on the direction of H, and precession frequency is proportional to H. Therefore, $f_m = \gamma H$, where $\gamma = 2.8\ MHz/Oe$ is the gyromagnetic constant. The propagation constant β can be obtained as

$$\beta \approx (2\pi\sqrt{\epsilon\mu'}/\lambda), \tag{2.27}$$

where μ' is the real part of the permeability and ϵ is the dielectric constant of the ferrite. Ferrimagnetic resonance occurs when the frequency of a microwave magnetic field equals the precession frequency ($f = f_m$). The opposite circularly polarized waves experience different probabilities, μ'_+ and μ'_-. We are able to change the permeability by tuning the magnetization (magnetic moment) M. When f_m is small compared to f, there is a significant difference between μ'_+ and μ'_- for the two polarization senses. In this case, it is shown that [107]

$$\mu'_{\pm} = 1 \mp \gamma 4\pi M/f \tag{2.28}$$

and the phase shift is given as

$$\Delta\phi = 2\pi\sqrt{\epsilon}[(\mu'_{+})^{1/2} - (\mu'_{-})^{1/2}]L/\lambda, \tag{2.29}$$

where L is the length of the ferrite section.

Ferrite phase shifters are divided into reciprocal and nonreciprocal, depending on whether the variable differential phase shift through the device is a function of the propagation direction [108–110]. Furthermore, ferrite phase shifters can be latching or non-latching, depending on whether a continuous current must be supplied to hold the magnetic bias field. There are generally three types of ferrite phase shifters, i.e., toroidal [111–113], dual mode [114–116], and rotary field [117–119].

Ferrite phase shifters have been widely studied due to their low loss performance and high power handling capability. However, old-fashioned ferrites are operated in fully saturated states with high external bias magnetic fields, which makes them bulky and power consuming. In the last few years, studies have been conducted to reduce the required bias field from several kilo-Oersteds to less than a hundred Oersteds [120–123]. Partially magnetized ferrite is a promising solution that requires low or zero bias field and has a fast micro-second tuning speed. It has $0 < \mu < 1$, which can be tuned by changing its magnetization M between 0 M_s (saturation magnetization) with a low field [124].The most important advantages is that the need for low tuning magnetic fields for partially magnetized ferrites provides a unique opportunity for dual H- and E-field tunable RF/microwave multiferroic devices, since the low tuning magnetic field can be provided by ferrite/piezoelectric structure under electric field.

2.3 PIN Diode and Capacitor

In this thesis, lumped elements including PIN diodes and capacitors are intensively used. The PIN diodes are employed as switches and the capacitors aim to provide RF continuity and DC isolation. This section presents the equivalent circuit, key parameter values, and mounting requirements of the employed PIN diodes and capacitors.

2.3.1 PIN diode

A microwave PIN diode is a semiconductor device that operates as a variable resistor at RF and Microwave frequencies [125]. It is a current control device and can be used for fast switching, when the control current is switched “On” and “Off”. Due to its small physical size compared to a wavelength, high switching speed, low package parasitic reactance, and low control power, the PIN diodes are adopted in this work as switches. Specifically, we chose the commercially available PIN diode with serial number of MA4FCP300 made by MA-COM Technology Solutions for its low resistance, compact size and low price.

According to its datasheet [126], the diode is fabricated on epitaxial wafers using a process designed for repeatable electrical characteristics and extremely low parasitics. It has a flip chip configuration that is suitable for pick and place insertion. Fig. 2.11 shows the top view of the PIN diode. This figure also gives the dimension requirements of the metallic pads supporting the diode.

The PIN diode is able to work in two states, the “On” state when it is forward biased, and the “Off” state when it is reverse biased or has no bias. Fig. 2.12(a) and 2.12(b) shows the equivalent circuits of the employed PIN diode in the On and Off states, respectively.

The equivalent circuit of the On-state PIN diode consists of a series combination of the series resistance $R_f = 2.6\,\Omega$ and a small inductance $L_f = 0.6\,nH$. For different PIN diodes, the values of the resistance and inductance can change. In this thesis, smaller

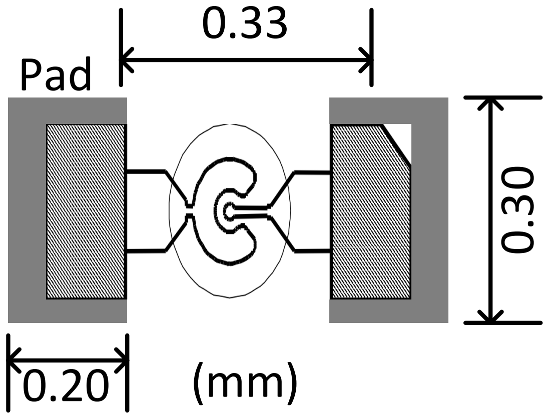

Figure 2.11: Top view of the PIN diode MAMA4FCP300.

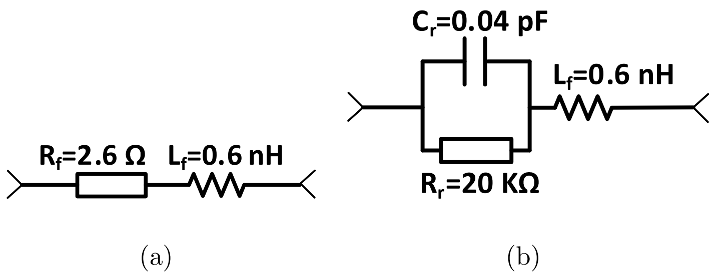

Figure 2.12: Equivalent circuit of the PIN diode in the (a) "On" and (b) "OFF" states.

resistance and inductance values are preferred for lower losses on the PIN diodes. The datasheet remarks that the PIN diode requires a forward DC current of 100 mA to work in the On state. However, according to our experiment results, a DC current of only 20 - 30 mA is enough to activate the diodes and presents no performance variation.

The "Off" state equivalent circuit consists of the PIN diode capacitance $C_r = 0.04pF$, a shunt loss element $R_r = 20K\Omega$, and the parasitic Inductance $L_f = 0.6nH$. In this state, the PIN diode blocks the RF currents and can be seen as ideal open circuit. The PIN diode doesn't need any bias current to work in this state. However, if the PIN diode is reversely biased, the capacitance C_r and R_r can be slightly lower. The maximum reversely biased voltage is 100 V before breakdown.

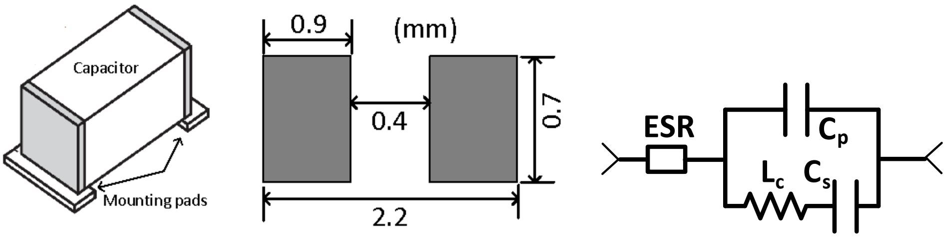

(a) (b)

Figure 2.13: (a) Outlet of the ATC 600L series capacitor with suggested mouting pad dimensions. (b) Equivalent circuit of the capacitor.

2.3.2 Capacitor

In this thesis, capacitors are used in phase shifter designs in blocking DC current while allowing RF current to pass. The ATC 600L Series thin-film capacitor [127] made by ATC Technology Inc. is adopted for its low resistance, high Q, and compact size. The thin-film capacitor can be fixed on metallic pads using epoxy technology. The outlet of the capacitor with its suggested mounting pad dimensions, and the equivalent circuit are depicted in Fig. 2.13(a) and 2.13(b), respectively.

As shown in Fig. 2.13(b), the capacitor has an intrinsic resistance of ESR, where $ESR \approx 0.1\ \Omega$ at 1 GHz, and increases slightly with frequency. A capacitor usually has both the series resonant frequency (F_{SR}) and the parallel resonant frequency (F_{PR}), respectively [108]. This is attributed to the existences of a serial capacitor C_s and a parallel capacitor C_p. The F_{SR} is defined by

$$F_{SR} = 1/2\pi\sqrt{L_c C_s}, \tag{2.30}$$

at which frequency, the capacitor's net reactance is zero and the impedance equals ESR. The magnitude of the transmission impedance the capacitor presents will be extremely low from the bottom frequency end determined by the capacitance value, right through the F_{SR} until one approaches the first F_{PR}. The first F_{PR} is frequently called simply the

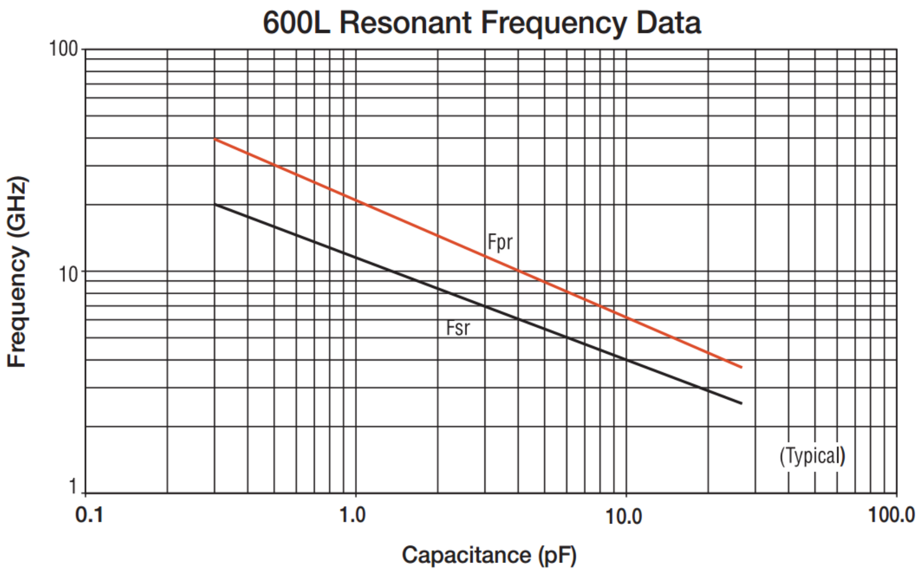

Figure 2.14: F_{SR} and F_{PR} curves of the ATC 600L capacitors.

F_{PR}. In reality, there is a second F_{PR}, third F_{PR}, and so on. Roughly, the F_{PR} is twice of the F_{SR}. At the F_{PR}, the impedance of the capacitor could be quite high, resulting in noticeable high IL.

When choosing the capacitor, it is preferred that the capacitor has the F_{SR} at the designed centre frequency, and has the F_{PR} above the maximum working frequency. This way, the employed capacitor can introduce minor insertion lo ss in the working band. Fig. 2.14 gives the F_{SR} and F_{PR} curves of the ATC 600L capacitors, which is used to find the suitable capacitor for our design. In this thesis, the centre frequency is 5.2 GHz for wireless local area network (WLAN) applications. To have the F_{SR} at 5.2 GHz, the capacitor with a total capacitance of 6.2 pF is selected.

2.4 Summary

This Chapter presented a literature review and background material related to this thesis for phased array antennas and phase shifters. Firstly, a brief introduction of the theory and architecture of phased array antennas was presented. Most significant design considerations of phased array antennas were described followed by reviews of advanced solutions published recently. Then we intensively reviewed various types of array feed networks, which is closely related to the main contributions of this thesis. Subsequently, phase shifters which are the most crucial component in phased arrays were introduced. A comprehensive review of different types of planar phase shifter was presented, including high-pass/low-pass, loaded-line, switched-line, reflective, slow-wave, and ferrite phase shifters. The working mechanism of these phase shifters were described and their progresses in the last ten years were summarized. Finally, in the last section, the Pin diode and capacitor that have been extensively used in this work were investigated.

Chapter 3

Phase Shifter Based on RDMS

3.1 Introduction

Beamforming is an effective way of improving the link performance of wireless communication systems. Conventionally, this is achieved by either digital [128–132] or analog beamforming [133–136]. Digital beamforming is the most flexible approach, and it can give the best system performance due to its ability to optimize the beam pattern according to the radio environment. A major disadvantage of digital beamforming is the high cost associated with the RF chains and signal processing units. By contrast, analog beamforming is a much less expensive approach, as the beams are formed via phase shifters and combiners that are located before the active devices. As a result, only one RF chain and a minimum amount of signal processing are required.

However, even in low-cost analog beamforming systems, for example, the phased array antennas, a number of phase shifters are employed, which could substantially increase costs. To minimize cost, the most effective way is to reduce the cost associated with the phase shifters. In low-cost analog beamforming, ferrite phase shifters are often used. However, these are relatively bulky and heavy compared to diode phase shifters, and they require significant switching power. Generally, phase shifters tend to be lossy or inconvenient for integration with the antenna array for low-cost and high-volume realizations. In the last few years, some novel phase shifters have been proposed based on defected ground structure (DGS) [137–140] which was originally used in filter, coupler, and oscillator designs. In [141], a novel phase shifter with DGS was presented that had a larger phase-shifting range. By using DGS in termination loads, the phase-shifting range was increased to 145^0 compared with a 65^0 phase shift for the same structure using conventional loads. Shafai et al. [142] introduced thin-film copper membranes in the ground plane below the transmission line to enable the ground plane reconfiguration. By actuating these membranes, the space between the transmission line and ground plane was tuned, and the line capacitance changed, which resulted in phase shift. In this design, the maximum phase shift realized was 55.5^0 at 14.25 GHz by applying a 405-V pull down voltage. Subsequently, this phase shifter was improved in [143] by using flexible microribbons that required significantly lower actuation voltage to replace the membranes. A 41^0 phase shift was obtained in the design with an actuation voltage of 120 V. In [144], the membrane in [142] was replaced by metallized polydimethylsiloxane (PDMS) elastomeric ground plane and the cost was reduced to some extent. The design described had an insertion loss of 2.5 dB and a phase shift of 170^0 at 50 GHz. In addition, a phase shifter giving a 45^0 phase shift was proposed in [145]. It employed DGS under parallel stubs, and this achieved a wider bandwidth and had a smaller size than a similar structure without DGS.

As a dual structure of DGS, the defected microstrip structure (DMS) [146] also has the potential to realize phase shifts. However, there have rarely been phase shifters based on DMS described in the literature. This chapter motivates to propose a low-cost low-loss phase shifter design, by developing the potential of DMS to be used as phase-shifting unit. In this Chapter, we propose a new type of reconfigurable DMS (RDMS)-based phase shifter. The proposed RDMS unit is a segment of microstrip line with a slot on it, and the slot is loaded with PIN diodes and capacitors. By applying different biasing voltages to switch the working states of the diodes, the current paths are changed, thus leading to a phase shift. In addition, by cascading a number of the RDMS units and controlling them separately using different DC voltages, stepwise phase shifters are realized with flexible phase-shifting range and step size. To verify the concept, phase shifters with three, six, and nine RDMS units have been designed, fabricated, and measured.

This chapter is organized as follows. In Section 3.2, the basics of the RDMS unit are presented, including the structure, working mechanism, equivalent circuit, and parameter analysis. Subsequently, the proposed RDMS units are cascaded, resulting in RDMS groups, which is studied in Section 3.3. Then, stepwise phase shifters employing RDMS groups are designed, fabricated, and measured. Finally, the conclusion is drawn in Section 3.4.

3.2 RDMS Phase-Shifting Unit

In this section, the RDMS is proposed and then studied as a phase-shifting unit. The structure is presented and the working mechanism is discussed. Moreover, physical dimensions of the RDMS are studied to demonstrate how they affect performance (IL and phase shift). The variation law obtained by simulations is then explained by equivalent circuits. Ultimately, with the understanding of its working mechanism and performance characteristics, an optimized RDMS phase-shifting unit is developed.

3.2.1 Structure Description

The proposed phase-shifting unit is made by etching a slot on a microstrip line and loading the slot with PIN diodes and capacitors. Such a structure can be realized in two steps,

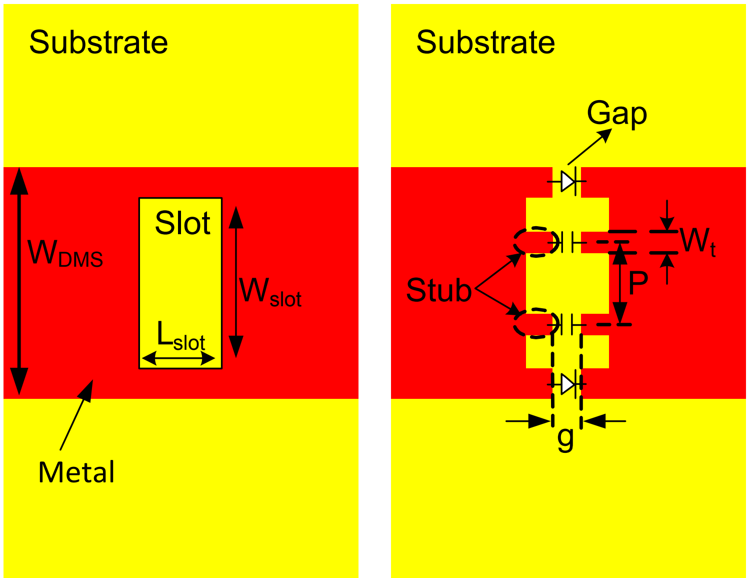

(a) (b)

Figure 3.1: Structure of the DMS unit. (a) Step 1: etching a slot on a microstrip line, (b) Step 2: loading PIN diodes and capacitors (complete structure).

which are illustrated in Fig. 3.1(a) and 3.1(b), respectively. The first step is to etch a rectangular slot with a size of $W_{slot} \times L_{slot}$ on a microstrip line with a width of W_{DMS}, as shown in Fig. 3.1(a). This creates a DMS. The second step is to insert the PIN diodes and capacitors to the slot. As shown in Fig. 3.1(b), two gaps are etched on the edges of the microstrip line to place the diodes, and stubs are employed as mounting pads for the capacitors. This way, the DMS is able to be reconfigured by controlling the working states of the PIN diodes.

Fig. 3.1(b) depicts the complete structure of the RDMS unit. The employed substrate used in this work is Rogers 4003, which has a substrate thickness of h, dielectric constant of ε, and loss tangent of δ. We remark that there are some key dimensions to be noticed, including the microstrip line width W_{DMS}, the slot size $W_{slot} \times L_{slot}$, the gap size $W_t \times g$, and the separation distance between the two stubs P. The values of the mentioned parameters are given in Table 3.1, for researchers and engineers who are interested in

Table 3.1: Dimension values of the RDMS unit

Parameter	Value	Description
W_{DMS}	10 mm	The width of microstrip line
W_{slot}	8 mm	The width of the slot
L_{slot}	2 mm	The length of the slot
P	4 mm	The distance between the two stubs
W_t	0.7 mm	The width of the stub
g	0.4 mm	The width of the gaps
h	1.524 mm	Substrate thickness
ε	3.55	Substrate dielectric constant
δ	0.0027	Substrate loss tangent

repeating this work. The presented dimension values are one set of the optimized results. The optimization details will be shown in Section 3.2.4.

3.2.2 Working Mechanism

The RDMS unit shown in Fig. 3.1(b) has two different states: the ON-state when the diodes are turned on, and the OFF-state when the diodes are turned off. Here we assume that the PIN diodes are ideal switches, which can be seen as segments of microstrip lines or an open circuit, when turned on and off, respectively. The capacitors are used for DC isolation and have minor resistances to RF signals. They are also replaced by segments of microstrip lines in our equivalent models. Fig. 3.2(a) and 3.2(b) shows the equivalent models of the RDMS and the current distribution in the ON- and OFF-states, respectively.

In the ON-state, the RDMS can be seen as conventional microstrip line with three slots. Since the currents on the microstrip line are concentrated at the edges, which is

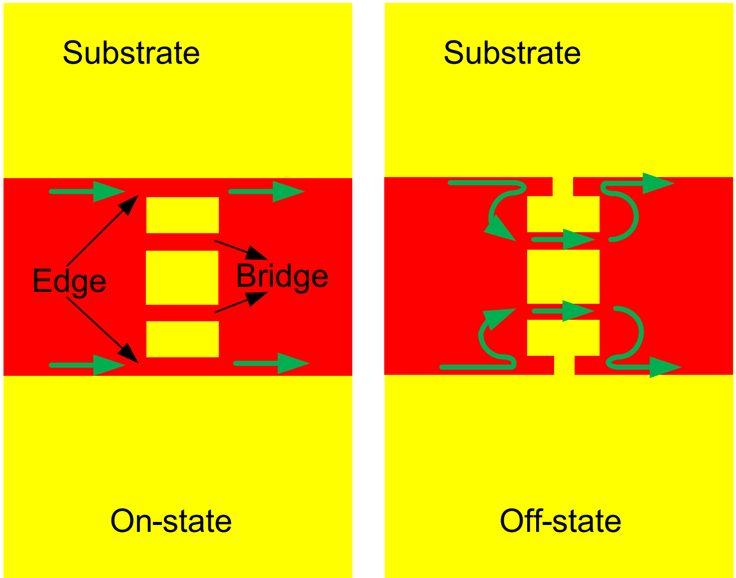

(a) (b)

Figure 3.2: Current distribution on the RDMS unit for (a) the "On" and (b) "Off" states.

a characteristic of the microstrip line, the relatively small slots have minor effects on the current distribution. In this thesis, we will only consider the working frequency of $f_{max} < C/(4 \times L_{slot})$. Within this frequency range, the resulted slots don't radiate at all. Therefore, the ON-state RDMS behaves just like a uniform microstrip line.

In the OFF-state, the RDMS has the new current paths passing through the bridges, due to the blocked path caused by the PIN diodes at the edges of the RDMS. The OFF-state current paths are obviously longer than those of the On-state. Considering the RDMS is a two-port device, the RF signals take more time to pass through this device in the OFF-state that in the ON-state, which introduces different phases of transmission coefficient S_{21}. Meanwhile, there will be more reflection caused by the discontinuity in the OFF-state, and therefore the magnitude of S_{21} will be different.

In this thesis, the phase shift of the RDMS is defined as the S_{21} difference between the On- and OFF-states ($\Delta\Phi = \Phi(S_{21\text{-}OFF}) - \Phi(S_{21\text{-}ON})$). And the insertion loss (IL) is

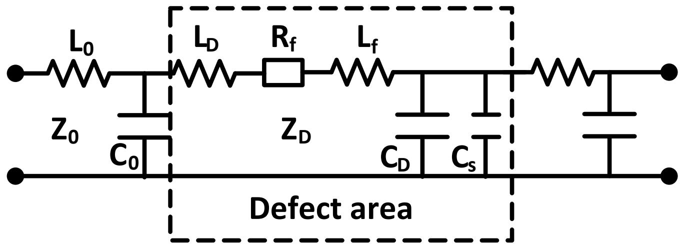

(a)

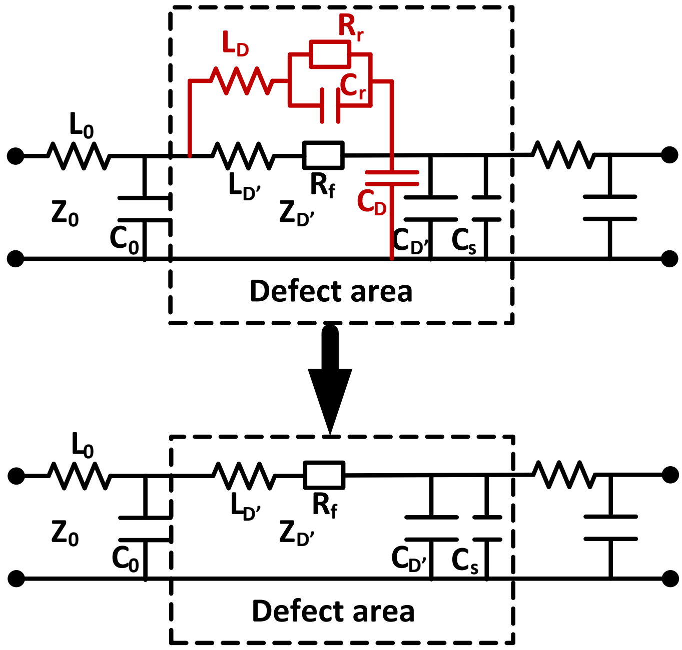

(b)

Figure 3.3: Equivalent circuit of the RDMS unit in (a) the "On" and (b) "Off" states.

defined as $-|S_{21}|$. These are the two most important performance indexes considered in this thesis.

3.2.3 Equivalent Circuit

To better understand how the RDMS phase-shifting unit shown in Fig. 3.1(b) works, equivalent circuits are derived based on the equivalent structures described in Section 3.2.2, and the equivalent circuits of the PIN diodes and capacitors given in Section 2.3.

Fig. 3.3(a) and 3.3(b) shows the ON- and OFF-states equivalent circuits of the RDMS unit, respectively.

The RDMS unit can be divided into the defect area and uniform connecting microstrip lines. As shown in Fig. 3.3(a), the connecting microstrip lines are replaced by the distribution model, where Z_0, C_0, and L_0 represent the characteristic impedance, distributed capacitance per unit length, and distributed inductance per unit length of the connecting lines, respectively. The defect area can also be seen as transmission line system and can be modelled as a serial conductor $L_D = L_0 \times L_{slot}$ and a ground capacitor $C_D = C_0 \times L_{slot}$. In the ON-state, the currents are concentrated at the edges, and the capacitors exhibit minor impedance. Therefore, the metal stubs and capacitors are neglected. The forward biased PIN diode is modelled as a serial combination of a resistor R_f and inductor L_f. In addition, the resultant slots in the defect area can introduce additional capacitance C_s, which is also considered in the equivalent circuit. The characteristic impedance of the defect area Z_D can be roughly calculated by $[(L_D + L_f)/(C_D + C_s)]^{1/2}$. Since $L_f \ll L_D$ and $C_s \ll C_D$, the characteristic impedance $Z_D \approx Z_0$, where Z_0 is the characteristic impedance of a uniform microstrip line. Given the line width W_{DMS}, dielectric constant ε, and substrate thickness h, it is calculated that $Z_0 = 23\Omega$. The connecting lines and the defect area have almost the same characteristic impedances, which avoids discontinuity and reflection. However, due to the presence of the forward biased diode with resistance Rf , a RDMS unit could have a slightly larger IL than a uniform microstrip line with the same length.

Fig. 3.3(b) shows the equivalent circuit of the RDMS unit in the OFF-state. The models of the connecting lines are the same with those in the ON-state. However, the equivalent circuit of the defect area is different. In the OFF-state, the diodes are turned off, and modelled as a parallel circuit consisting of a large resistor and a small capacitor. This leads to a fact that there is minor current go through the diodes located at the edges of the microstrip line (highlighted in red font in Fig. 3.3(b)). Therefore, the red path is neglected, and the defect area in the OFF-state can be seen as a transmission line with a characteristic impedance of $Z_{D'}$. It can be calculated by $[L_{D'}/(C_{D'} + C_s)]$, where $L_{D'}$ and $C_{D'}$ are the distributed inductance and capacitance per unit length, respectively, of a microstrip line with a width of P, dielectric constant of ε, and substrate thickness of h. C_s is determined by the area of the resulted "T-slot" in Fig. 3.2(b).

From $P < W_{DMS}$, it is conducted that $Z_{D'} > Z_D \approx Z_0$, $L_{D'} > L_D \approx L_0$, and $C_{D'} < C_D \approx C_0$. Due to the mismatch of the connecting line (Z_0) and defect area (Z'_D), reflection is introduced by the discontinuity and IL is increased in the OFF-state.

3.2.4 Parameter Analysis

Physical Dimensions

In this subsection, parameter sweeps of the four physical dimensions: W_{slot}, L_{slot}, and W_{DMS}, and P are made. These four parameters are found to have significant effects on the IL and the phase shift of the RDMS unit. The parameter sweep aims to elaborate on how the dimensions of the RDMS affect the performance. The parameter sweep is made by sweeping one of the parameters each time while the others are fixed at the value given in Table 3.1. The dimension values are the optimized results based on simulations using CST Microwave Studio [147]. They were obtained by trial and error based optimization process with two goals. The first goal was to achieve the greatest phase shift with an acceptable IL (below 1 dB). The second was to create the smallest possible RDMS unit on the premise of the first goal.

The sweep of W_{slot} was made from 5 mm to 8 mm due to the fact that $P < W_{slot} < W_{DMS}$. Fig. 3.4(a) and 3.4(b) shows the simulated magnitudes and phases of S_{21} with different W_{slot}, respectively. It was observed that the transmission coefficient S_{21} in the

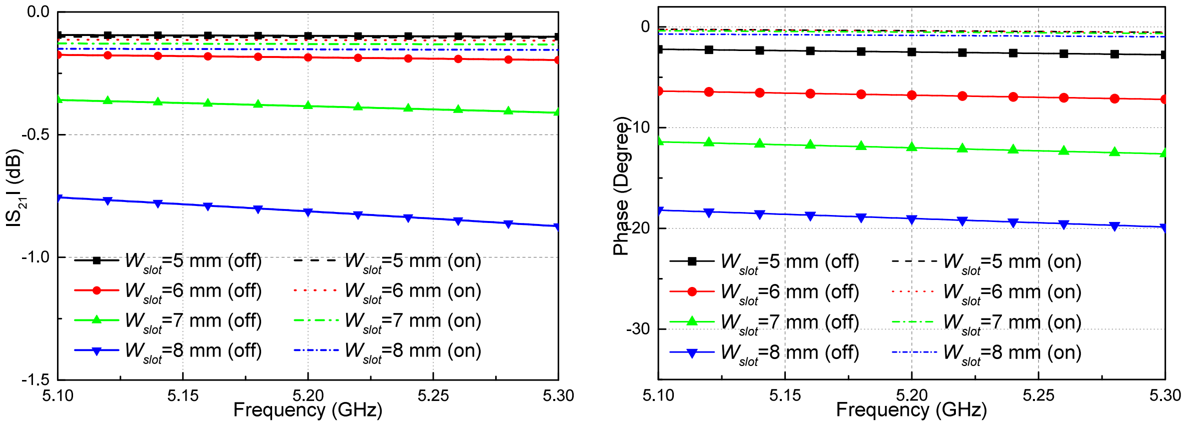

(a) (b)

Figure 3.4: Simulated (a) magnitudes and (b) phases of S_{21} when W_{slot} sweep from 5 mm to 8 mm.

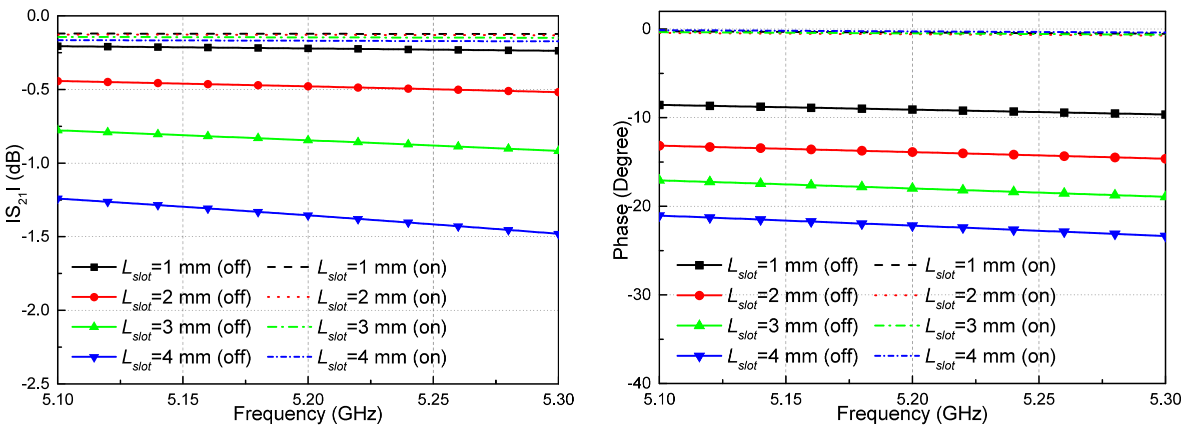

(a) (b)

Figure 3.5: Simulated (a) magnitudes and (b) phases of S_{21} when L_{slot} sweep from 1 mm to 4 mm.

ON-state showed good stability with increased W_{slot}. In the OFF-state, however, both the magnitude and the phase of S_{21} decreased with W_{slot}. It is thus concluded that both the IL and the phase shift increase with W_{slot}.

The sweep of the slot length L_{slot} was made from 1 mm to 4 mm with the results shown in Fig. 3.5. The S_{21} in the ON-state exhibits minor variations with different L_{slot}.

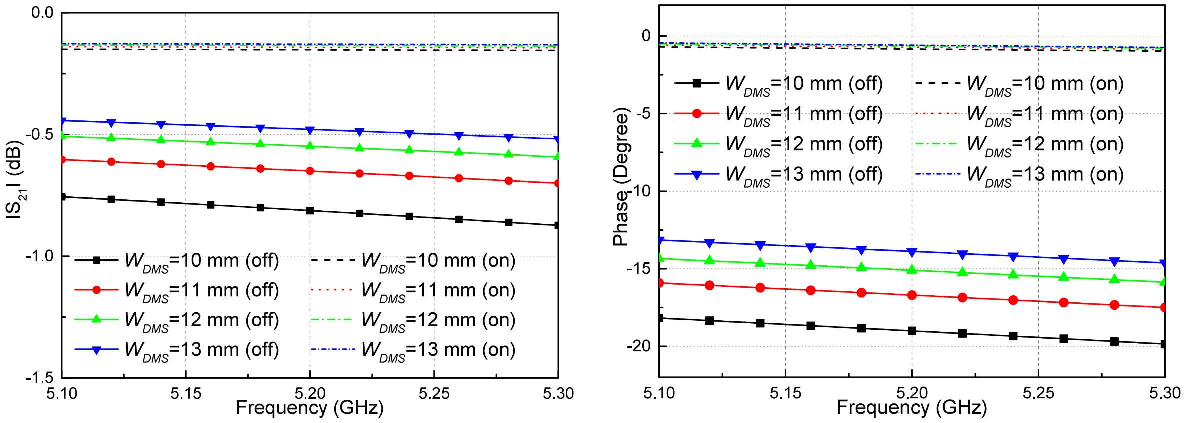

(a) (b)

Figure 3.6: Simulated (a) magnitudes and (b) phases of S_{21} when W_{DMS} sweep from 10 mm to 13 mm.

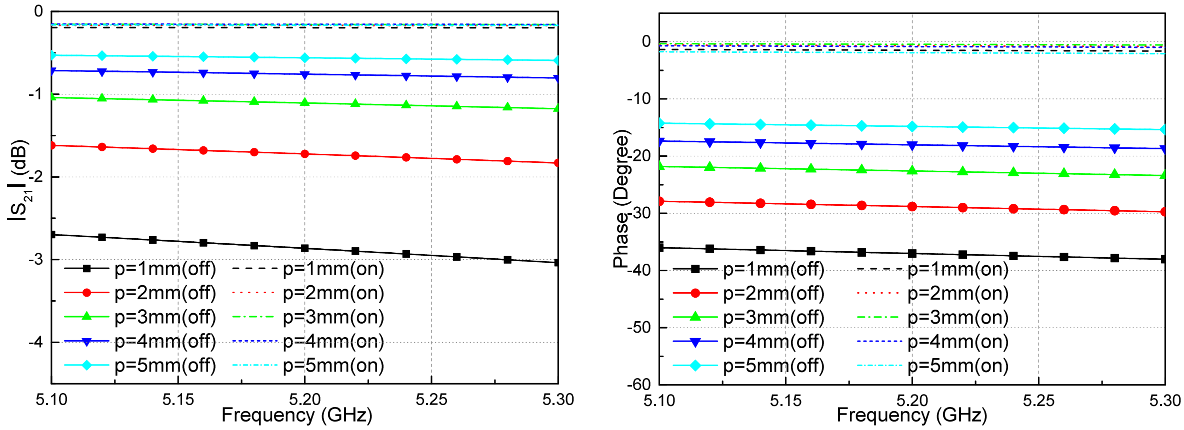

(a) (b)

Figure 3.7: Simulated (a) magnitudes and (b) phases of S_{21} when p sweep from 1 mm to 5 mm.

In the OFF-state, both the magnitude and the phase of S_{21} decrease with L_{slot}. This indicates that both the IL and the phase shift increase with L_{slot}. It should be noted that L_{slot} also affects the size of the RDMS unit. Clearly, a larger L_{slot} implies a longer RDMS unit, and the size increase will be amplified if several RDMS units are cascaded.

The width of the microstrip line W_{DMS} is a parameter of significant importance as

Table 3.2: Variation law of the performance with some key dimensions of the DMS unit

Parameter	$P \nearrow$	$W_{slot} \nearrow$	$L_{slot} \nearrow$	$W_{DMS} \nearrow$
IL (ON-state)	$--$	$--$	$--$	$--$
IL (OFF-state)	$\searrow$	$\nearrow$	$\nearrow$	$\searrow$
Phase of S_{21} (on-state)	$--$	$--$	$--$	$--$
Phase of S_{21} (off-state)	$\nearrow$	$\searrow$	$\searrow$	$\nearrow$
Phase shift	$\searrow$	$\nearrow$	$\nearrow$	$\searrow$

it not only determines the characteristic impedance of the microstrip line but imposes an upper limit on W_{slot}. Since L_{slot} is fixed at 8 mm and W_{DMS} should be no less than $W_{slot} + 2W_t$, the parameter sweep of W_{DMS} was made from 10 mm to 13 mm. Fig. 3.6(a) and 3.6(b) shows the simulated magnitudes and phases of S_{21}, respectively. According to the figures, both the IL and the phase shift decrease with W_{DMS}.

Fig. 3.7(a) and 3.7(b) depicts the effects of P on the magnitude and phase of S_{21} in both the ON- and OFF-states with P varying from 1 mm to 5 mm. In the ON-state, both the magnitude and the phase of S_{21} have little variation with the varying P. For the OFF-state, both the magnitude and the phase of S_{21} increase dramatically with P.

The effect of these parameters on the performance of the DMS unit is summarized qualitatively in Table 3.2. The variation ranges of the parameters given in the table are determined according to the dimension limitations. The symbols "$\nearrow$", "$\searrow$", and "$--$" in the table signify that the corresponding value increases, decreases, and almost remains unchanged, respectively. For example, when P increases, the OFF-state IL and also the phase shift values decrease, while in the ON-state the IL and the phase barely change. It is noted that during the parameter sweep, the OFF-state IL were always larger than those in the ON-state. The variation law of the dimensions on the performance can be explained using the varied current path lengths between the ON- and OFF-states of the RDMS unit. As shown in Fig. 3.2, there exists a current path change when the RDMS unit works in the two different states. Generally, the value of the change is proportional to the IL and the phase shift values.

A single RDMS unit with the dimension values given in Table 3.1 has an IL of 0.8 dB with a phase shift of 17° at 5.2 GHz. The width of the RDMS unit W_{DMS} is 10 mm, which results in a characteristic impedance of $Z_0 = 23\,\Omega$. Tapered microstrip lines were used as impedance transformers to connect the DMS unit to the 50 Ω system, which will be shown in the next section. The length of the slot in the RDMS unit L_{slot} is 2 mm (0.06 wavelengths at 5.2 GHz). In addition, the simulated results show that a RDMS unit has radiation losses below -50 dB in both the ON- and OFF-states. The radiation losses are included in the IL and are not shown separately for the phase shifters described in this work.

Diodes and Capacitors

There are diodes and capacitors employed in the proposed RDMS unit. The diodes are used as switches and the capacitors are used to provide RF path and to block DC current. It is concerned that they might have negative effects on the performance. Simulations have been made based on a RDMS unit with the dimension values given in Table 3.1 to investigate the effects of the employed diodes and capacitors.

Firstly, the magnitudes and phases of S_{21} are calculated assuming the RDMS unit is a pure microstrip-based device as shown in Fig. 3.2. Then, we put the diodes at the edges and recalculate the results. Subsequently, capacitors are also considered in the third calculation. Finally, all the obtained results are compared in Fig. 3.8. In these simulations, all the diodes and capacitors are modelled as described in Section 2.3.

As shown in Fig. 3.8(a), it is noticed that the diodes introduce an additional IL in

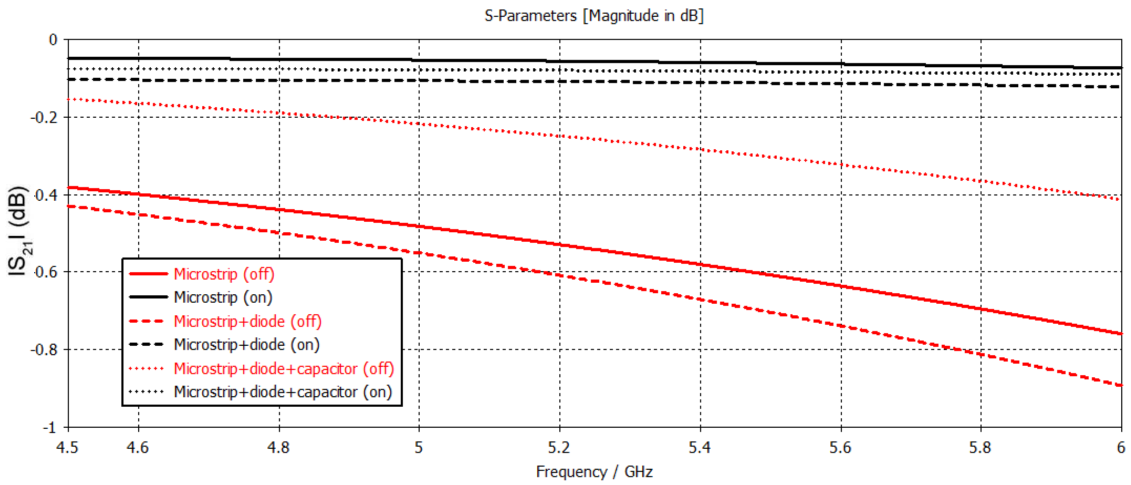

(a)

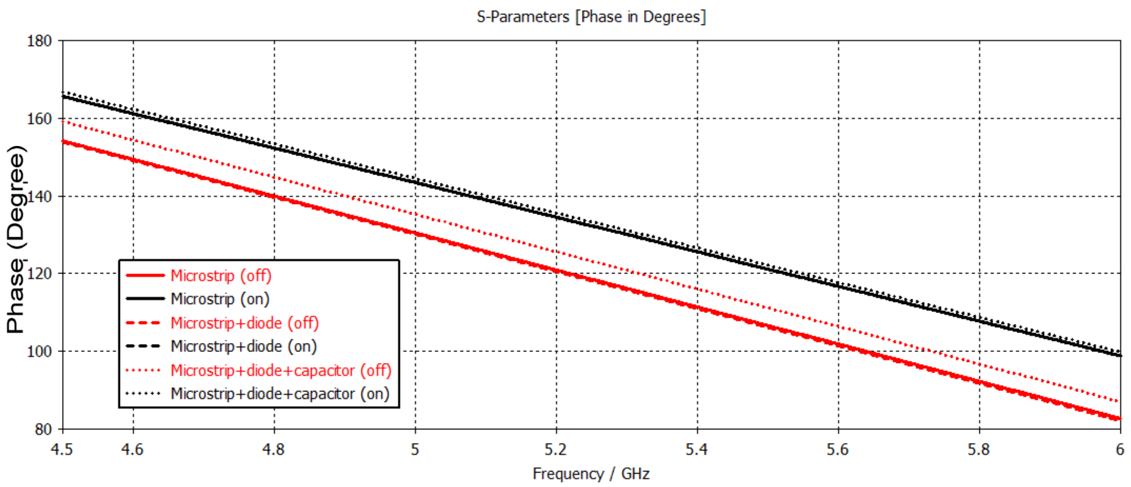

(b)

Figure 3.8: Simulated (a) magnitudes and (b) phases of S_{21} of the RDMS units with or without diodes and capacitors.

the ON-state, which is due to the small resistances of the diodes. Since the ON-state ILs are always small compared to the OFF-state ILs, the losses attributed to the diodes are acceptable. Moreover, we notice that the ON-state IL can be reduced with the presence of the capacitors. In the OFF-state, the diodes and capacitors have the same effects as that in the ON-state. According to the results shown in Fig. 3.8(b), the diodes have minor effect on the phase shift of the RDMS unit. However, the capacitors slightly decrease the phase shift value. By employing capacitors with smaller capacitances, the phase shift values can be increased with an increased IL in the OFF-state. It is summarized that the employed diodes and capacitors have minor effects on the IL, phase shift value, and bandwidth.

3.3 Cascaded RDMS Phase-Shifting Group

As described in the previous section, the phase shift produced by a single RDMS unit is 17^0. By changing the dimensions, this phase shift value can either be reduced or increased. However, a larger phase shift value is always accompanied by a larger IL. In this section, we aim to obtain greater phase shifts while maintaining low IL by cascading the RDMS units described in Chapter 3.2.

3.3.1 Mutual Coupling Analysis

As shown in Fig. 3.9, 3 RDMS units are simply cascaded with the separation distance of d. With the fixed dimension values of the RDMS units, each RDMS unit individually introduces a phase shift of 17^0 and an IL of 0.8 dB. However, when the RDMS units are put together and formed into a phase-shifting group, the IL and phase shift values are changed due to the mutual interaction between the RDMS units. The intensity of the mutual interaction depends on the separation distance d. Therefore, a parameter sweep of d is conducted to study its effects on the performance of the RDMS phase-shifting group.

Fig. 3.10(a) and 3.10(b) shows the simulated S_{21} magnitudes and phases of the RDMS group. According to the figure, the ON-state IL is very small and remains almost constant for different values of d. For the OFF-state, however, the insertion loss increases with the distance d. This loss is still comparable to the IL of a single RDMS unit, which makes

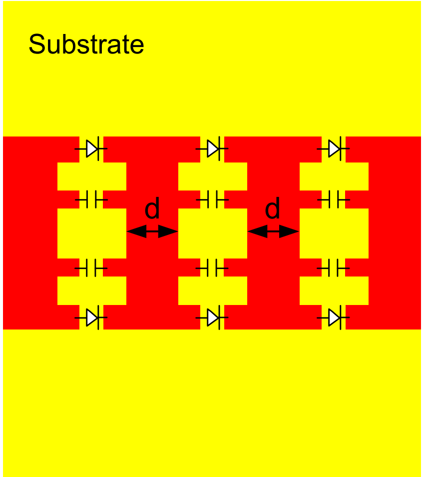

Figure 3.9: RDMS phase-shifting group consisting of 3 RDMS units.

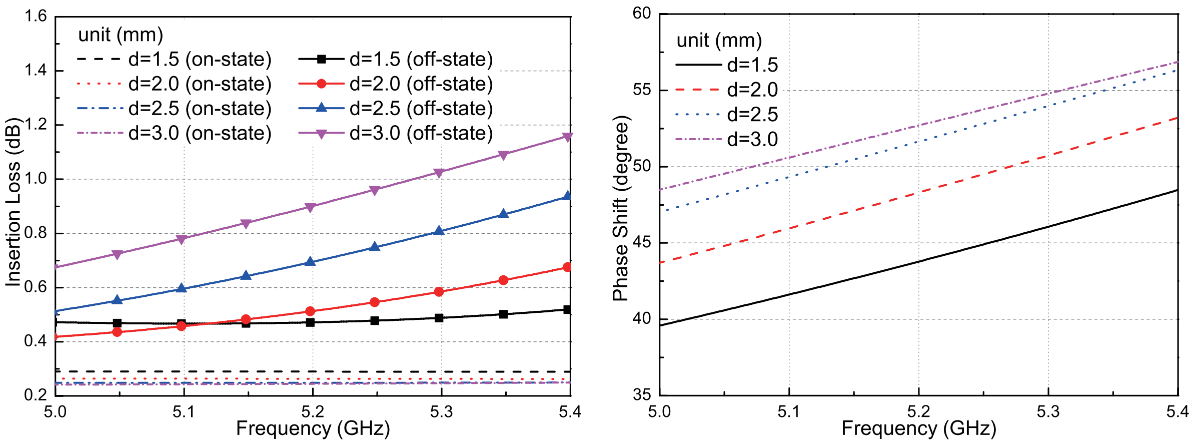

(a) (b)

Figure 3.10: Simulated S_{21} (a) magnitudes and (b) phases of the RDMS group.

phase shifters using RDMS units practical. With a 1 dB loss criteria, d should be < 3 mm. Meanwhile, the phase shift obtained by RDMS units increases with d. As the IL also increases with d, a compromise on spacing d needs to be made between the achieved phase shift value and the IL. With such considerations, d was chosen to be 2 mm in the phase shifter designs that are described in the next subsection.

3.3.2 Phase Shifter Design

In this section, phase shifters are proposed based on RDMS units. Fig. 3.11(a)-3.11(c) shows the structures of the phase shifters made by cascading three, six, and nine RDMS units, respectively. They are correspondingly defined as 3-, 6-, and 9-RDMS phase shifters. The basic structures of the three phase shifters are similar, which consist of RDMS groups, tapered microstrip lines for impedance matching, and DC biasing networks for states control. According to the previous study, a RDMS group consisting of three RDMS units has a phase shift of nearly 45^0 and an IL < 1 dB at 5.2 GHz. As shown in Fig. 3.11(a), a DC biasing network is employed to control the working states of the RDMS group. It consists of a square pad for DC source connecting, a low-pass filter composed of a surface-mount inductor ($L = 15nH$), a capacitor ($C = 6.2pF$), and a grounded via for isolation of the DC biasing voltage from the RF signal. We remark that the characteristic impedance of the RDMS is $23\,\Omega$. In order to connect the RDMS group with 50-Ω microstrip systems, tapered microstrip lines are employed. It is proved that the tapered microstrip lines are able to reduce the reflection without affecting the S_{21} phase shifts for the RDMS working in the ON- and OFF-states. In this work, the length of the tapered microstrip lines have an optimized value of $d_2 = 12\,mm$.

In the proposed designs, every RDMS group can be controlled separately by means of the DC biasing networks. With different combinations of the DC voltages applied on the pads, the phase shifters are able to work in different states with different phases. The working states of the phase shifters are summarized in Table 3.3. In fact, for the 6- and 9-RDMS phase shifters, there is more than one biasing method to realize some of the states listed in Table 3.3. For example, the Half-on state for the 6-RDMS phase shifter can be realized either by turning Group 1 on and Group 2 off, or by turning Group 2 on and Group 1 off. The phase shifter presents minor differences in performance using these alternative symmetric biasing methods. In this thesis, for the sake of clarity, only

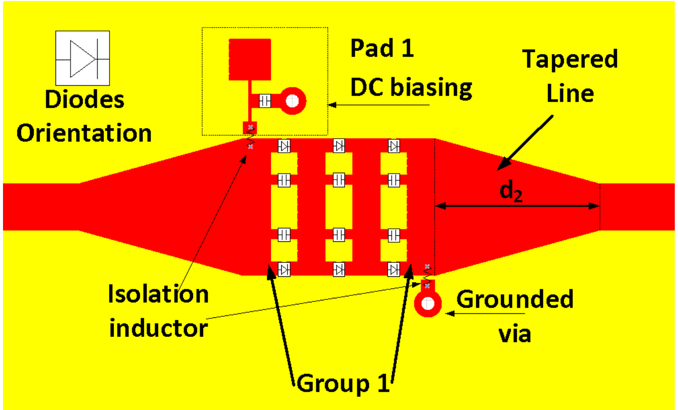

(a)

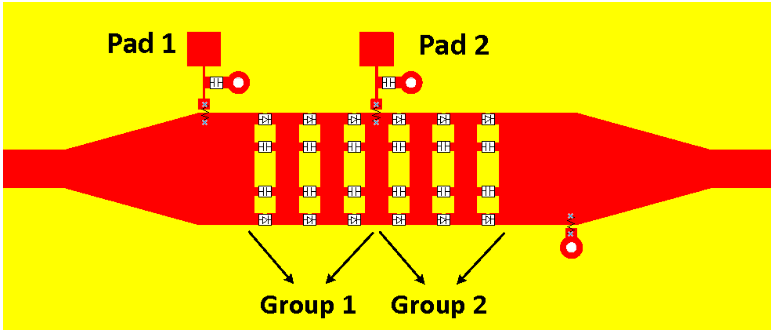

(b)

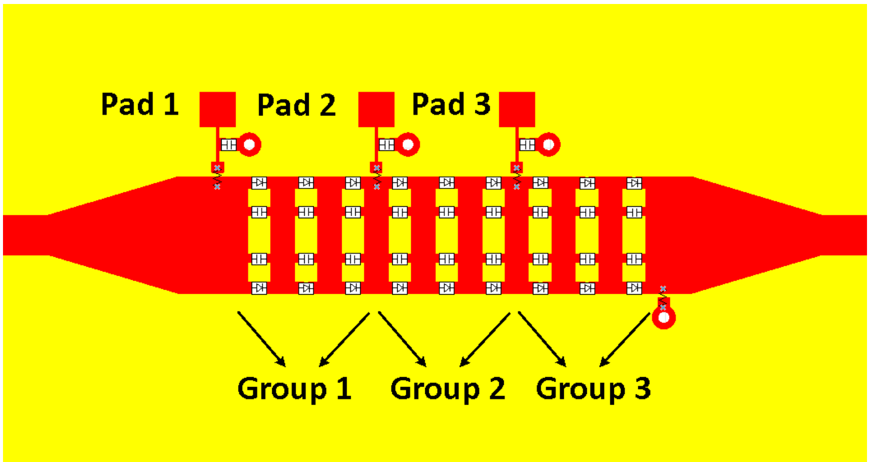

(c)

Figure 3.11: Prototypes of the (a) 3-RDMS, (b) 6-RDMS, and (c) 9-RDMS phase shifters.

Table 3.3: Definitions and descriptions of the proposed phase shifters' working states

Phase shifters	States name	Group1	Group2	Group3
3-DMS phase shifter	All-on state	on	–	–
	All-off state	off	–	–
6-DMS phase shifter	All-on state	on	on	–
	Half-on state	on	off	–
	All-off state	off	off	–
9-DMS phase shifter	All-on state	on	on	on
	6-on state	on	on	off
	3-on state	on	off	off
	All-off state	off	off	off

the results of one biasing method are given.

The 3-, 6-, and 9-RDMS phase shifters are also fabricated and measured. The fabricated phase shifters are pictured in Fig. 3.12. In order to evaluate the performance, the simulated and measured IL and phase shifts are compared and shown in Figs. 3.13 to 3.15 for each of the three phase shifters. The phase shifts shown in Figs. 3.13(b) to 3.15(b) are given by Phase(other states) - Phase(All-on state). Therefore, the results in the All-on states are not given as separate plots.

As shown in Figs. 3.13 to 3.15, the measured transmission coefficient S_{21} agrees well with the simulated results. For the 3-RDMS phase shifter, the measured IL are < 1 dB in both the All-on and All-off states at 5.2 GHz. The measured phase shift between the two states is 45°. For the 6-RDMS phase shifter, the worst case of the measured IL is 1.81 dB in the All-on state. With reference to the phase of the All-on state, measured phase

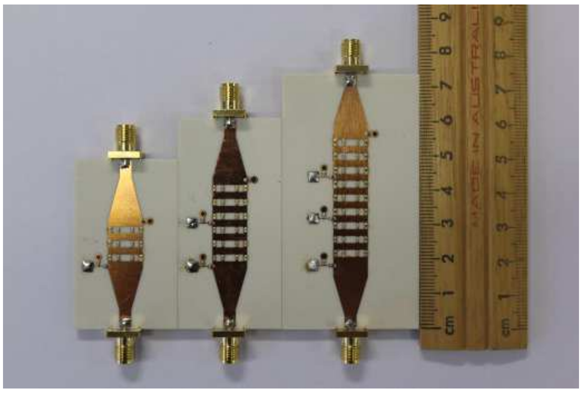

Figure 3.12: Fabricated prototypes of the 3-, 6-, and 9-RDMS phase shifters.

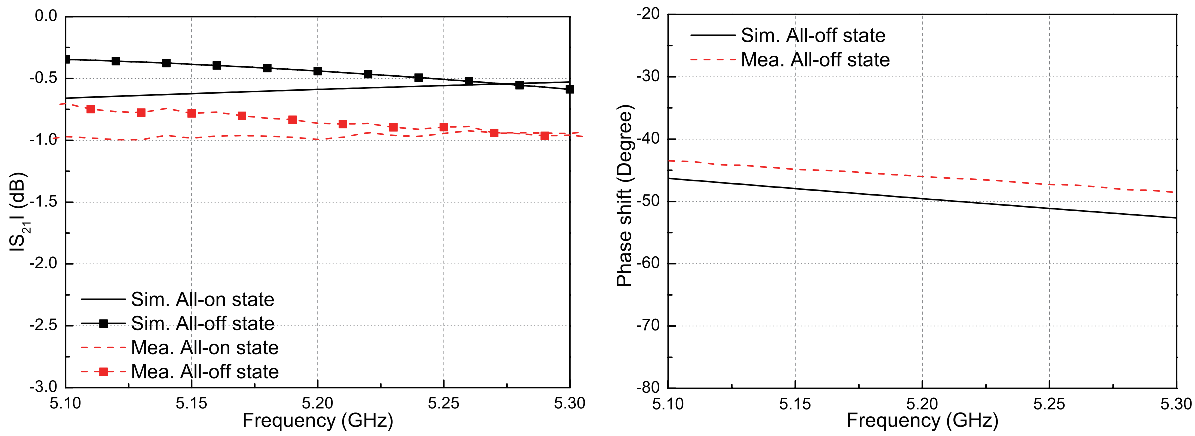

(a) (b)

Figure 3.13: Simulated and measured (a) IL and (b) phase shift of the 3-RDMS phase shifter.

shifts of 45° and 90° for the Half-on and All-off states are realized, respectively. For the 9-RDMS phase shifter, the worst case of the measured IL is 2.3 dB in the All-off state. With the All-on state phase as a reference, the measured phase shifts of the other 3 states are 44°, 95°, and 143°, respectively.

According to the results, the three phase shifters have different ranges of phase shift with a same phase step size of 45°. The experimental results agree well with the simulated ones, which validates the flexibility and practicability of the design method. Regarding the

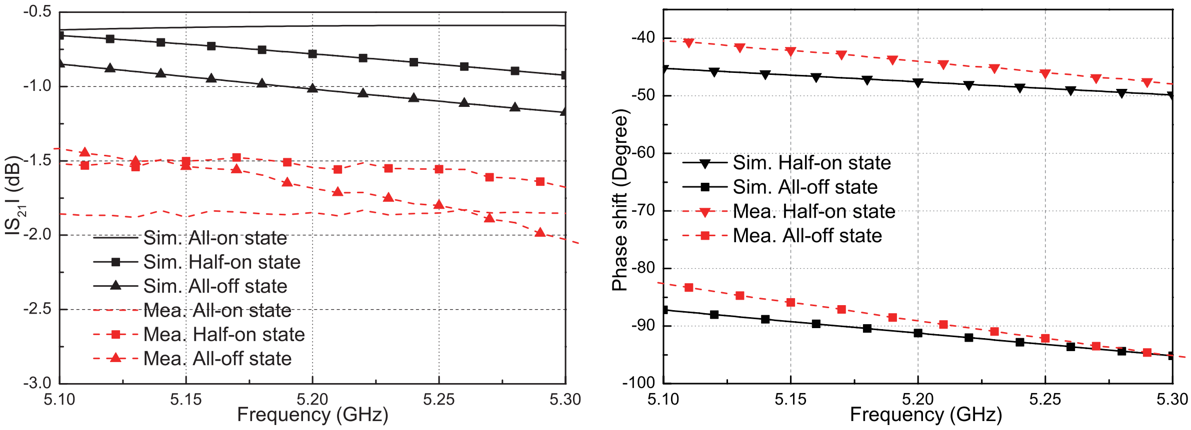

(a) (b)

Figure 3.14: Simulated and measured (a) IL and (b) phase shift of the 6-RDMS phase shifter.

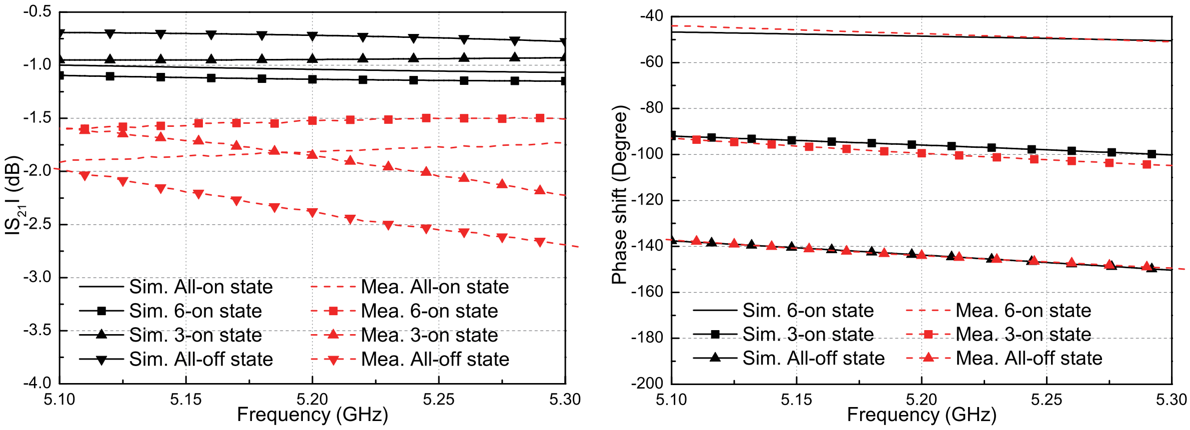

(a) (b)

Figure 3.15: Simulated and measured (a) IL and (b) phase shift of the 9-RDMS phase shifter.

IL, the measured results are larger than the simulated ones. This is due to the fabrication inaccuracies and uncertainties in the discrete component values that are obtained from the datasheet, which leads to mismatches that deteriorate the impedance matching. This could be improved by better characterizing all the models.

Compared to DGS based phase shifters [141–145], RDMS based phase shifters have a number of advantages. Firstly, the proposed phase shifter has a larger phase shifting range compared to the designs in [141–143, 145], and a lower IL than those of the designs in [142, 144]. A maximum phase shift of 143° is obtained with the present approach. Secondly, this RDMS based phase shifter is more flexible in its ability to meet various system requirements. Specifically, different ranges of phase shift can be obtained by changing the phase shift value of a single RDMS unit, the number of the cascaded RDMS units, and the distance d between the adjacent RDMS units. Also, the phase step size can be altered by changing the number of the RDMS units in a RDMS group that are controlled simultaneously. Thirdly, compared to the designs which require high voltages [142, 143], the control method of the proposed phase shifter is simpler and likely to be more reliable as only low DC voltages are required for biasing. Fourthly, the fabrication process for the RDMS phase shifter is much simpler compared to designs [142–144] employing multilayer substrates. Finally, the phase shift obtained by the RDMS phase shifter is in proportional to frequency, which indicates that the RDMS phase shifter provides true time delay. This can alleviate the beam squint problem when the phase shifters are used in phased arrays. However, the proposed phase shifter has some disadvantages, including a large number of lumped elements and a large electrical size. It is noted that the large number of lumped elements does not necessarily lead to a high fabrication cost compared to phase shifters involving microelectromechanical systems (MEMS) [142–144], especially during mass production. In addition, the quantity of the lumped elements and the size of the phase shifter can be reduced by further optimizing the structure, which will be discussed in the following chapter.

3.4 Summary

This chapter proposed a RDMS phase-shifting unit made by etching a slot on a microstrip line and loading the slot with PIN diodes and capacitors. Such a RDMS unit is able to work in two different states by altering its biasing currents to have a phase shift. The working mechanism was discussed and the relationships between the key dimension values and performance were studied. A RDMS unit with optimized dimension values considering size, IL, and phase-shifting value was obtained. It is able to provide 17^0 phase shift with 0.8 dB IL at 5.2 GHz.

Then, the RDMS group was proposed by cascading the 3 RDMS units. By tuning the separation distance between the RDMS units relating with the intensity of the mutual coupling effect, a RDMS group was realized with multiplied phase-shifting range but comparable IL. Subsequently, stepwise phase shifters were built by cascading the RDMS groups and controlling each group separately using biasing networks. The resultant stepwise phase shifters were also fabricated and measured. Comparisons were made between the measured RDMS-based phase shifters and the comparable DGS-based phase shifters, which validated the superiority of the proposed RDMS phase-shifting unit.

Chapter 4

Phase Shifter Based on MRDMS

4.1 Introduction

In the previous chapter we proposed a RDMS phase-shifting unit to design low-cost stepwise phase shifters. The RDMS unit is able to provide phase shift by tuning the working states of the employed PIN diodes. However, it was shown that the IL increased with the phase shift value. Then CRDMS group was obtained by cascading 3 RDMS units, which has a multiplied phase-shifting range but comparable IL. Stepwise phase shifters employing CRDMS groups were fabricated, measured, and compared with comparable phase shifters in the literature. It was concluded that the RDMS-based phase shifters have the advantage of low cost, low loss, simple fabrication process, and easy integration with microstrip system. However, it has the disadvantages of large electrical size and high volume of lumped elements that could affect its applications and increase the implementation cost.

In this chapter, we investigate a modified RDMS (MRDMS) unit with a compact size and a simpler structure. Based on this MRDMS unit, a complete design scheme of stepwise phase shifters consisting of three steps is presented. Each step is supported by simulations and experiments and its mechanism is explained using qualitative equations. Various phase shifters are obtained by following the proposed design scheme. Comparing the obtained phase shifters with the ones obtained in the previous chapter, significant reductions in size, cost and IL are achieved, while the phase-shifting range remains at the same level.

The rest of the chapter is organised as follows. Section 4.2 presents the structure, working mechanism, and some characteristics of the MRDSM units. Several samples of MRDMS units are also fabricated and tested. In Section 4.3, the MRDMS units are cascaded, resulting in MRDMS groups, which have multiplied phase shifts but lower IL. Insights of the performance improvement are also given in this section. Then, the MRDMS groups are used to design stepwise phase shifters in Section 4.4. Finally, this chapter is concluded in Section 4.5.

4.2 MRDMS Phase-Shifting unit

4.2.1 Structure Description

The structures of the original RDMS unit described in the previous chapter and the MRDMS in this chapter are given in Fig. 4.1(a) and 4.1(b), respectively. As shown in the figures, both of the units are built by etching a rectangular slot with a size of $W_{slot} \times L_{slot}$ on the microstrip line to introduce a defect. PIN diodes are inserted into the edges of the slot area, which enables structural reconfiguration and results in a RDMS unit. Capacitors and metal stubs used for capacitor mounting are placed in the middle of the slot to achieve RF continuity when the diodes are turned off. The dimensions $g_1 = 0.4$ mm and $g_2 = 0.7$ mm are determined by the mounting requirements of the lumped elements [126, 127]. The two units employ the same substrate Rogers4003 ($h = 1.524mm, \varepsilon = 3.55$, $\delta = 0.0027$).

It is noted that the main differences between two RDMS units shown in Fig. 4.1

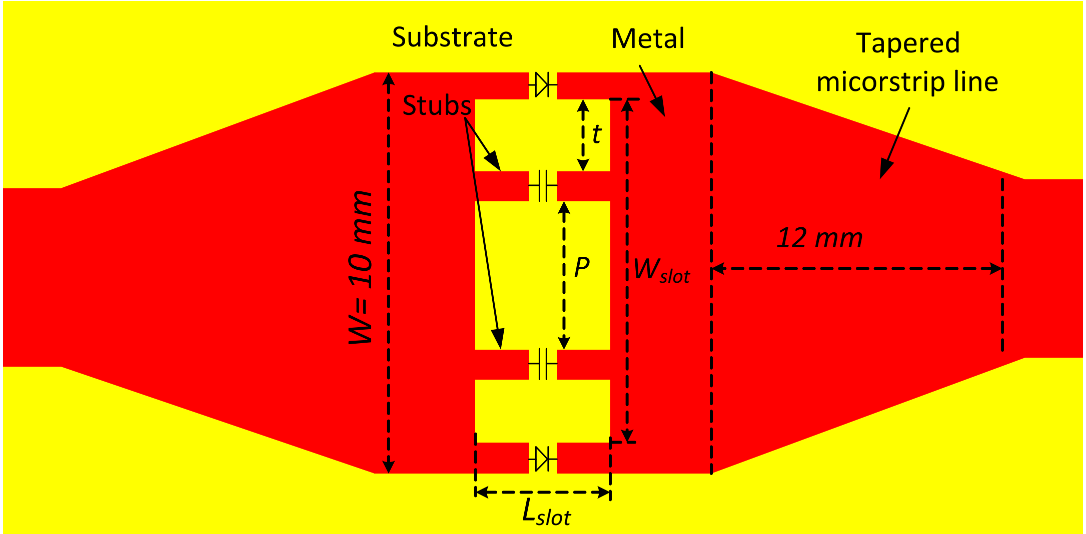

(a)

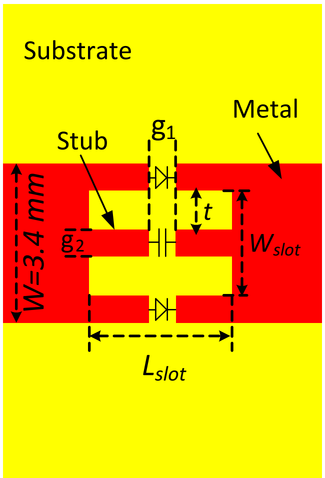

(b)

Figure 4.1: Configurations of (a) the original RDMS unit and (b) MRDMS unit.

manifested in the width of the microstrip line, the presence of the tapered microstrip lines, and the number of the stubs. We use only one pair of stubs in the MRDMS unit [Fig. 4.1(b)] rather than two pairs in the original RDMS unit [Fig. 4.1(a)], so that the width of microstrip line W can be reduced from $10\,mm$ to $3.4\,mm$. This way, the tapered microstrip lines used to connect the RDMS unit to the 50 Ω port are eliminated.

4.2.2 Working Mechanism

By comparing the MRDMS unit shown in Fig. 4.1(b) with the original RDMS unit shown in Fig. 4.1(a), it is noticed that significant size reduction has been achieved. Meanwhile, the size reduction does not lead to any performance deterioration. The phase shift and IL can remain almost the same by tuning the slot dimensions W_{slot} and L_{slot}.

1) Phase-shifting range

The phase shift is achieved by controlling the PIN diodes to obtain different current paths. By turning the diodes "on" or "off", the RDMS and MRDMS units can work in two different states, namely, the ON- and OFF-states, respectively. In the ON-state, both the diodes and capacitors allow the currents to go through them with minor losses. Numerical simulations find that the currents concentrate at the edges of the units, which is similar to that of a uniform microstrip line. In the OFF-state, the currents concentrate on the stub since the OFF-state diodes can be seen as open circuits. Therefore, phase shift is realized due to the different current path in the two states. It can be deduced that the phase shift θ is a function of $t$and L_{slot} which affects the current path and can be expressed as

$$\theta = F(t, L_{slot}). \tag{4.1}$$

Although the width of the MRDMS unit W in this paper has been significantly reduced (from $10\,mm$ to $3.4\,mm$), the value of t [$t = (W_{slot} - g_2)/2$ for the MRDMS unit] can be remain similar to that of the RDMS by tuning W_{slot}. Therefore, the width reduction does not degrade the phase shift of the MRDMS unit.

2) IL in the ON-state

The IL of the MRDMS unit is very small in the ON-state, since the unit behaves like a uniform microstrip line. It can be expressed by

$$L_u(\mathit{All\text{-}on}) = L_m + L_{dr}, \tag{4.2}$$

where L_m represents the loss of a conventional microstrip line and L_{dr} represents the sum of the diode loss and radiation loss. L_m increases with the line length and the loss tangent of the substrate. The experimental results show that a 50-mm long microstrip line made on Rogers4003 substrate has a line loss of about 0.2 dB. L_{dr} is dominated by the loss of the PIN diodes since the radiation of the MRDMS is neglectable in our working band. Considering the two parallel diodes employed in a MRDMS unit is a pair, each pair of diodes can introduce approximately 0.1 dB IL.

3) IL in the OFF-state

In the OFF-state, both the MRDMS and the RDMS units introduce noticeable reflection which results in the extra transmission degradation. Here we define the degradation caused by the reflection as $F_1 = F_1(W_{slot}, L_{slot})$. As a consequence, the IL of the phase-shifting units in the OFF-state can be expressed by

$$L_u(\textit{All-off}) = L_m + L_{dr} + F_1(W_{slot}, L_{slot}). \tag{4.3}$$

The reflection is attributed to the step in the phase-shifting units as shown in Fig. 4.2(a) and 4.2(b). The transmission line model of the RDMS and MRDMS units are given in Fig. 4.2(c).

The characteristic impedances of the defect area and the microstrip line surrounding the defect area are Z_D and Z_0, respectively. The Y_L and Z_L caused by the loads have minimum effects on the characteristic impedance. Therefore, given the dimensions of W, P, and g_2, it is calculated that $\{Z_D, Z_0\}$=$\{22\,\Omega, 45\,\Omega\}$ and $\{50\,\Omega, 106\,\Omega\}$ for the original RDMS and MRDMS units, respectively. It is noticed that due to the width reduction, the MRDMS has larger Z'_D and Z_0 compared to those of the RDMS unit. However, the normalized characteristic impedances Z_D/Z_0 for the two units are similar. Therefore, the reflection F_1 can be maintained at the same level with the same L_{slot}. This explains why the width reduction of the MRDMS unit does not increase the IL.

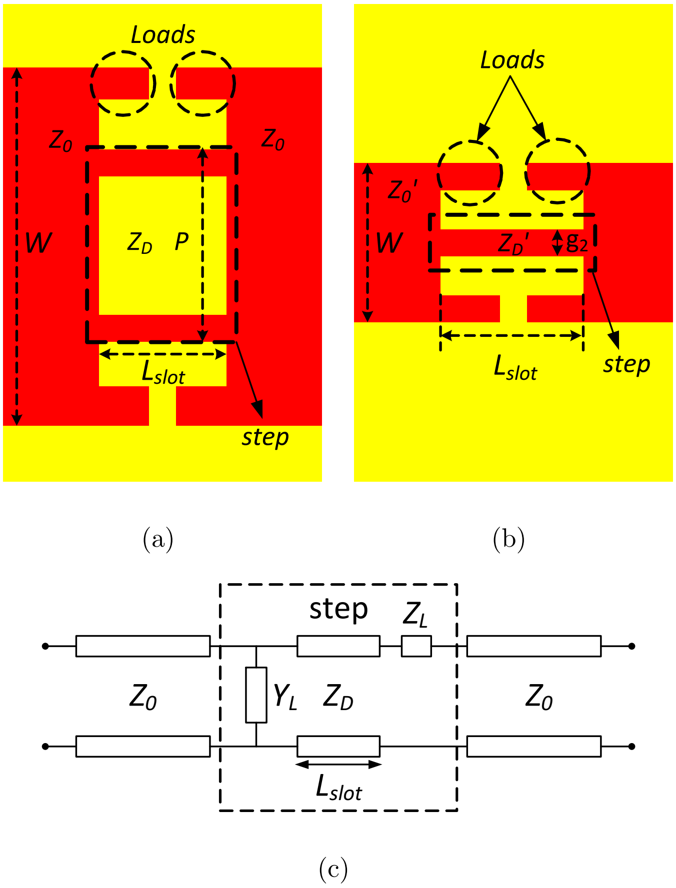

Figure 4.2: Equivalent structure of (a) the original RDMS unit and (b) the MRDMS unit in the OFF-state, and (c) their transmission line model.

4.2.3 Variation Law

It is found in equations 4.2 and 4.3 that the IL can be seen as a constant in the ON-state, and a function of W_{slot} and L_{slot} in the OFF-state, respectively. The phase shift is also a function of the slot dimensions and can be expressed by

$$\theta = F_2(W_{slot}, L_{slot}), \tag{4.4}$$

since the variable t in equation (4.1) is a linear function of W_{slot} ($W_{slot} = 2t + g_2$). To demonstrate the performance of the MRDMS unit shown in Fig. 4.1 relative to the slot dimensions, parametric studies on W_{slot} and L_{slot} are conducted using CST Microwave

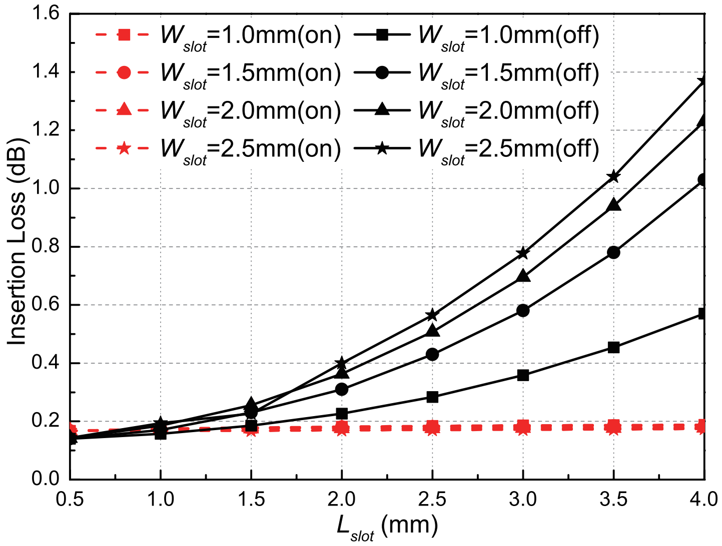

(a)

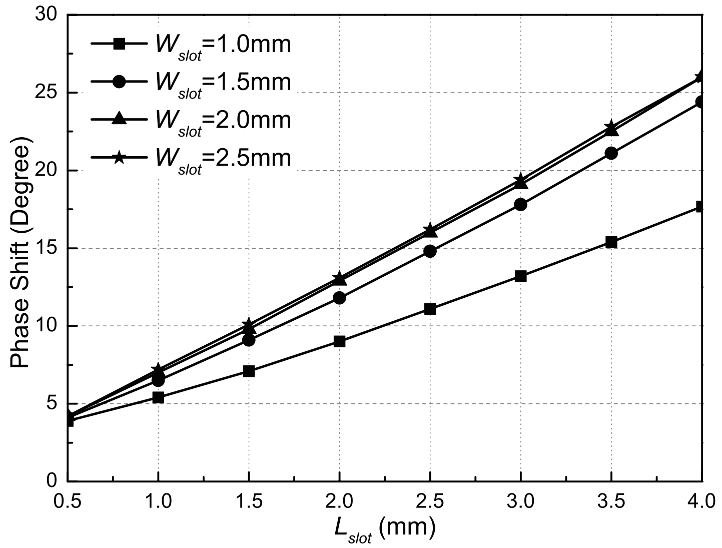

(b)

Figure 4.3: Simulated (a) IL and (b) phase shifts of the RDMS unit with different slot dimensions.

Studio [147].

Fig. 4.3(a) and 4.3(b) gives the simulated IL and phase shift of the MRDMS unit at 5.2 GHz, respectively. It is observed in Fig. 4.3(a) that the MRDMS unit in the ON-state has a low IL that remains unchanged with different W_{slot} and L_{slot}, which is expected from equation (4.2). However, the OFF-state IL increases with the slot dimensions. As shown in Fig. 4.3(b), there is a significant increase in the phase shift of the MRDMS unit by increasing W_{slot} and L_{slot}. It is concluded from these results that both the F_1 and F_2 in equations (4.1) and (4.3) are monotonic increasing functions of W_{slot} and L_{slot}. Theoretically, any phase shift value can be obtained using a single MRDMS unit. However, a higher phase shift is accompanied by a higher IL in the OFF-state.

4.2.4 Fabricated MRDMS Units

To verify the design concept, four MRDMS units have been designed with $\{W_{slot}, L_{slot}\}$ = $\{1\,mm, 1\,mm\}$, $\{2\,mm, 2.4\,mm\}$, $\{2\,mm, 3.3\,mm\}$, and $\{2\,mm, 6.2\,mm\}$ to achieve phase shifts of $\theta = 5°$, $15°$, $22.5°$, and $45°$, respectively, at 5.2 GHz. The four MRDMS units are correspondingly defined as MRDMS$_i$, where $i = 1, 2, 3$ and 4, respectively. Fig. 4.4 presents the photo of the MRDMS units and a microstrip line with the same length for comparison. It is noted that the microstrip line surrounding the MRDMS unit is only for connection and its length is immaterial. As a consequence, the effective length of the MRDMS unit is considered as L_{slot} rather than the length of the microstrip line. All the MRDMS units are fabricated on $50\,mm$ long microstrip lines for ease of measurement and comparison. It should be pointed out that the MRDMS unit working in the OFF-state does not need a bias voltage. For the MRDMS unit working in the On-state, a bias voltage of 0.9 V with the current of 40 mA is required to keep the two PIN diodes "on".

The simulated and measured IL and phase shifts of the fabricated MRDMS units are pictured in Figs. 4.5 and 4.6, respectively. The measured IL of the 50 mm long microstrip line is also presented in Fig. 4.5(a) as a reference. It is observed from Fig. 4.5(a) that the measured loss of a microstrip line $L_m \approx 0.5$ dB, which is mainly attributed to the loss on the line (about 0.3 dB) and on the two SMA connectors (about 0.2 dB). Since all the ON-state MRDMS units have similar low IL as a uniform microstrip line

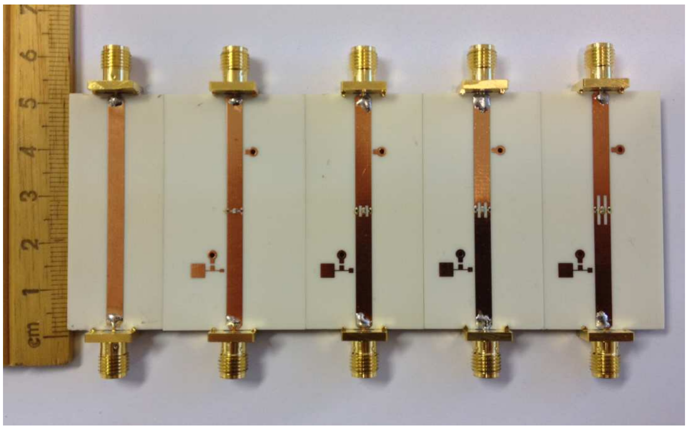

Figure 4.4: Photo of the fabricated RDMS units. They are (from left to right) the 50 mm long uniform microstrip line, $MRDMS_1$, $MRDMS_2$, $MRDMS_3$, and $MRDMS_4$ units, respectively.

(L_u*(All-on)* $= L_m + L_{dr} \approx L_m$), it is concluded that the sum of the diode loss and radiation loss $L_{dr} \ll L_m$. As shown in Fig. 4.5(b), the IL in the OFF-state increases with the slot dimensions and can be very high when a large size slot is employed for a higher phase shift, which is in accordance with Fig. 4.3. The measured OFF-state IL are 0.5, 0.7, 1.1, and 4.5 dB for the four MRDMS units, respectively. Fig. 4.6 shows that the fabricated MRDMS units can achieve phase shifts of $\theta = 6°$, 15°, 20°, and 47° at 5.2 GHz, respectively. This validates the fact that various phase shifts can be obtained by varying W_{slot} and L_{slot}.

The proposed MRDMS unit can serve as a good phase-shifting unit to obtain a phase shift $\theta \leq 15°$. However, to obtain a higher phase shift $\theta > 15°$, the MRDMS unit can introduce a remarkably high IL in the OFF-state. This can be mitigated by using the cascaded structure described in the next section.

Compared to the RDMS unit introduced in Chapter 3, the MRDMS is much smaller in size, has a lower IL, and can attain to obtaine a comparable phase shift, due to its improved configuration. Taking the $MRDMS_2$ as an example, it has a comparable performance with a size of only 40.8% of the original RDMS unit, which is illustrated in Table 4.1.

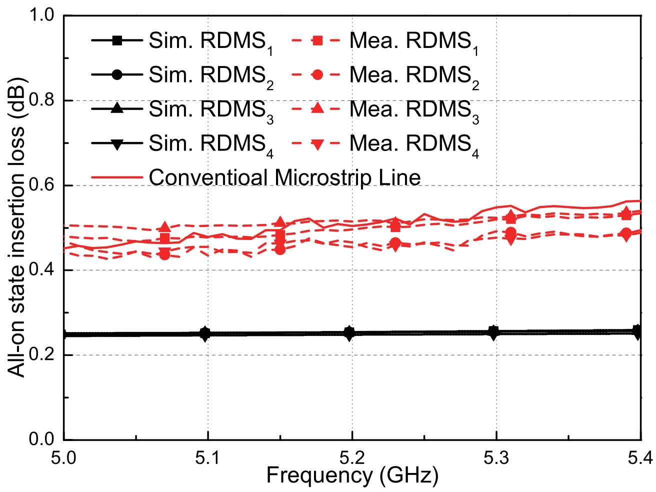

(a)

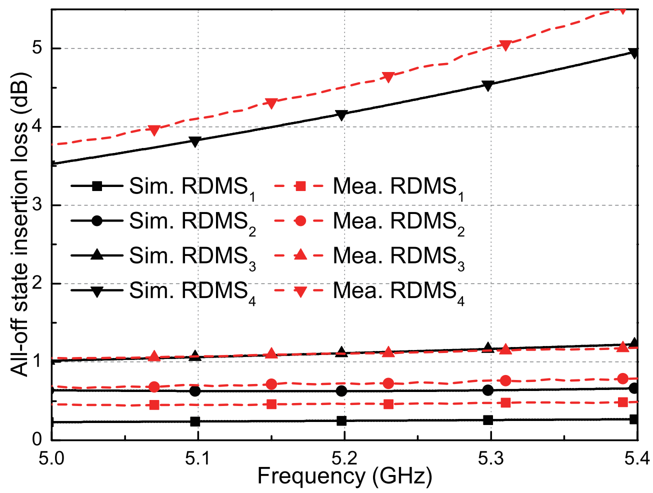

(b)

Figure 4.5: Simulated and measured (a) ON-state and (b) OFF-state IL of the fabricated MRDMS units.

4.3 Cascaded MRDMS Phase-Shifting Group

In this section, MRDMS groups are produced by cascading several MRDMS units described in the previous section. Numerical results show that the phase shift introduced by the MRDMS group of exactly $\phi = n\theta$ can be achieved, where θ and n are the phase shift of each MRDMS unit and the number of the cascaded units, respectively. Meanwhile, the

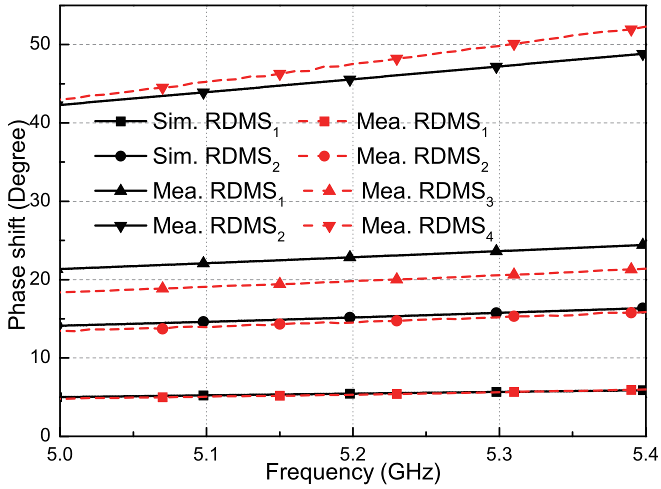

Figure 4.6: Simulated and measured phase shift of the fabricated MRDMS units.

IL is substantially reduced compared to a single MRDMS unit.

4.3.1 Cascading Analysis

To illustrate the change of the IL and phase shift when MRDMS units are cascaded, a MRDMS group consisting of two MRDMS_3 units is proposed as shown in Fig. 4.7. The two MRDMS units are separated from each other by a distance of d. Two DC voltages are used to control the two MRDMS units independently. As a result, the MRDMS group has four working states named "All-on", "On-off", "Off-on" and "All-off" states when the two MRDMS units work in the "ON, ON", "ON, OFF", "OFF, ON" and "OFF, OFF" states, respectively. It is found that the "On-off" and "Off-on" states have almost the same performance due to their symmetric structures. Therefore, we only present the results of one of them and define it as the "Half-on" state.

The performance (IL and phase shift) of a MRDMS group is not only affected by the performance of the MRDMS unit employed and the number of the MRDMS units cascaded, but also the mutual interaction between the two units, which is related to the distance d. A parameter sweep of d from 1 mm to 4 mm is conducted using CST microwave

Table 4.1: Comparison between the original RDMS and $MRDMS_2$

Parameter	original RDMS	$MRDMS_2$
Phase shift (degree)	17^0	15^0
IL (dB)	0.8	0.6
Width (W) (mm)	10	3.4
Length (L_{slot}) (mm)	2	2.4
Area ($W \times L_{slot}$) (mm^2)	20	8.16
Normalized Area	1	0.4

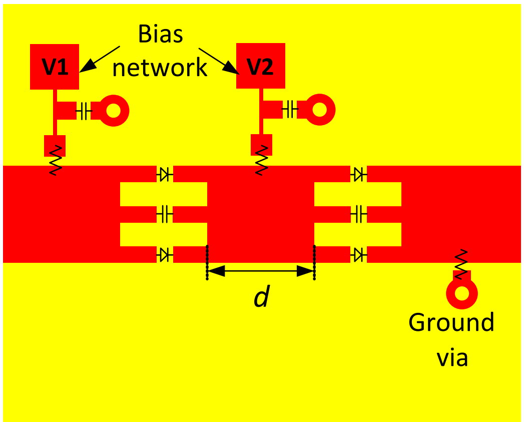

Figure 4.7: Structure of the cascaded MRDMS units

studio to study the relationships between the mutual interaction and the performance of the MRDMS group. Larger distance d > 4 mm are not considered since this will increase the size of the phase shifter too much.

Fig. 4.8(a) and 4.8(b) shows the computed IL and phase shifts of the MRDMS group, respectively, with different d. As shown in Fig. 4.8(a), the IL in the All-on and Half-on states are independent of d. This is due to the fact that a MRDMS unit in the All-on state can be simply seen as a uniform microstrip line. Consequently, one of the employed

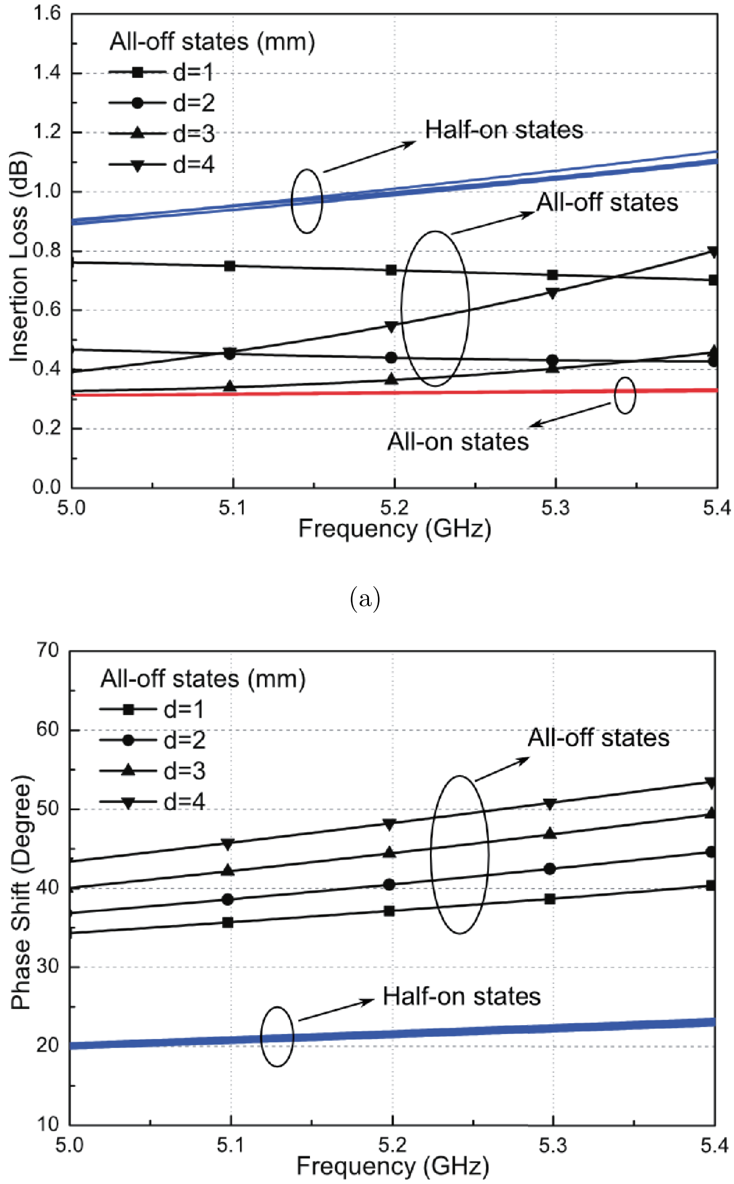

(a)

(b)

Figure 4.8: Parameter sweep results of the (a) IL and (b) phase shifts of the MRDMS group.

All-on state MRDMS units in the group can be replaced by a segment of microstrip line, thus the MRDMS group in the All-on and Half-on states are equivalent to one MRDMS unit working in the All-on and All-off states, respectively. Therefore, the IL in these two states can be expressed by

$$L_g\,\textit{(All-on)} = L_m + 2L_{dr}, \tag{4.5}$$

$$L_g\,\textit{(Half-on)} = L_m + 2L_{dr} + F_1(W_{slot}, L_{slot}), \tag{4.6}$$

respectively. For the MRDMS group in the All-off state, the insertion loss changes with d and is always smaller than that in the Half-on state. In other words, compared to that of a single MRDMS unit, the All-off state IL is reduced when two MRDMS units are cascaded. This is due to the fact that when the MRDMS units are connected by a segment of uniform microstrip line, the input impedance of the MRDMS group is changed to be closer to that of the input/output port (50 Ω), resulting in less reflection. Consequently, the All-off state IL is given as

$$L_g\,\textit{(All-off)} = L_m + 2L_{dr} + F_1(W_{slot}, L_{slot}) - M_1(d), \tag{4.7}$$

where $M_1(d) > 0$ represents the reduction in the IL due to the canceled reflection.

The phase shift of the MRDMS group in the Half-on state shown in Fig. 4.8(b) is independent of d and is equal to that of a single MRDMS unit in the All-off state shown in Fig. 4.3(b). This is expected and can be attributed to the same reason that we used to explain the IL. With the All-on state phase as a reference, the phase shift in the Half-on state can be expressed as

$$\phi\ \textit{(Half-on)} = F_2(W_{slot}, L_{slot}) = \theta. \tag{4.8}$$

In the All-off state, the phase shift of the MRDMS group is doubled since the current path change is doubled compared to that of a single MRDMS unit. In addition, as observed in Fig. 4.8(b), the phase shift is also affected by the reflection change. Therefore, the phase shift can be expressed by

$$\phi\ \textit{(All-off)} = 2F_2(W_{slot}, L_{slot}) + M_2(d), \tag{4.9}$$

where $M_2(d)$ is the phase variation with respect to the reflection change and can be either positive or negative with different d. For a specific MRDMS group, we can always find a d to satisfy

$$| M_2(d) | = minimum, \tag{4.10}$$

and

$$M_1(d) > 0, \tag{4.11}$$

thereby the MRDMS group can have an exactly doubled phase shift of $\phi = 2\theta$ and a smaller IL $L_g(\textit{All-off}) < L_u(\textit{All-off})$ concurrently, compared to those of the employed MRDMS unit.

As shown in Fig. 4.8(a), it is noted that the IL in the Half-on state is obviously larger than those in the All-on and All-off states. As a consequence, we choose to bias the two MRDMS units simultaneously rather than control them separately. This way, only one bias network is required and the MRDMS group works in two discrete states, the All-on and All-off states.

Moreover, we could also cascade more than two MRDMS units to produce a MRDMS group. The equations (4.5), (4.7), and (4.9) presenting the insertion losses and phase shift of a MRDMS group cascading 2 RDMS units can also be applied to a MRDMS group cascading n MRDMS units. The expressions of the IL and phase shift can be written as

$$L_g(\textit{All-on}) = L_m + nL_{dr}, \tag{4.12}$$

$$L_g(\textit{All-off}) = L_m + nL_{dr} + F_1(W_{slot}, L_{slot}) - M_1(n, d), \tag{4.13}$$

$$\phi = n\theta + M_2(n, d), \tag{4.14}$$

where $F_1(W_{slot}, L_{slot}) - M_1(n, d)$ in (4.13) and $M_2(n, d)$ in (4.14) could be very small with an optimized d.

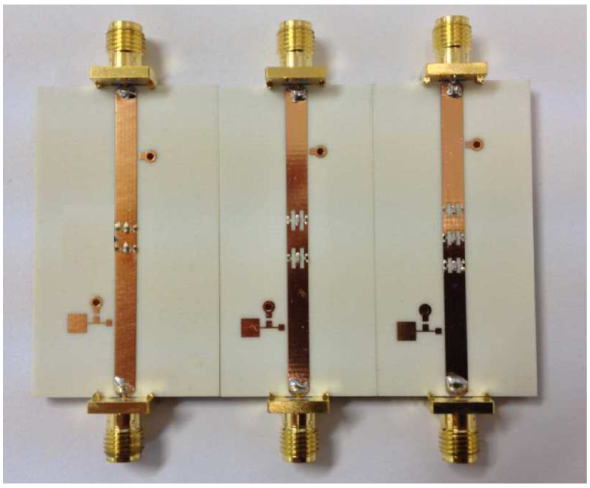

Figure 4.9: Photo of the fabricated ^{2}RDMS$_1$, ^{2}RDMS$_3$, and ^{3}RDMS$_2$ groups (from left to right).

4.3.2 Fabricated MRDMS groups

For simplicity, a MRDMS group cascading n MRDMS$_i$ units is defined as ^{n}MRDMS$_i$ group, where i represents the serial number of the MRDMS unit proposed in the previous section, and n is the quantity of the cascaded MRDMS units. Two MRDMS groups ^{2}MRDMS$_1$ and ^{2}MRDMS$_3$ are designed with $d = 2\,mm$ and $2.8\,mm$ to obtain phase shifts of $\phi = 2\theta_1$ and $2\theta_3$, respectively, where θ_i is the phase shift of the MRDMS$_i$ unit. Also, a MRDMS group ^{3}MRDMS$_2$ is designed with $d = 2.4\,mm$ to achieve a phase shift of $\phi = 3\theta_2$. The fabricated MRDMS groups are pictured in Fig. 4.9. To bias a MRDMS group cascading n MRDMS units, the required DC voltage and current are $n \times 0.9V$ and 40 mA, respectively.

Figs. 4.10 to 4.12 present the simulated and measured results of the ^{2}MRDMS$_1$, ^{2}MRDMS$_3$, and ^{3}MRDMS$_2$ groups, respectively. It is seen that the measured results agree well with the simulated ones. As shown in the figures, the IL for these MRDMS groups are all $<$ 1 dB in both of the two states. Regarding the phase shift, the measured results shown in Figs. 4.10 and 4.11 demonstrate that the ^{2}MRDMS$_1$ and ^{2}MRDMS$_3$

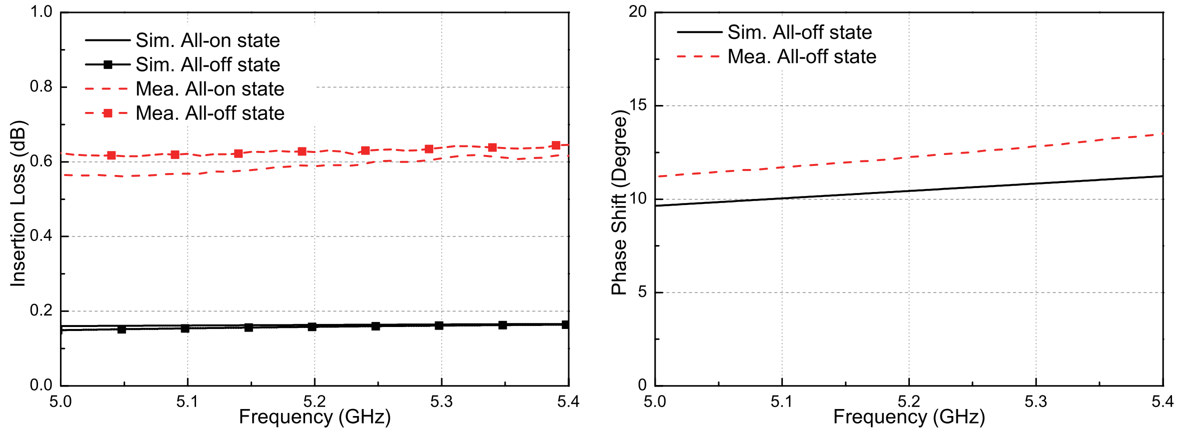

(a) (b)

Figure 4.10: Simulated and measured (a) IL and (b) phase shifts of the ^{2}MRDMS$_1$ group.

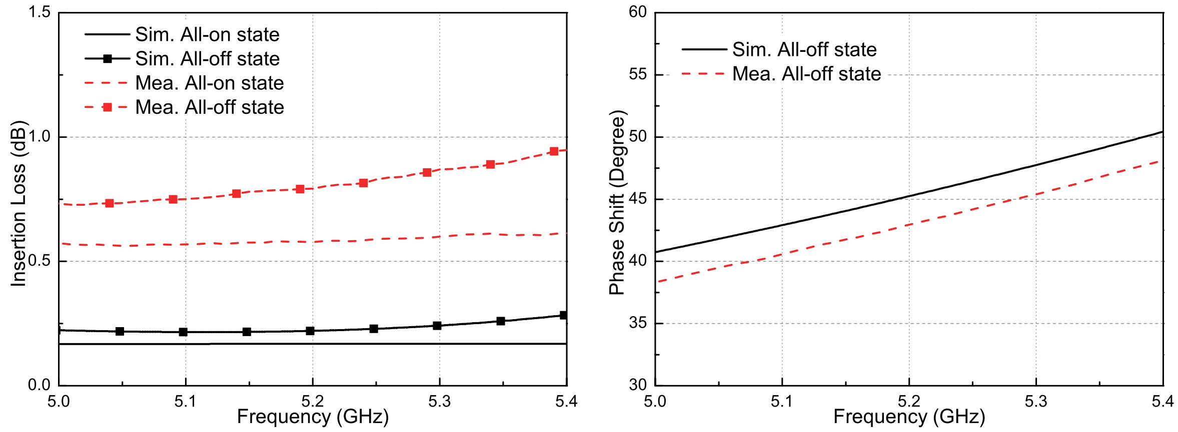

(a) (b)

Figure 4.11: Simulated and measured (a) IL and (b) phase shifts of the ^{2}MRDMS$_3$ group.

groups can realize phase shifts of $\phi = 12°$ and $43°$, respectively, which are two times of those realized by the MRDMS$_1$ ($\theta = 6°$) and MRDMS$_3$ ($\theta = 20°$) units. It is observed in Fig. 4.12 that the phase shift achieved by the ^{3}MRDMS$_2$ group is $\phi = 45°$, which is exactly three times that of the MRDMS$_2$ unit $\theta = 15°$.

It is concluded from the measured results that a ^{n}MRDMS$_i$ group can achieve a phase

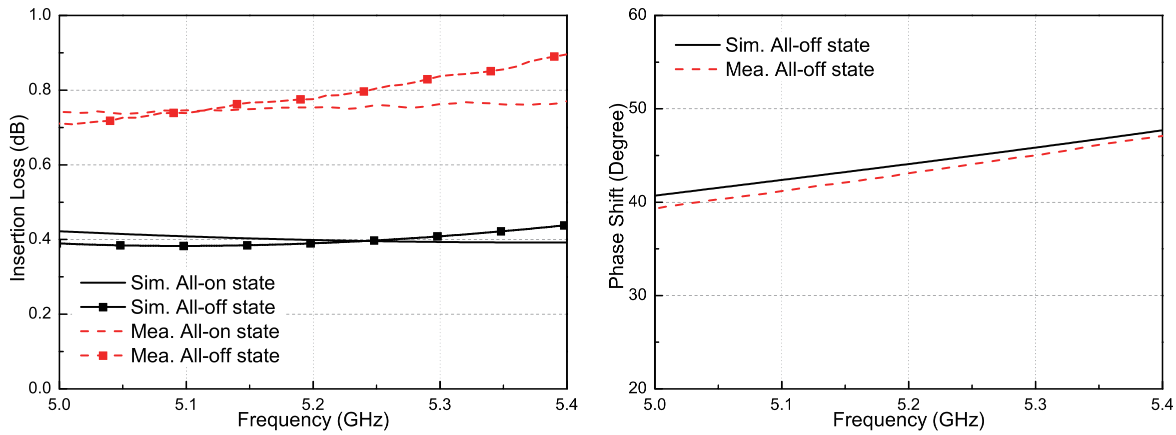

(a) (b)

Figure 4.12: Simulated and measured (a) IL and (b) phase shifts of the ^{3}MRDMS$_2$ group.

shift of $\phi = n\theta_i$ with low IL, where θ_i is the phase shift of a MRDMS$_i$ unit. Compared to the MRDMS unit, the MRDMS group proves to be a better phase shift unit to obtain a phase shift $\phi > 15°$. For example, to realize a phase shift of 45°, the IL of a MRDMS unit is 4.5 dB while that of a MRDMS group is < 0.8 dB.

4.4 Stepwise Phase Shifter

4.4.1 Design and measurement

Stepwise phase shifters can be obtained by cascading m MRDMS groups and employing more bias networks, where m is a positive integer. This way, a total phase shift of $m\phi$ with a step of ϕ can be realized, where ϕ is the phase shift of a MRDMS group. In order to verify the design scheme, three stepwise phase shifters are designed, fabricated, and tested. The first one is made by cascading two ^{2}MRDMS$_3$ groups with two bias networks. The second employs two ^{3}MRDMS$_2$ groups with two bias networks. Both of these phase shifters are designed to have a maximum phase shift of 90° with a step of 45°. The third

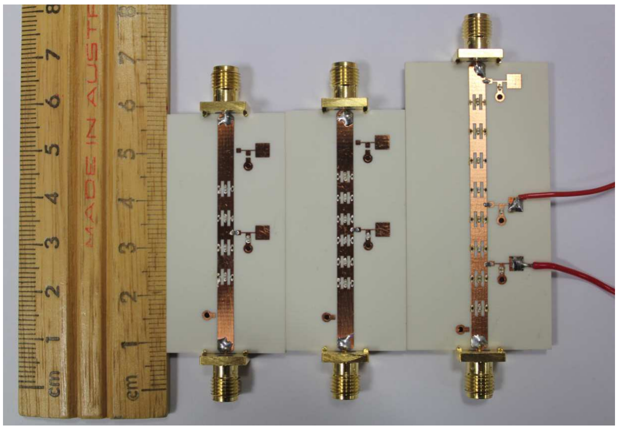

Figure 4.13: Photo of the fabricated stepwise phase shifters. They are the 4-, 6-, and 8-MRDMS phase shifters from left to right, respectively.

phase shifter is made by cascading four ^{2}MRDMS$_3$ groups to obtain a phase shift of 180°. The three phase shifters are named 4-, 6-, and 8-MRDMS phase shifters, respectively. The photo of the fabricated phase shifters are given in Fig. 4.13.

As shown in Fig. 4.13, the stepwise phase shifters have employed 2 bias pads for the 4- and 6-MRDMS phase shifters and 3 bias pads for the 8-MRDMS phase shifters. The bias pads are named Pads 1, 2, and 3, from top to bottom. By manipulating the DC voltages on the bias pads, the stepwise phase shifters are able to work in different states. The 4- and 6-MRDMS phase shifters have three states while the 8-MRDMS phase shifter has five states in terms of phase shift they achieve. The working states, bias voltages, and the ideal phases of the phase shifters are summarized in Table 4.2. The required bias current is always 40 mA since the MRDMS units are connected in series. It should be pointed out that not all the bias pads are connected to a DC source for a certain state. For example, for the All-on state of the 4-MRDMS phase shifter, bias pad 2 is not used and marked as "−−" in the table. In addition, for some states of the phase shifters, there is more than one bias method to realize the same phase shift with a similar IL. In this paper, only one way is presented in Table 4.2 for the sake of brevity.

Figs. 4.14 to 4.16 show the simulated and measured IL and phase shift of the 4-, 6-,

Table 4.2: Bias method of the stepwise phase shifters and their ideal relative phases of S_{21} in different states.

Phase shifters	Pad 1	Pad 2	Pad 3	States name	Ideal phase
4-MRDMS phase shifter	3.6 V	−−	N/A	All-on	0°
	G	1.8 V	N/A	Half-on	−45°
	−−	−−	N/A	All-off	−90°
6-MRDMS phase shifter	5.4 V	−−	N/A	All-on	0°
	G	2.7 V	N/A	Half-on	−45°
	−−	−−	N/A	All-off	−90°
8-MRDMS phase shifter	7.2 V	−−	−−	All-on	0°
	5.4 V	−−	G	3-on	−45°
	3.6 V	G	−−	Half-on	−90°
	−−	−−	1.8 V	1-on	−135°
	−−	−−	−−	All-off	−180°

and 8-MRDMS phase shifters in all the states listed in Table 4.2. It is observed in Fig. 4.14 that phase shifts of 0°, 44°, and 88° are obtained by the 4-MRDMS phase shifter in the All-on, Half-on, and All-off states, respectively, at 5.2 GHz. The measured IL in all the three states are $<$ 1.3 dB. The 6-MRDMS phase shifter introduces phase shifts of 0°, 44°, and 87° in the All-on, Half-on, and All-off states, respectively, as shown in Fig. 4.15. The IL in all the three states are $<$ 1.2 dB. As shown in Fig. 4.16, measured phase shifts of 0°, 45°, 92°, 138°, and 184° are realized by the 8-MRDMS phase shifter. The IL in all the 5 states are $<$ 2 dB at 5.2 GHz.

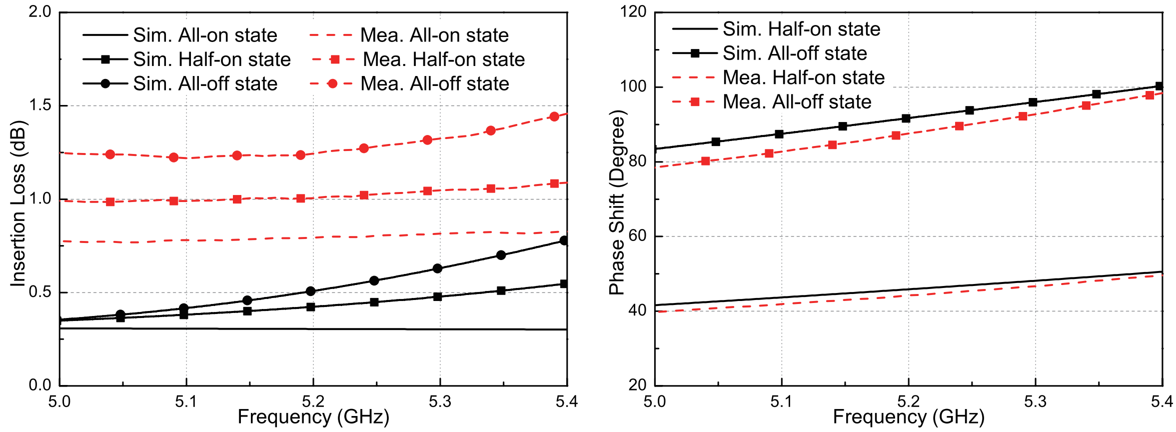

(a) (b)

Figure 4.14: Simulated and measured (a) IL and (b) phase shifts of the 4-MRDMS phase shifter.

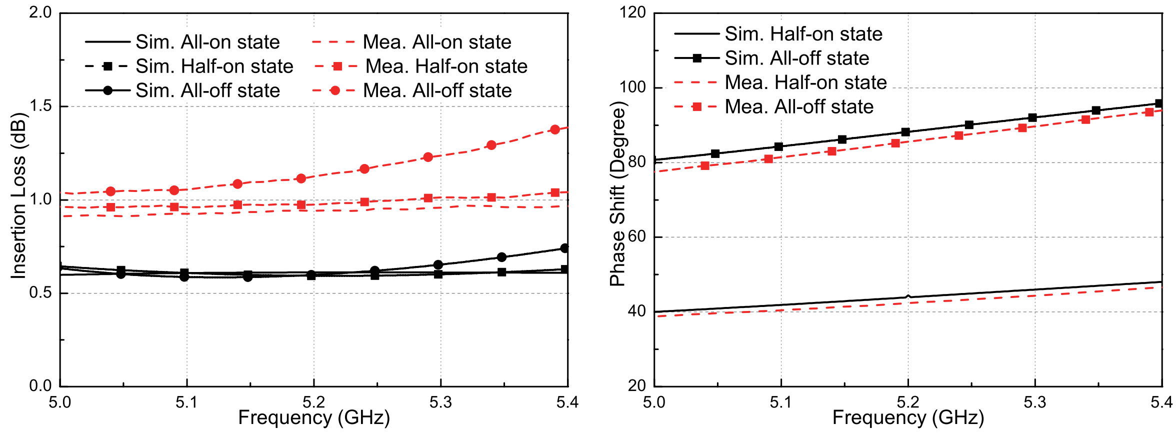

(a) (b)

Figure 4.15: Simulated and measured (a) IL and (b) phase shifts of the 6-MRDMS phase shifter.

4.4.2 Summarized design scheme of the stepwise phase shifter

Sections II – IV have described a complete design scheme of the stepwise phase shifter using the proposed MRDMS units. To obtain a stepwise phase shifter with a step size of ϕ and a total phase-shifting range of $m\phi$ (where m is a positive integer), three steps are

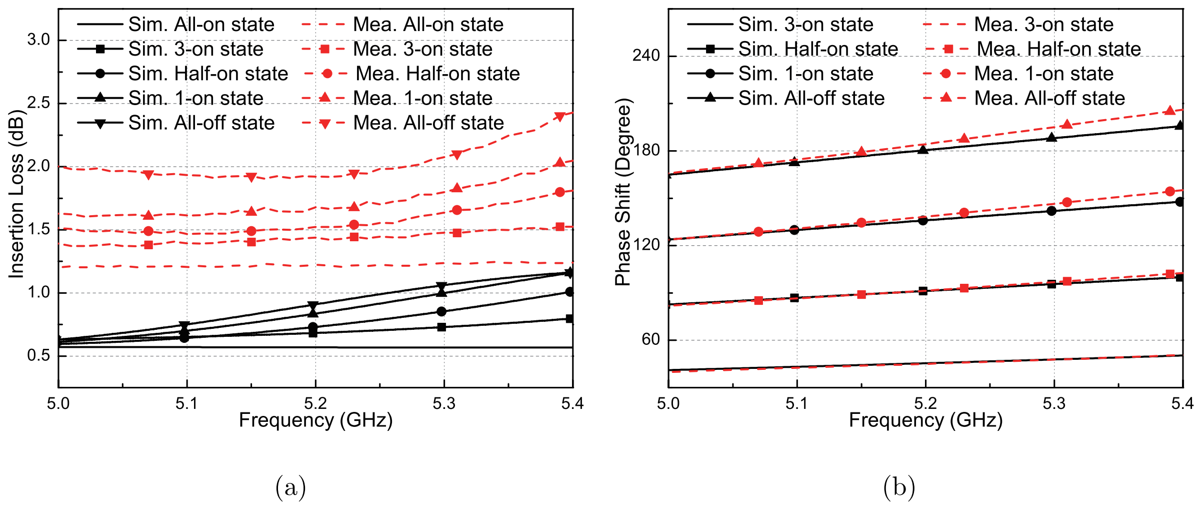

Figure 4.16: Simulated and measured (a) IL and (b) phase shifts of the 8-MRDMS phase shifter.

required. The first step is to optimize the dimensions of a single MRDMS unit to obtain a phase shift of $\theta = \phi/n$ (where n is also a positive integer) at the design frequency. The second step is to obtain a MRDMS group with a phase shift of ϕ by cascading n MRDMS units and optimizing the separation distance. The last step is to cascade m MRDMS groups and control each group separately using additional bias networks.

More specifically, some guidelines are described below to choose the value of n in the second step depending on the step size ϕ.

1) Case 1 ($n = 1$): To obtain a step size $\phi \leq 15°$, a single MRDMS unit should be used to realize the step. This is due to the fact that it has the smallest size while the IL are also small as observed in Fig. 4.5. If using a MRDMS group cascading n MRDMS units ($n > 1$) to realize such a phase shift, the reduction in IL would be negligible, while the size is noticeably increased.

2) Case 2 ($n = 2$): For the step size $15 < \phi \leq 50°$, a MRDMS group cascading 2 MRDMS units is the best option, due to the fact that the IL can be fairly high using a single MRDMS unit to realize such a phase shift. For example, the measured IL of the

$MRDMS_4$ unit is 4.5 dB with a 45° phase shift. Actually, a similar small IL can also be obtained using MRDMS groups cascading more than 2 MRDMS units, but this would increase the size.

3) Case 3 ($n > 2$): To obtain higher step size $\phi > 50°$, a MRDMS group cascading n ($n > 2$) MRDMS units is required. However, it should be borne in mind that the size of the MRDMS group increases with n. Therefore, if the size rather than the IL is the main concern, a smaller n is preferred.

4.4.3 Discussion

The significant improvements to the RDMS phase shifters demonstrated in Chapter 3 show that the MRDMS not only inherents all the advantages of the RDMS, but they possess other noticeable merits as follows. Firstly, the size of the phase shifter has been significantly reduced without affecting the phase shift. Compared with the original phase shifters that can achieve phase shifts of 45° and 90°, the sizes of the new phase shifters in this paper have been reduced to only 10.6% and 17.5%, respectively, with unchanged phase shifts. The significant size reduction is due to the smaller size of the proposed MRDMS unit and the elimination of the impedance matching part. Secondly, the quantity of the lumped elements employed in the new phase shifters is only half of the number of those employed in the original models. This can be attributed to the new configuration that reduces the number of the capacitors used in a MRDMS unit and the quantity of the MRDMS units in a MRDMS group. Thirdly, the new phase shifters have lower IL. The loss reduction is result of the smaller quantity of lumped elements and a lower dielectric loss due to the smaller size. In addition, unlike the original models, the new phase shifters do not need tapered microstrip lines for impedance matching when connected to a 50-Ω microstrip system, which leads to smaller losses.

4.5 Summary

This chapter introduced the improved MRDMS phase-shifting unit which inherited all the advantages of the RDMS unit described in Chapter 3, but with significantly reduced size and cost. Firstly, the structure of the MRDMS unit was introduced and compared with that of the RDMS unit. Working mechanisms were discussed, which also explained the fact that the reduced size did not degrade performance. Then, by cascading the MRDMS units, the MRDMS groups were obtained which are actually controllable slow-wave structures. Better performance was achieved and an explanation of this achievement was given. Subsequently, by cascading such RDMS groups, stepwise phase shifters with different phase-shifting ranges were obtained. Several samples of the MRDMS units, MRDMS groups, and phase shifters were fabricated and tested. The tested results agreed well with the simulated results, which validated the design concept. Finally, the complete design scheme was summarized and can be used as a guidance to design this type of phase shifter.

Chapter 5

Phased Array Antennas

5.1 Introduction

Phased array antennas can achieve analogue beamforming with high gains and are extensively utilized in satellite communications, radar systems, and other military applications. However, there are not many consumer applications of phased arrays so far. This is because they can be quite expensive, due to the need for many microwave phase shifters and their control signals. In this thesis, a novel type of phase shifter is proposed for phased array antennas. The phase shifters have a simple structure, low loss, low cost, simple control method, and are easy to integrate with microstirp systems, which can significantly reduce the cost of a phased array. Moreover, the proposed phase shifters are true time-delay devices, which can help to reduce beam squint in a phased array. In this Chapter, we firstly use the RDMS phase-shifting unit in the array design and then its updated version, the MRDMS unit is advocated for its smaller profile.

This chapter demonstrates two examples of the proposed phase shifters' applications in phased array antennas. In a primary implementation, a 4-element linear array is designed. Firstly, the RDMS-based phase shifters are employed in the feed network, providing required phase shifts for the array to steer its beam to different directions. Then, the RDMS-based phase shifters are replaced by the MRDMS-based phase shifters, which significantly reduces the size and cost of the phased array while maintaining the same performance. Both the phased arrays employing the RDMS- and MRDMS-based phase shifters are fabricated and tested to validate the practicability of the phase shifters in arrays.

Another example is a reconfigurable partially reflective surface (PRS) antenna fed by a two-element phased array. The antenna consists of two main parts, a phased array antenna as the exciter and a reconfigurable PRS. The RDMS-based phase shifters are employed in the phased array antenna exciter to steer the beam. The antenna with the reconfigurable PRS can only steer its beam from $-5°$ to $5°$ if fed by a patch antenna with fixed beam. By replacing the sole patch radiator with the 2-element phased array as the source, the beam steering range can be substantially increased.

This chapter is organized as follows. Section 5.2 presents the work of the 4-element phased array employing the MRDS-based phase shifters. Then the RDMS-based phase shifters are replaced by the MRDMS-based phase shifter in Section 5.3, resulting in a more cost effective phased array. The reconfigurable PRS antenna employing MRDSM-based phase shifter is proposed in Section 5.4. Finally, Section 5.5 concludes this chapter.

5.2 Phased Array Antenna Employing RDMS

A 4-element patch antenna array was designed for beam steering based on the RDMS phase shifters described in Chapter 3. The feed network of the phased array consists of three Wilkinson power dividers [148], two 6-RDMS phase shifters, and four 3-RDMS phase shifters. The phase shifters in the array allow phase delays or advances to be introduced between different antenna elements. By controlling the working states of the phase shifters to manipulate the phases of the array elements, the beam switching of the antenna array between different directions can be realized. In this section, the feed networks are described where 3- and 6-RDMS phase shifters are connected to the power dividers. Then by connecting these feed networks to 4 patch antennas, a steerable 4-element patch antenna array is formed. Simulated and measured results of the feed networks and the antenna array are also presented in this section.

5.2.1 Corporate Feed Network

Figs. 5.1(a) and 5.1(b) show the structures of the feed networks consisting of a power divider with two 3-RDMS phase shifters and two 6-RDMS phase shifters, respectively. In this paper, to differentiate them, they are identified as the 3-RDMS power divider and the 6-RDMS power divider, respectively. For each power divider, two RDMS phase shifters that were described in Chapter 3 (3- or 6-RDMS phase shifter) are connected to the two ports of a Wilkinson power divider. By controlling the DC biasing voltages, the two phase shifters can work in different states, which results in different phase shifts between Ports 2 and 3. The 3-RDMS power divider has four operating states: All-on, All-off, Left-on-right-off, and Left-off-right-on states. For the sake of future discussion, these four states are labelled as States 1, 2, 3, and 4. When the divider network works in these four states, the phase shifters on the left- and right-hand sides are correspondingly both turned on, both turned off, left turned on right turned off, and left turned off right turned on. The 6-RDMS power divider has the same states as the 3-RDMS power divider.

The simulated and measured results of the 3- and 6-RDMS power dividers are shown in Figs. 5.2 and 5.3, respectively. Figs. 5.2(a) and 5.3(a) give the IL of States 1 and 2 for the 3- and 6-RDMS power divider, respectively. Figs. 5.2(b) and 5.3(b) show the IL of States 3 and 4 for the 3- and 6-RDMS power divider, respectively. The power dividers have two branches where each branch has an IL. Ideally, the IL of the two branches are

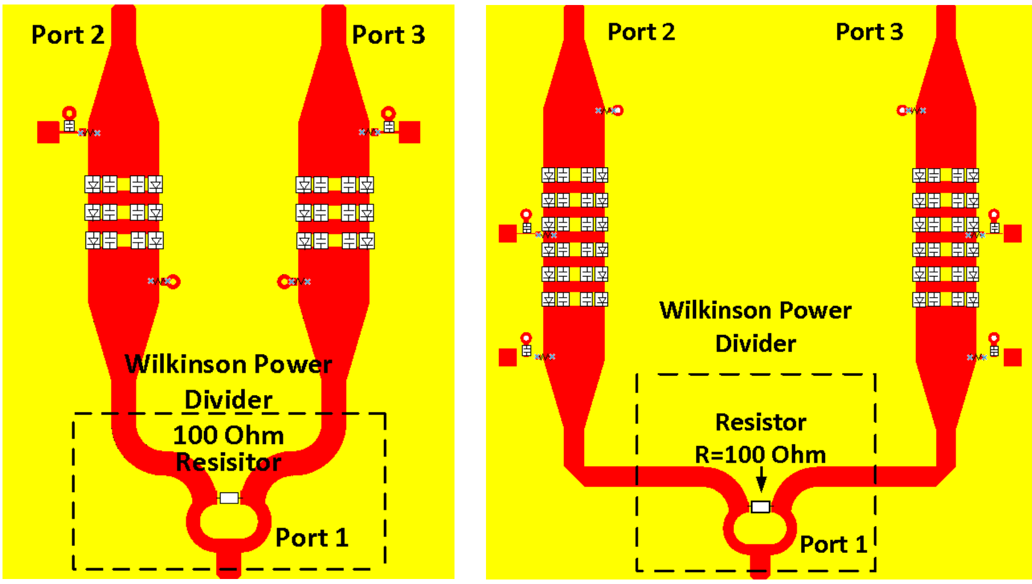

(a) (b)

Figure 5.1: The structures of the (a) 3-RDMS power divider and (b) the 6-RDMS power divider.

the same. In practice, there is usually a difference between the IL in each branch, which is known as the imbalance of a power divider. For the simulated results of States 1 and 2 shown in Figs. 5.2(a) and 5.3(a), the IL of the two ports are assumed to be balanced and therefore the simulated IL for only one of the branches are presented. However, in practice, the measured IL of the two branches are different due to the nonuniform lumped elements inserted in the branches. In Figs. 5.2(b) and 5.3(b), the simulated IL of State 4 are not plotted here because they are the same as the IL of State 3 due to the symmetrical structure when working in these two states. Nevertheless, the measured results of State 4 are included because they are different in practice because of the fabrication errors and nonuniform lumped elements.

According to the measured results, it is found that the IL of all the states are ≤ 2.2 dB and ≤ 1.8 dB for the 3- and the 6-RDMS power dividers, respectively. The predicted imbalances of the two branches are < 0.1 dB for both two power dividers. The measured

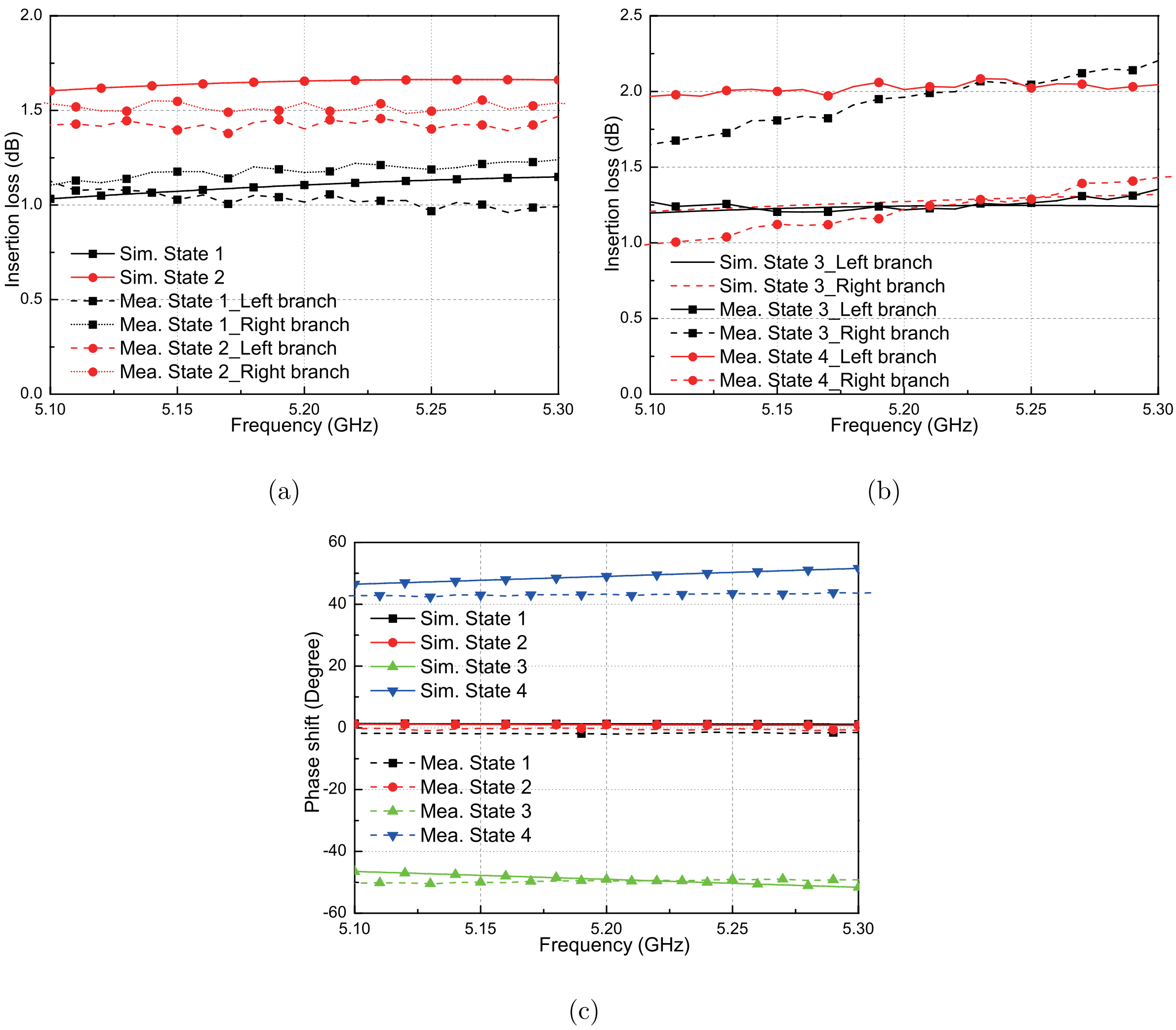

Figure 5.2: Simulated and measured results of the 3-RDMS power divider (State 1: All-on state; State 2: All-off state; State 3: Left-on-right-off state; State 4: Left-off-right-on state). (a) The IL of the two branches for States 1 and 2. (b) The IL of the two branches for States 3 and 4. (c) The phase shift values between port 2 and port 3 for States 1, 2, 3 and 4.

imbalances are slightly higher than the simulated results but they are still small. Figs. 5.2(c) and 5.3(c) give the phase shifts of the 4 states of the 3- and 6-RDMS power dividers, respectively. The phase shifts are the relative phase differences between port 2 and port 3, which are calculated from Phases(port 3) − Phases(port 2). Ports 2 and 3 are the output ports on the left- and right-hand side as shown in Fig. 5.1. The measured phase

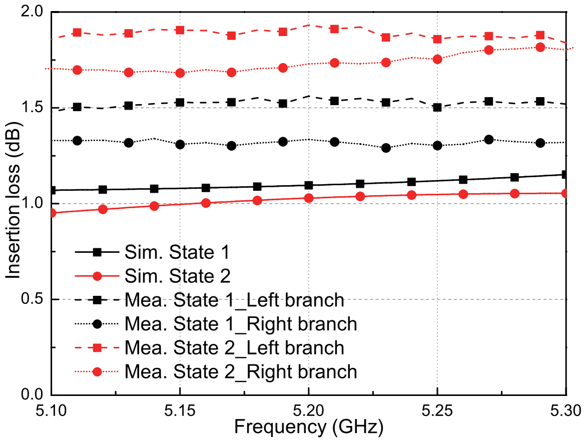

(a)

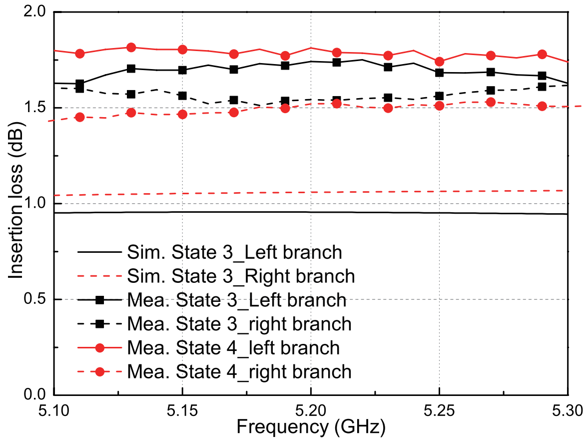

(b)

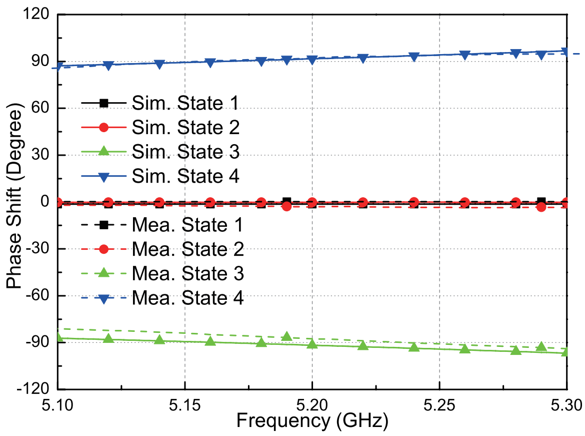

(c)

Figure 5.3: Simulated and measured results of the 6-RDMS power divider (State 1: All-on state; State 2: All-off state; State 3: Left-on-right-off state; State 4: Left-off-right-on state). (a) The IL of the two branches for States 1 and 2. (b) The IL of the two branches for States 3 and 4. (c) The phase shift values between port 2 and port 3 for States 1, 2, 3 and 4.

shifts agree well with the simulated results. The 3-RDMS power divider has phase shifts of 0°, 0°, 42°, and −45° in States 1, 2, 3, and 4, respectively. While for the 6-DMS power divider, phase shifts of 0°, 0°, 87°, and −91° are realized in the four states.

The above results demonstrate that when combined with a power divider, the phase shifters still produce the expected phase shifts. The measured IL is higher than expected.

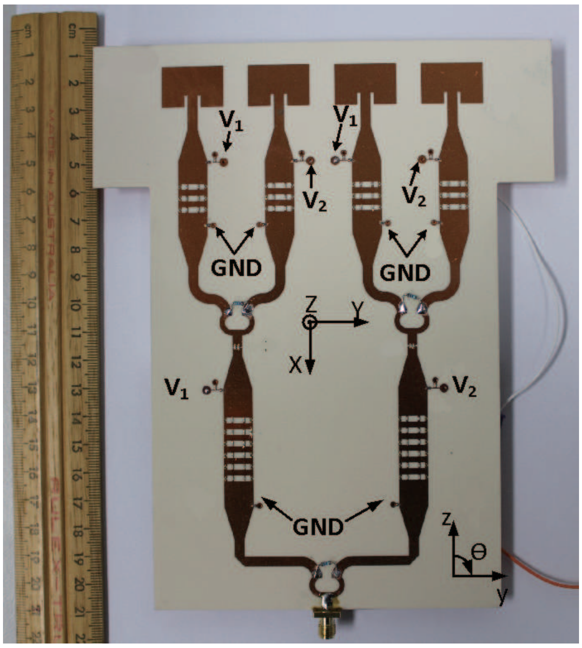

Figure 5.4: Prototype of the beam steering antenna array employing RDMS.

This is actually attributed to the reflection due to the mismatch of the structure. When the power divider is connected with the antenna array, the mismatch will be reduced. Therefore, the feed network will not reduce the antenna gain.

5.2.2 Phased Array Antenna

One 6-RDMS power divider and two 3-RDMS power dividers are combined with four patch antennas to form a 4-element steerable phased array. The fabricated array is shown in Fig. 5.4. The array has four working states where all three power dividers employed in the feed network produce the four working states given by All-on, All-off, Left-on-right-off, and Left-off-right-on states, respectively. In both the All-on and All-off states, the four patches are in phase, thereby producing a boresight beam direction in the H plane ($Z-Y$ plane). In the Left-on-right-off state, all the three power dividers work in the Left-on-right-off state, leading to regular phase advances of 45° between the adjacent patches. As

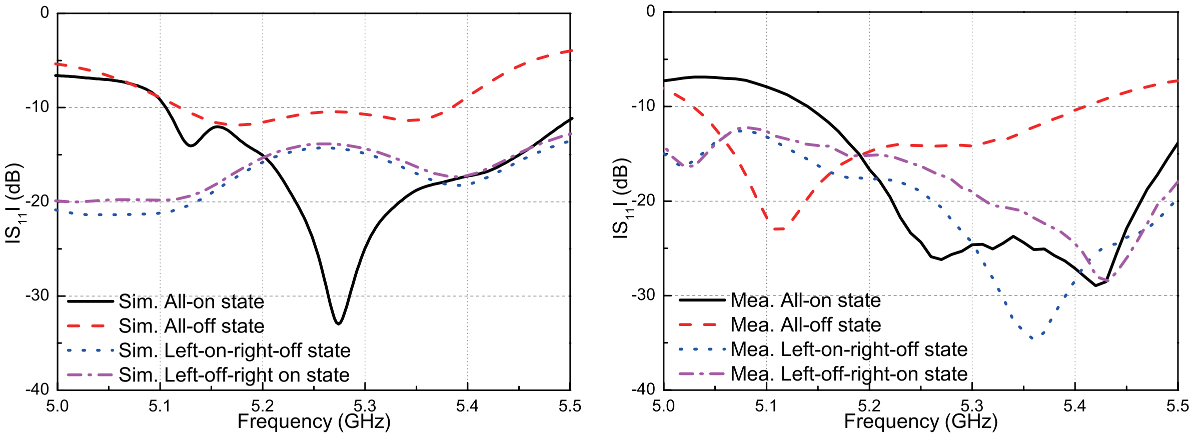

(a) (b)

Figure 5.5: (a) Simulated and (b) measured S_{11} of the beam steering array employing RDMS in the All-on, All-off, Left-on-right-off, and Left-off-right-on states.

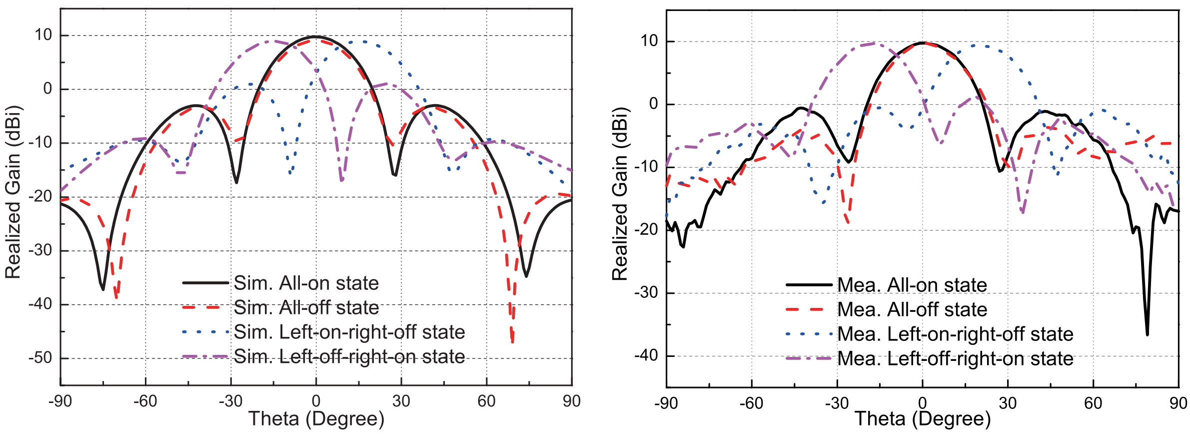

(a) (b)

Figure 5.6: (a) Simulated and (b) measured far-field pattern of the beam steering array employing RDMS in the All-on, All-off, Left-on-right-off, and Left-off-right-on states.

a result, the main lobe is shifted to $\theta = -15°$ in the H plane. In the Left-off-right-on state, all the power dividers work in the Left-off-right-on state which results in regular phase delays of 45° between the adjacent patches. In this case, the beam is shifted to $\theta = 15°$ in the H plane. Since the three power dividers always work in the same state for all the array working states, we connect the corresponding biasing pad using conducting wires at the back of the antenna array to reduce the level of the required DC bias. In practice, only two independent DC sources V_1 and V_2 (labelled in Fig. 5.4) are employed in the measurement. The employed bias networks have minor effects on the radiation patterns since they do not resonant in the working band. But they slightly reduces the antenna gain by 0.1 dB by comparing the simulation results of the antenna with and without the bias networks.

The simulated and measured results of the reflection coefficient S_{11} in the four states are shown in Figs. 5.5(a) and 5.5(b), respectively. It is seen that the measured overlapped impedance bandwidth in the four states covers the wireless local area network (WLAN) 5.2 GHz band (e.g. 5.15-5.35 GHz in the USA, 5.15-5.25 GHz in Japan, and 5.15-5.35 GHz in Europe). Figs. 5.6(a) and 5.6(b) give the simulated and measured far-field gain patterns in the H-plane in all the four states at 5.2 GHz. The radiation patterns and realized gains of the proposed antenna were measured by using a spherical near-field (SNF) antenna measurement system NSI-700s-50 located at CSIRO, Marsfield, NSW, Australia. According to the measured results, the main lobes of the antenna array in the All-on and All-off states are at 0°. In the Left-on-right-off and Left-off-right-on states, the main lobe directions in H plane are at $-15°$ and $15°$, respectively. It is observed in Fig. 5.6(b) that the antenna array can switch its main beam direction to 0°, $-15°$, and 15°, with minor gain reductions. The average realized gain is 10 dBi. In addition, the measured maximum sidelobe level (SLL) is -7 dB in the Left-off-right-on state. The SLL in the other three states are all below -10 dB.

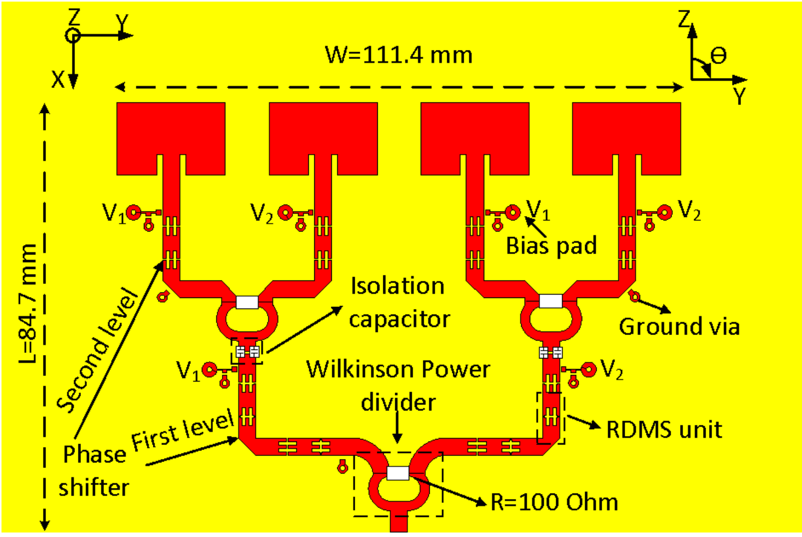

Figure 5.7: Prototype of the phased array employing MRDMS.

5.3 Phased Array Antenna Employing MRDMS

In this section, we use the MRDMS to provide required phase shifts for the 4-element phased array antenna described in Section 5.2.2, resulting in a significantly reduced profile and cost. Meanwhile, the revised array employing MRDMS can also switch its main beam to $-15°$, $0°$, and $15°$ in its H-plane as the array described in Section 5.2. This is due to the fact that the same antenna elements are used, and the MRDMS phase shifters are designed to provide the same phase shifts as the RDMS phase shifters.

In this design, three Wilkinson power dividers are employed to split the power while eight phase shifters are integrated in the feed network to realize 50° progressive phase differences between the array elements at 5.2 GHz. Each phase shifter is composed of one MRDMS phase shifter consisting of two MRDMS units with $W_{slot} = 2mm$, $L_{slot} = 3.6mm$, and $d = 3\,mm$. As shown in Fig. 5.7, for the first-level power divider, there are 2 phase shifters at each of the two branches. For the second-level, there is one phase shifter at each of the 4 branches. Two bias DC voltages labelled by V_1 and V_2 are employed to control the phase shifters. The biasing mechanism is the same as the phased array in Section 5.3.

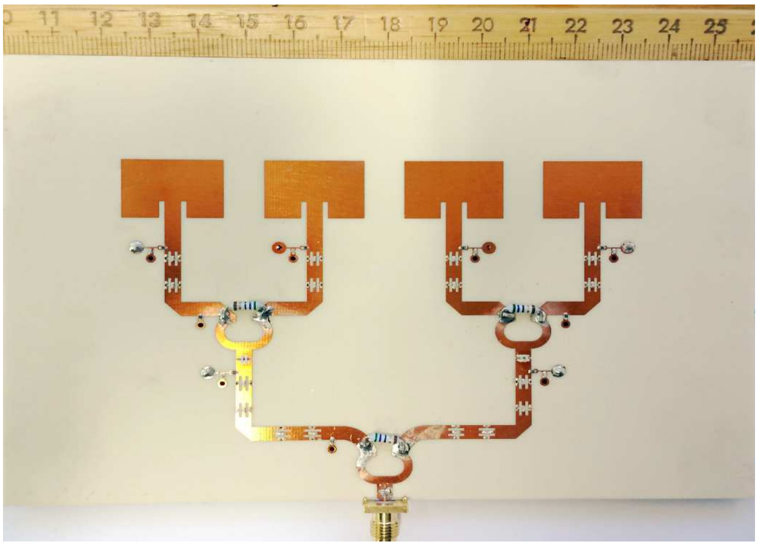

Figure 5.8: Photo of the fabricated phased array employing MRDMS.

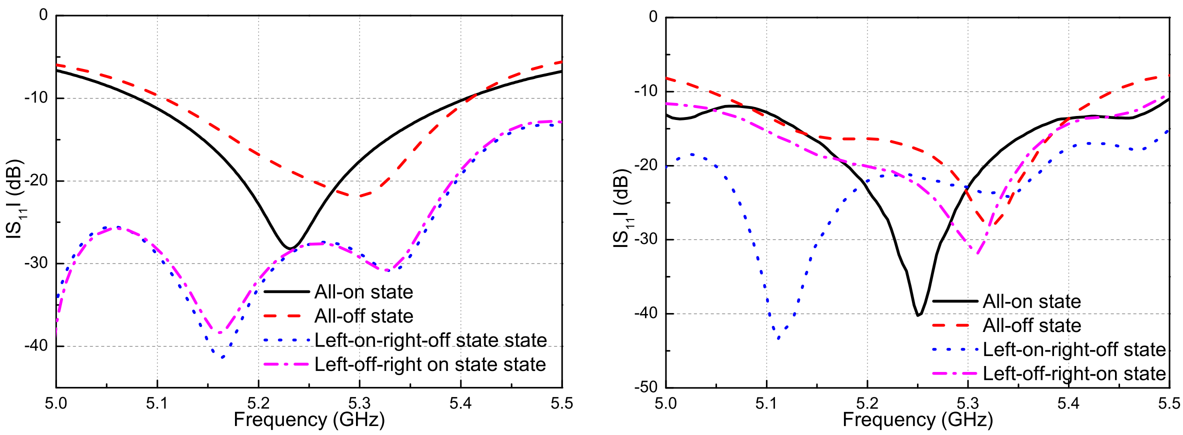

(a) (b)

Figure 5.9: (a) Simulated and (b) measured reflection coefficient S_{11} of the phased array employing MRDMS.

There are four different working states of the phased array. When voltages V_1 and V_2 are "+,+", "–,–", "+,–", and "–,+", the phased array can work in the "All-on", "All-off", "left-on-right-off", and "Left-off-right-on" states, respectively. In the All-on and All-off states, the array elements are in phase so that the beam is not tilted. In the left-on-

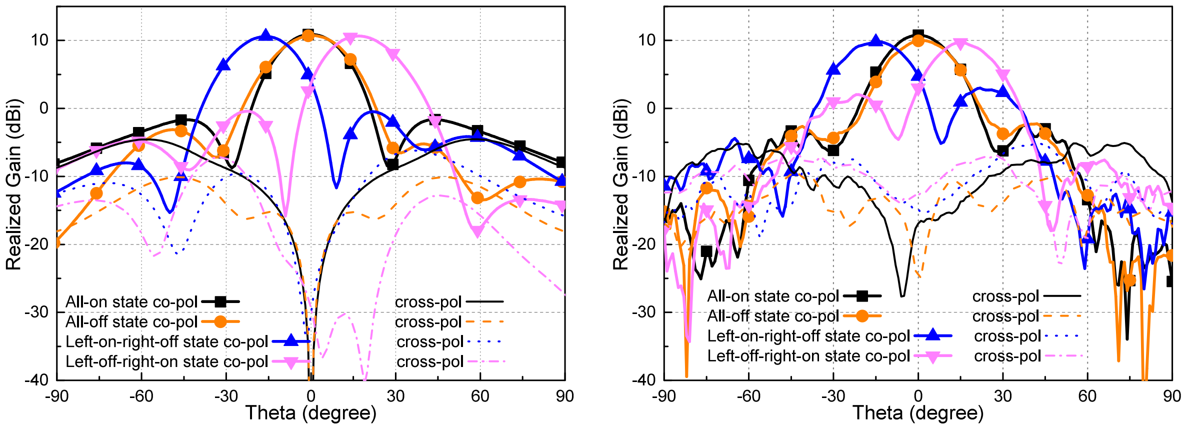

(a) (b)

Figure 5.10: (a) Simulated and (b) measured far-field pattern in the H-plane of the phased array employing MRDMS.

right-off and Left-off-right-on states, phase advances and delays of 50° between the array elements are obtained, respectively. Therefore, beam tilts of $-15°$ and $15°$ are realized.

The 4-element phased array antenna is fabricated and tested. Fig. 5.8 shows a picture of the fabricated antenna array. The simulated and measured reflection coefficient S_{11} is depict in Fig. 5.9. According to the figure, the overlapped impedance bandwidth of the 4 states can cover the wireless local area network (WLAN) 5.2 GHz band (e.g. 5.15-5.35 GHz in the USA, 5.15-5.25 GHz in Japan, and 5.15-5.35 GHz in Europe). Fig. 5.10 shows the simulated and measured co-polarization and cross-polarization patterns in the H-plane (Z–Y plane) of the antenna. As shown in Fig. 5.10, the phased array can switch its main beam towards 0°, 0°, $-15°$, and 15° in the H-plane with minor gain variations for the All-on, All-off, Left-on-right-off, and Left-off-right-on states, respectively, at 5.2 GHz. The co-polarization radiation pattern of phased array at 5.1, 5.2, 5.3, and 5.4 GHz are tested and depicted in Fig. 5.11. The results show that the phased array have a steady radiation pattern across the 10 dB impedance working band (5.1 – 5.4 GHz). This is due to the fact that the proposed MRDMS phase shifters provide true time delays, which

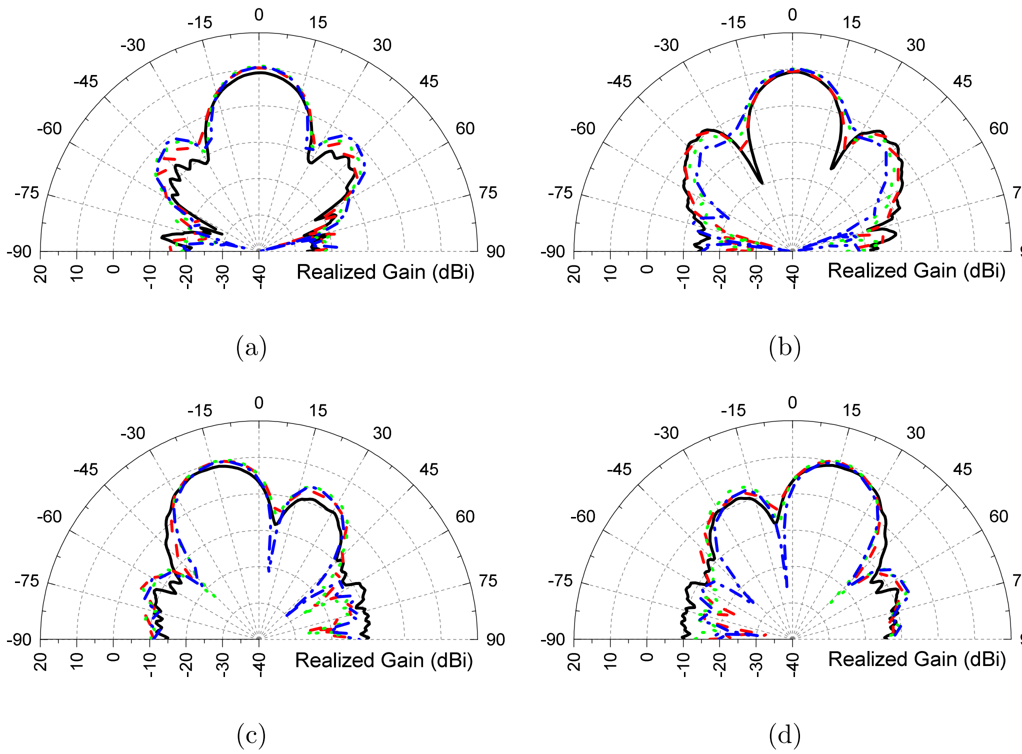

Figure 5.11: Measured H-plane far-field pattern in the (a) All-on, (b) All-off, (c) Left-on-right-off, and (d) Left-off-right-on states. (5.1 GHz ——— ; 5.2 GHz – – – –; 5.3 GHz · · · · · ·; 5.4 GHz – · –)

reduces the beam squint. The measured average gain of the antenna array is 10 dBi. The measured maximum SLL is -8 dB in the Left-on-right-off state. All the SLL in the other states are below -10 dB.

The obtained antenna is designed for WLAN systems in Australia rural areas. In those areas, residents usually live quite far away from each other. Base station antenna or optical fibres are too expensive to be used since the number of users is too small to cover the expenses. In this case, a economic solution is to use high gain directional relay antenna to transmit the WIFI signal from one house to another. One issue that should be taken into consideration is that the strong wind can make the antenna shaking, resulting in mis-alignment and reducing the signal intensity. The proposed phased array based on

MRDMS units is low cost, high gain, and is able to switch its main beam from $-15°$ to $15°$, thereby serving as an excellent candidate for this application.

By comparing the 4-element phased array employing MRDMS (shown in Fig. 5.8) and the phased array employing RDMS (shown in Fig. 5.4), it is noticed that significant achievements have been realized by replacing the RDMS by MRDMS in the array design. Firstly, the size of the array has been reduce by 55%. Secondly, the quantity of the lumped element has been halved with the more compact MRDMS. Thirdly, the performance of the phased array employing MRDMS is better than the one employing RDMS, including the impedance bandwidth and SLL. Therefore, the phase shifters based on MRDMS serve as a better candidate for phased array applications.

5.4 A Partially Reflective Surface Antenna Fed by a 2-Element Phased Array Employing MRDMS

This section proposes a beam-steering pattern reconfigurable PRS antenna which employs a new non-uniform reconfigurable PRS structure with a 2-element microstrip patch phased array as the source. The proposed reconfigurable PRS structure employs 6×6 reconfigurable cells and is divided into the left and right parts with respect to the center of the structure. Each reconfigurable cell is composed of a square patch in which two PIN diodes are inserted. The reflection phase of the cell element can be varied by switching the diodes on and off to produce a reflection phase inconsistency between the two parts of the entire PRS structure, which in turn switches the beam of the PRS antenna. However, the beam can be only steered from $-5°$ to $5°$ with respect to the broadside direction. To increase the tilt range, a phased array is employed as the source for the PRS antenna, where MRDMS phase shifters are incorporated in the feed network to provide phase shift. Therefore, a large beam steering angle is achieved with comparable realized gains. The

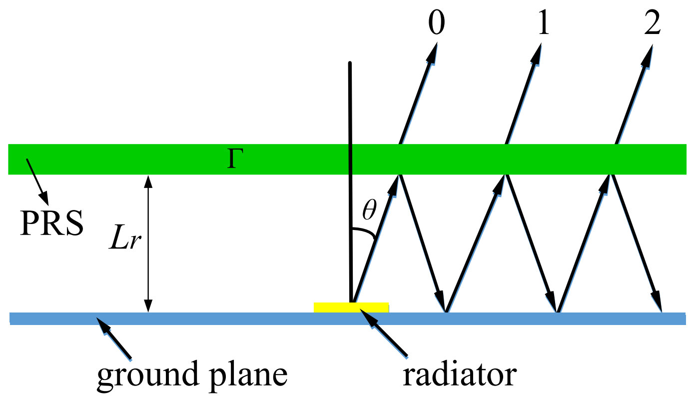

Figure 5.12: Schematic model of a conventional PRS antenna

antenna can switch its beam between $-15°$, $0°$, and $15°$ in an overlapped frequency range that goes from 5.5 GHz to 5.7 GHz with a realized gain over 12 dBi. Moreover, the proposed scheme achieves a nearly constant beam-tilt angle across a relatively wide frequency range due to the true time delay of the phase shifter. Furthermore, instead of using a separate power divider and a reconfigurable matching network as in [149], the proposed antenna employs an integrated aperture-feed network for the phased array source and does not require an extra impedance matching network, thereby leading to a more compact structure.

5.4.1 Reconfigurable PRS Structure

The schematic model of a conventional PRS antenna is shown in Fig. 5.12. It is composed of a source antenna (exciter) embedded between a ground plane and a dielectric superstrate employed as the PRS. The PRS is placed at a distance L_r above the ground plane with a reflection coefficient $\Gamma = R \cdot exp(j\phi)$. The electromagnetic waves radiating from the source experience multiple reflections and transmissions within the cavity. It is well known that a center-fed PRS antenna can radiate a broadside pattern when a uniform PRS is employed. By introducing non-uniformity to the PRS, a progressive phase shift

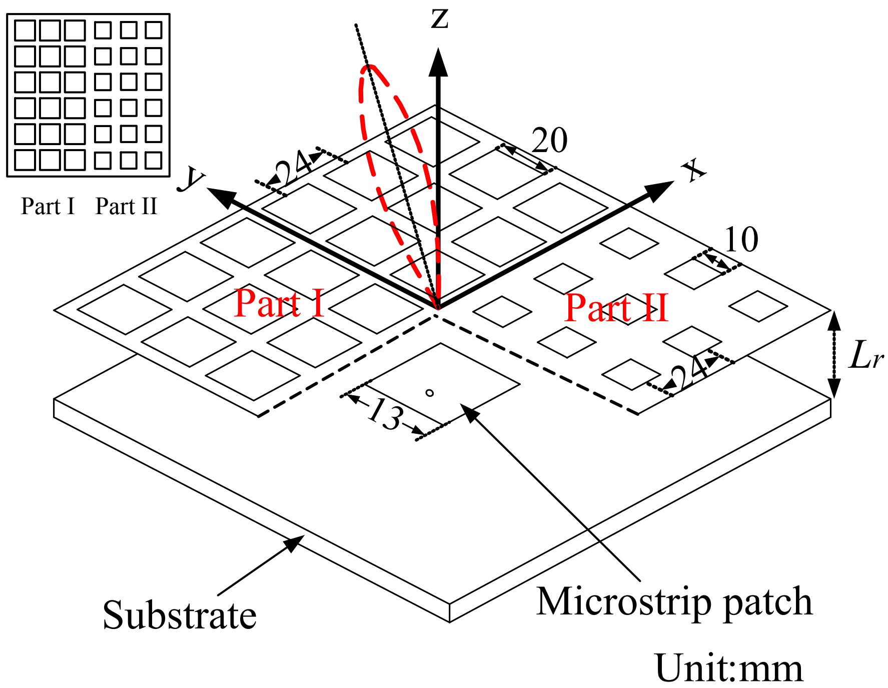

Figure 5.13: Oblique view of the PRS antenna with differing patch cells belonging to the two parts

and therefore a tilted beam can be achieved [150]. Regarding the direction of the beam tilt, the phased array concept can be utilized to consider each PRS unit cell as an element of a phased array. It is found that the phase and magnitude of the reflection coefficient are highly dependent on the patch size. Therefore, in this work, the entire PRS structure is divided into two equal parts, with individual phases and magnitudes of the reflection coefficients. By treating each part of the PRS as an element of a phased array, a beam tilt towards the part whose phase lags behind that of the other can be achieved.

Fig. 5.13 shows the schematic of the PRS antenna fed by a microstrip patch. The PRS surface is divided into two parts, Parts I and II, where patch cells with different sizes are employed to achieve beam tilting. In order to electronically change the size of the patch with a view to steering the beam over a full range (both left and right with respect to the broadside), here we uses a reconfigurable PRS unit cell rather than two different patch cells in the PRS antenna. The configuration of the reconfigurable patch

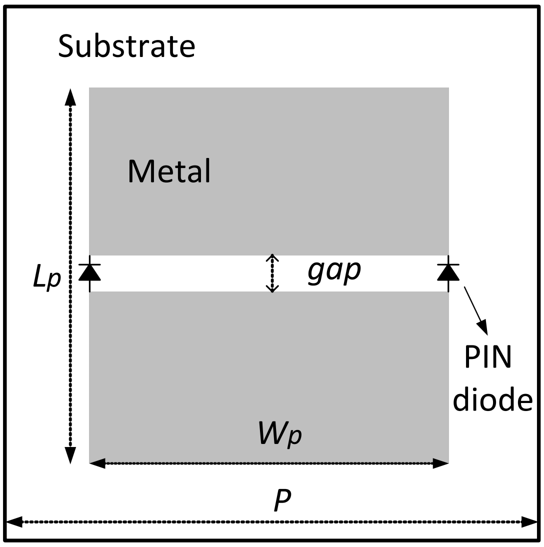

(a)

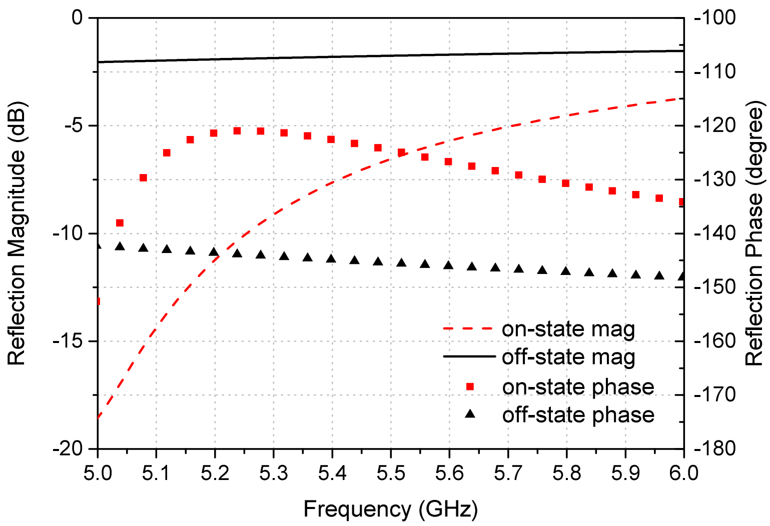

(b)

Figure 5.14: (a) Structure of the reconfigurable PRS cell. (b) Simulated reflection coefficient of the cell in the On- and Off-states.

cell is shown in Fig. 5.14(a). It is comprised of a $20.5mm \times 20.5mm$ microstrip patch etched on a $24mm \times 24mm \times 0.8mm$ FR4 substrate ($\varepsilon = 4.4, \delta = 0.0018$). A $1mm$ slot is inserted in the middle of the patch. PIN diodes [126] are placed at the two sides of the slot. The performance of the reconfigurable PRS cell has been calculated in a waveguide

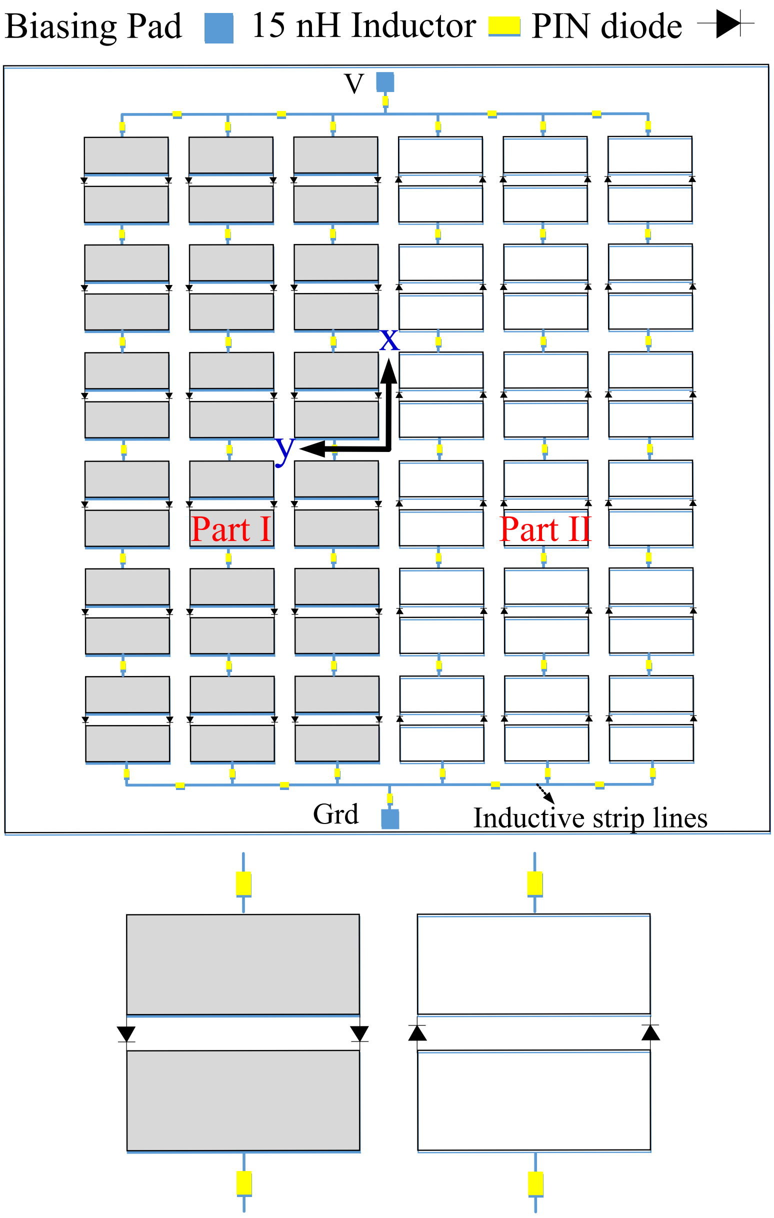

Figure 5.15: Schematic of the reconfigurable PRS structure.

environment by using a periodic boundary condition. Fig. 5.14(b) shows the simulated reflection magnitude and phases of the reconfigurable patch cell. When the PIN diodes are switched off, the two halves of the patch disconnect from each other, which results in a surface with a high reflectivity and a small phase. When the PIN diodes are switched on, a larger phase value is obtained compared to that of the off-state.

The schematic of the PRS structure employing the reconfigurable patch cell and its feed network is shown in Fig. 5.15. The PRS structure is divided into two halves and the PIN diodes in each part are oriented in opposite directions, though the diodes have the same orientation in each individual part. In terms of the DC signal, the PRS cells in each column are connected in series by using very thin (0.15 mm) metallic biasing striplines. In order to mitigate the effects of these biasing lines on the performance of the PRS, the striplines are broken down into small sections and the gaps between them are bridged with surface-mounted RF chock inductors (0402HP, 20 nH). For simplicity, we name such biasing striplines inductive biasing lines. Subsequently, all the columns are connected in parallel by using the same inductive biasing lines. Due to the reverse orientation of the PIN diodes in the two halves of the PRS, only one DC biasing voltage is utilized to control the diodes. When the voltage V is positive, the diodes in the left part (Part I) are switched on while the diodes in the right part (Part II) are switched off, and vice versa. The simulation results show that the proposed PRS antenna can switch to $-5°$ and $5°$ in the $Y-Z$ plane with an gain of 14.3 dBi.

5.4.2 Phased Array Source Employing MRDMS for PRS Antenna

In order to increase the tilt range of the PRS antenna described in the previous section, a phased array antenna is employed as the source (exciter). To obtain phase shifts between the array elements, MRDMS phase shifters are incorporated in the feed network as shown in Fig. 5.16. The feed network is comprised of two phase shifters etched on each branch of a Wilkinson power divider. Each phase shifter consists of three identical MRDMS units described in Chapter 4, as shown in the inset of Fig. 5.16. Each unit has a slot size of $L_{slot} \times W_{slot} = 3.5\,mm \times 2.0\,mm$ which are separated from each other by a distance of $4.2\,mm$. For this design, the Off-state generates a $30°$ phase delay with respect to the

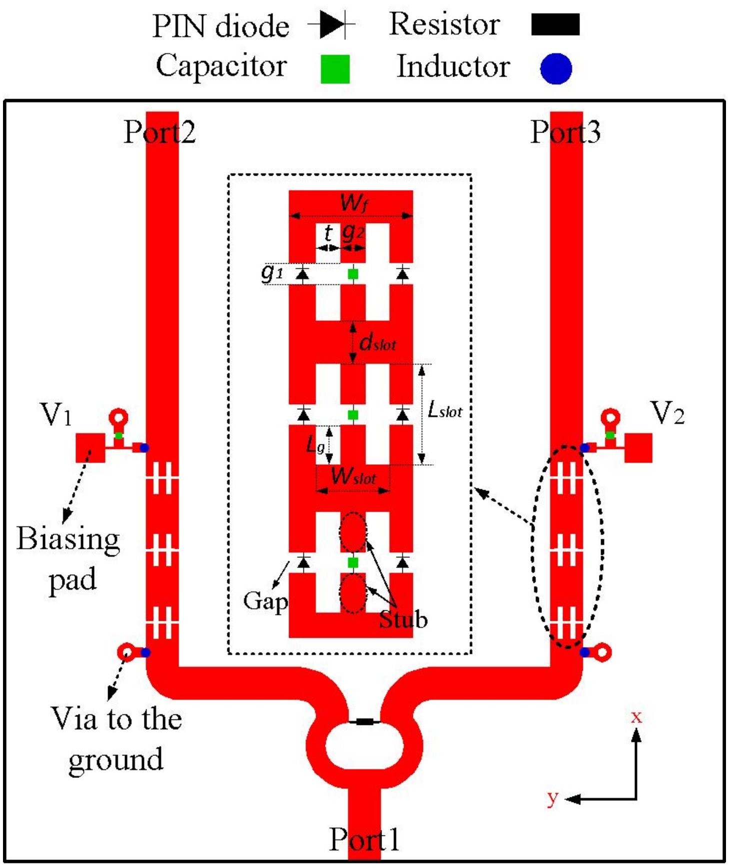

Figure 5.16: Structure of the feed network employing MRDMS.

On-state for a single unit. By cascading three MRDMS units, a 90° phase shift can be obtained. If the PIN diodes on both branches of the power divider are "All-on", no phase shift is acquired and this state is referred to "S1" in this work. When the diodes on the left branch are switched on and those of the right branch are switched off, the right branch can achieve a 90° phase delay with respect to the left branch. This state is named "S2" and results in a tilted beam towards the right side ($-y$ direction). On the other hand, the diodes on the network with a state of left-off-right-on (named as "S3") leads to a beam that titled towards the left side ($+y$ direction).

The feed network employing MRDMS phase shifters are designed on $80\,mm \times 80\,mm \times 1.524\,mm$ Rogers4003 substrate, and its simulation results are given in Fig. 5.17. For

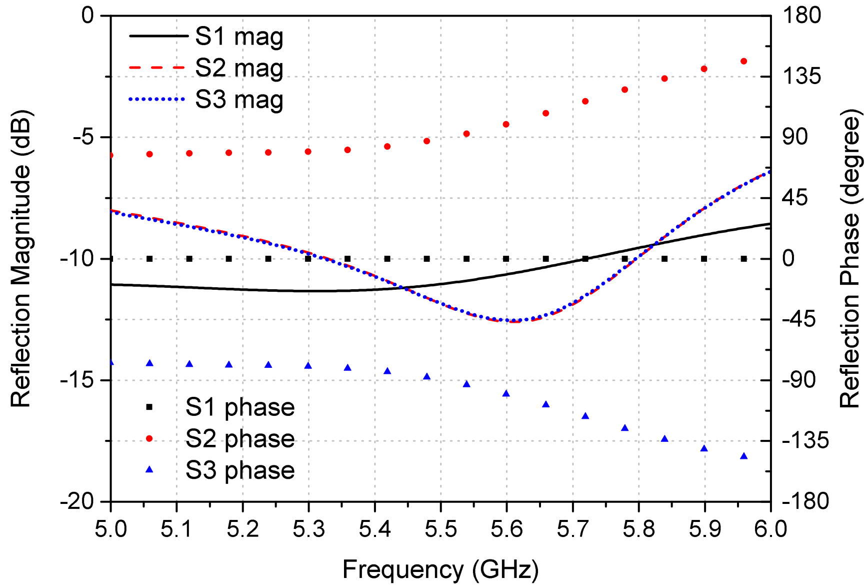

Figure 5.17: Simulated reflection coefficient S_{11} and the phase shift feed network.

brevity, we only studied the magnitude of the input reflection coefficient for Port1 and the phase difference between Port2 and Port3. It is observed that the return loss is below -10 dB for all the three states across the frequency band ranging from 5.3 GHz to 5.7 GHz. Furthermore, the phase difference Φ_{23} values for the three states (S1, S2 and S3) remain at approximately $0°$, $90°$, and $-90°$ respectively in this frequency band.

Based on the above results, an entire two-element microstrip phased array system is designed as the source (exciter) for the PRS antenna. The schematics of the phased array PRS antenna are shown in Fig. 5.18. The dimensions of the antenna are $150mm \times 150mm$. The phased array source is a two-layer structure. For the first layer, two square patches, each with a size of 13.2 mm, are placed at one side of a 1.524-mm-thick Rogers4003 substrate and aligned symmetrically along the y direction; hence the beam-scanning would only be realized in the H-plane. The spacing between the patches is chosen to be 43 mm ($0.8\lambda_0$) at 5.5 GHz, to achieve a compromise between the array coupling and the grating lobes. On the other side of the substrate, two slots with a dimension of $7mm \times 1.5mm$ for

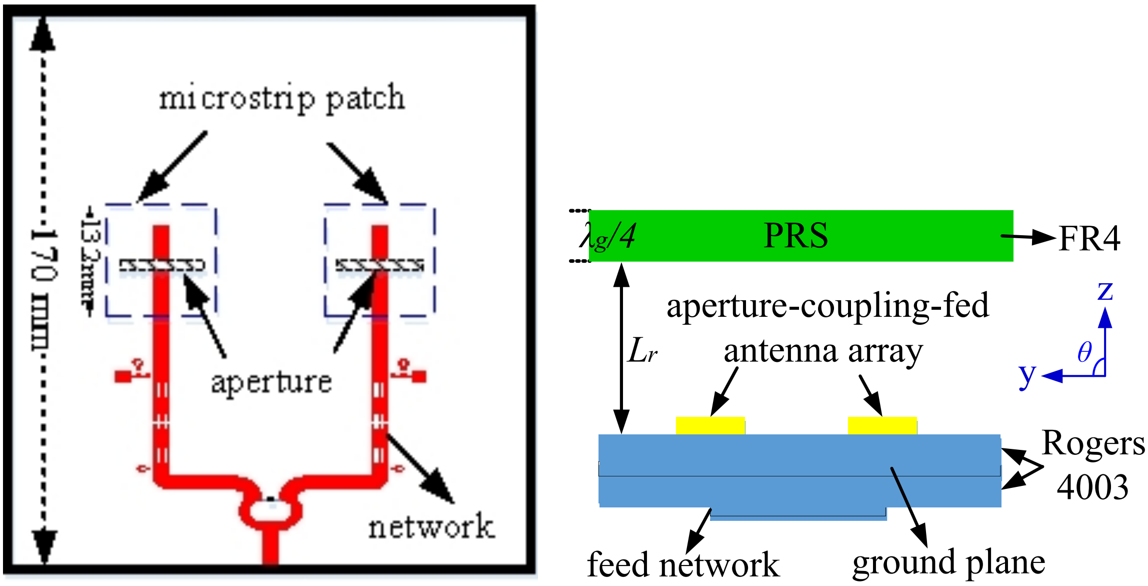

(a) (b)

Figure 5.18: (a) Top view and (b) side view of the Phased array fed PRS antenna.

Table 5.1: Simulated Beam-Scanning Capability of The Phased Array Source

Fr (GHz)	Beam Direction (degree)			Max Gain (dBi)		
	S1 state	S2 state	S3 state	S1 state	S2 state	S3 state
5.3	0	-10	10	12.6	10	10
5.5	0	-10	10	13	11.5	11.5
5.7	0	-9	9	9	9.2	9.2

an aperture coupling are etched on the ground at the position of the patch center. For the second layer, the feed network is printed on one side of another 1.524-mm-thick Rogers4003 substrate and the metal of the other side of this substrate is etched off. By following the conventional design rules of the traditional single superstrate PRS antenna [151], a 6.5-mm-thick FR4 substrate ($\lambda_g/4$ at 5.5 GHz) is used as the PRS structure. It is located 27 mm ($0.5\lambda_0$) from the patch antenna array.

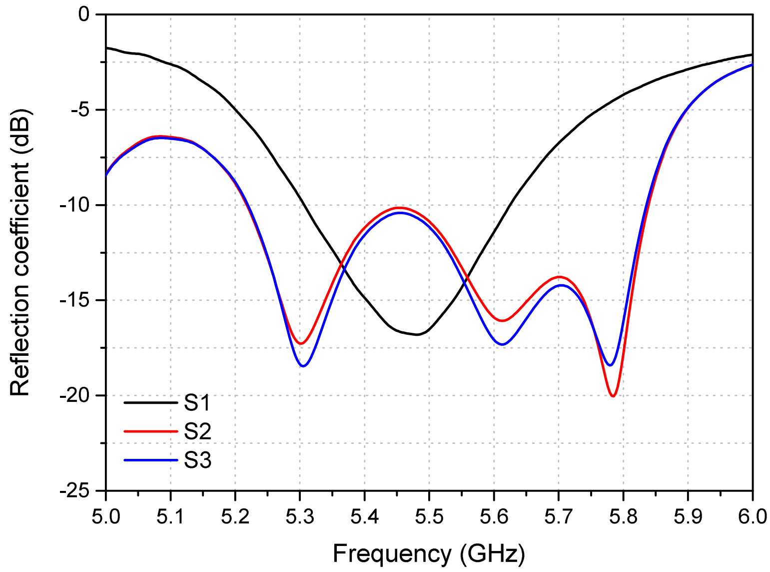

Figure 5.19: Simulated reflection coefficients of the phased array fed PRS antenna.

Simulated results for the reflection coefficients and the radiation patterns are shown in Fig. 5.19 and Table 5.1, respectively. It can be seen from Fig. 5.19 that the overlapped impedance bandwidth for the three states ranges from 5.3 GHz to 5.63 GHz. As listed in Table 5.1, the PRS antenna can steer its beam towards 0°, $-10°$, and 10° in the H-plane for the S1, S2 and S3 states, respectively, in the frequency range of 5.3 GHz to 5.7 GHz. The realized gains at the three frequency points are also given in Table 5.1. For the broadside beam, the realized gains are 12.6 dBi, 13 dBi and 9 dBi at 5.3 GHz, 5.5 GHz and 5.7 GHz, respectively. For the beam-scanning states, the realized gains are 10 dBi, 11.5 dBi and 9.2 dBi at 5.3 GHz, 5.5 GHz and 5.7 GHz, respectively.

5.4.3 Measurement Results

Based on the analysis and results obtained in Section 5.4.1 and Section 5.4.2, a PRS antenna with a reconfigurable PRS structure and a phased array source has been designed, fabricated, and measured. The reconfigurable PRS structure is the same as that shown

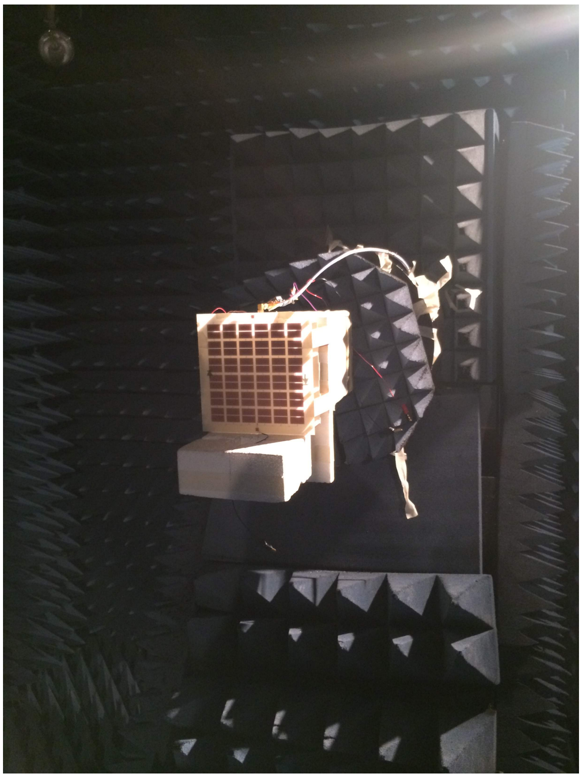

Figure 5.20: Prototype of the proposed antenna.

in Fig. 5.15, which consists of 6×6 reconfigurable cells, with dimensions of $20.5\,mm \times 20.5\,mm$, printed on the lower side of a 0.8-mm-thick FR4 substrate. The structure of the phased array source and its feed network are the same as that shown in Fig. 5.18. However, the size of the array elements is changed to $12.2\,mm$ after optimization. In this design, $\phi = -145.5°$ for an Off-state is chosen as an initial value (shown in Fig. 5.14(b)) to calculate L_r. After optimization, L_r is set to be 30 mm. A photograph of the PRS antenna prototype is shown in Fig. 5.20. Nylon spacers and M3 nylon bolts are used to support the PRS material above the ground plane. Visible at the back of the antenna is a low-loss bias tee, used to supply the biasing currents to the reconfigurable PRS unit cells in the measurement.

As discussed in Section 5.4.1, the reconfigurable PRS structure has three states corresponding to three radiation patterns at 5.5 GHz. Similarly, the phased array source also has three states, as discussed in Section 5.4.2; hence, there are nine states altogether. The simulated beam directions and their corresponding diode states are shown in Table IV for the nine states. As can be seen from the table, the beam can be primarily steered to three directions, namely 5° , 10°, and 15° . For the cases of 5° and 10°, they have already been discussed in Sections 5.4.1 and 5.4.2, respectively. The focus of this paper is to have a wider steering range for the reconfigurable PRS antenna. Therefore, in this section, only the states of 15° beam steering angle are measured and compared with the simulated results.

Table 5.2: Working States of the Obtained PRS Antenna

State	PRS state		Array state		Beam Direction	Gain (dBi)
	Left	Right	Left	Right		
1	off	off	on	on	0°	16.3
2	on	off	on	off	−15°	11.7
3	off	on	off	on	15°	11.7
4	on	off	on	on	−4°	14.2
5	off	on	on	on	4°	14.2
6	off	off	on	off	−9°	14.4
7	off	off	off	on	9°	14.4
8	off	on	on	off	−6°	12.7
9	on	off	off	on	6°	12.7

Fig. 5.21 plots the simulated and measured input reflection coefficients for the three states. The measured results show that an overlapped impedance bandwidth from 5.5 GHz to 5.74 GHz is achieved and that they agree well with the simulated results. The radiation patterns in the H-plane ($Y - Z$ plane) for the three states are shown in Fig.

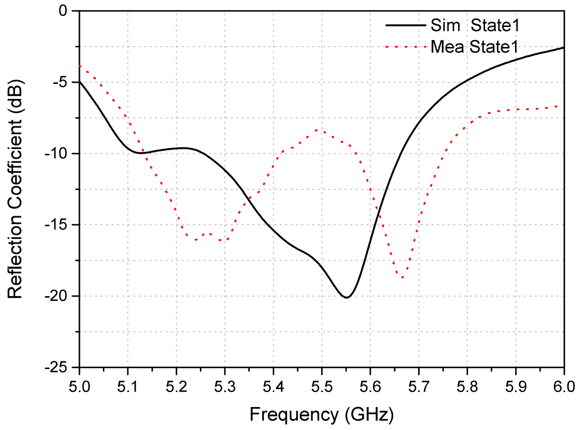

(a)

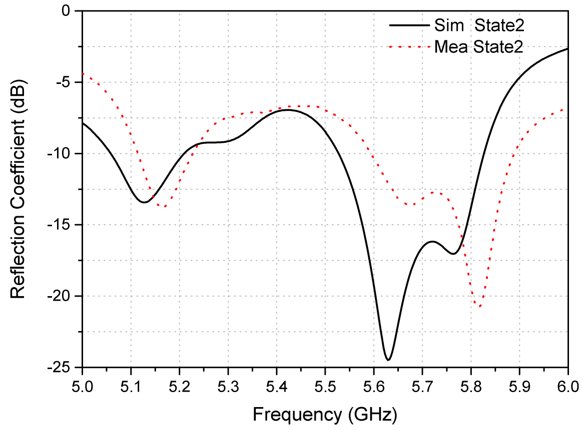

(b)

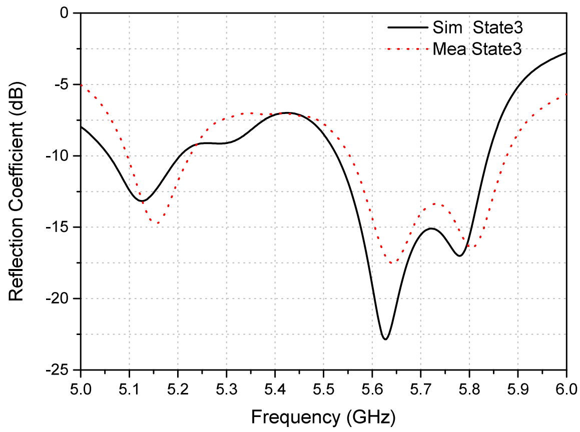

(c)

Figure 5.21: Input reflection coefficient of the proposed antenna in (a) State 1, (b) State 2, and (c) State 3.

5.22. The simulated and measured results are seen to be in agreement with each other. It is observed that a broadside radiation is obtained at State 1. For State 2 and State 3, the beam directions are tilted towards $-15°$ and $15°$ from the broadside, respectively, in a frequency band that ranges from 5.3 GHz to 5.7 GHz.

The realized gain is measured by using the gain comparison technique and the results are also given in Fig. 5.22. For State 1, the simulated realized gain is from 11.4 dBi to 16.2 dBi for a frequency range from 5.3 GHz to 5.7 GHz; while the measured one is from

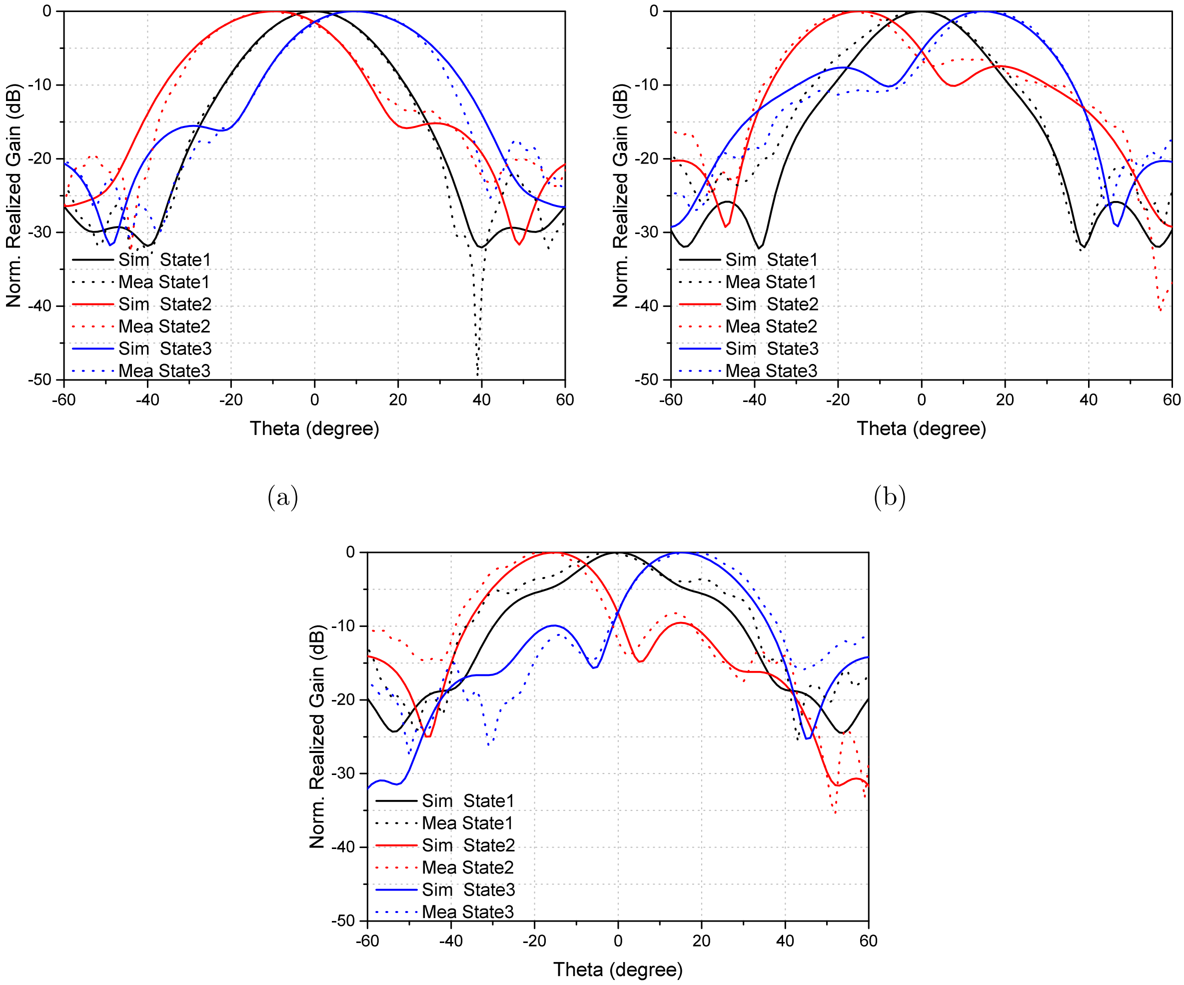

(a)

(b)

(c)

Figure 5.22: Simulated and measured far-field pattern of the proposed antenna at (a) 5.3 GHz, (b) 5.5 GHz, and (c) 5.7 GHz.

12.6 dBi to 15.5 dBi. For States 2 and 3, the simulated result is from 11.4 dBi to 12 dBi; while the measured gain varies from 10.2 dBi to 12.7 dBi. The difference between the simulated and measured results is less than 1.6 dB for the three states and can be attributed to the measurement errors and the inaccuracies in the fabrication process, such as alignment errors and the potential air gap between the two layers of the patch antenna array. In addition, it is observed that the measured realized gains for States 2 and 3 are

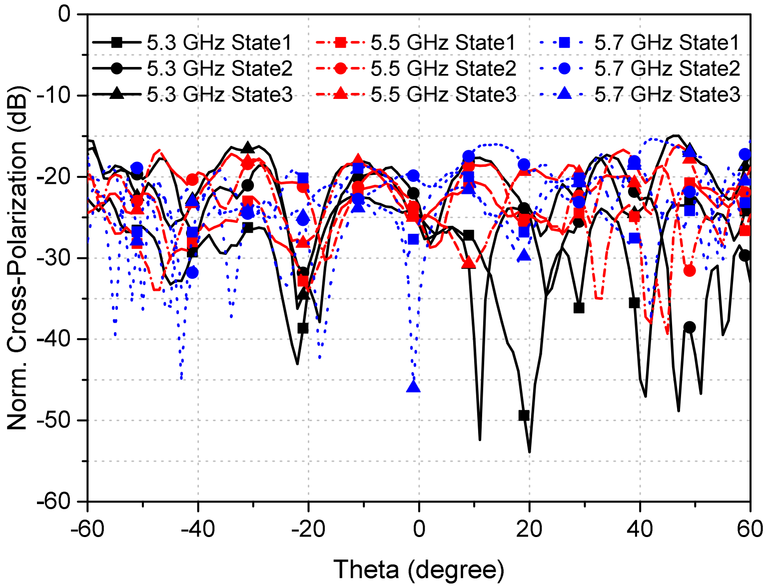

Figure 5.23: Measured reflection coefficients of the phased array fed PRS antenna.

almost the same, though small differences can be found at some certain frequencies. This is due to the variations in the characteristics of the PIN diodes employed in the phase shift network and the two halves of the PRS structure. The measured cross-polarization radiation patterns of H plane are shown in Fig. 5.23. It is seen that for all the operating states, the level of the cross-polarization is below -15 dB at the three frequency points. The E-plane (x-z plane) patterns and their corresponding cross-polarizations have been investigated by simulation. It is found that for State 1, the maximum realized gain is the same as that in the H-plane. While for State 2 and 3, the maximum gains are lower than those in the H-plane due to the beam tilting. Those patterns are omitted here for the sake of brevity.

From Section 5.4.1 to Section 5.4.3, it is seen that by using a reconfigurable PRS structure, a beam tilt of ±5° can be realized with a gain around 12 dBi. The PRS antenna fed by a 2-element phased array antenna source employing MRDMS phase shifters can achieve a beam tilt of ±10° with a gain of 10 dBi. The beam steering angle can then be increased further to $\pm 15°$ by employing a combined reconfiguration mechanism without compromising the antenna gain. Therefore, more flexibility can be realized in terms of the beam tilt angle and the antenna gain by using the proposed reconfigurable PRS antenna. Moreover, due to the true time delay characteristic of the MRDMS phase shifters, it can be seen from Fig. 5.22 that the proposed antenna can realize nearly consistent beam steering angles from 5.3 to 5.7 GHz; however, the reflection coefficient is above -10 dB for $f < 5.5$ GHz. To address this problem, an impedance matching network can be used to further increase the impedance bandwidth, and we plan to examine this issue in our future work.

5.5 Summary

In this Section, the proposed phase shifters described in the previous two sections were used in phased arrays. Two phased arrays that have the same radiating elements but different feed networks constructed by the RDMS- and MRDMS-based phase shifters were designed, fabricated, and tested. Both the phased arrays can switch their main beams to $-15°$, $0°$, and$15°$ in the H-plane with an average gain of 10 dBi. The phased arrays can work in the WLAN 5.2 GHz band with a steady beam pattern due to the true time-delays provided by the phase shifters. The tested results prove that the proposed RMDS- and MRDMS-based phase shifters can work properly in phased arrays, offering a simple low-cost solution to provide phase shift. In addition, the proposed phase shifters have a simple structure, easy control method, and are easily integrated into microstrip systems, which makes them cost effective candidates to be used in phased arrays. Moreover, by comparing the phased array that employs RDMS-based phase shifters with the one that employs MRDMS-based phase shifters, we noted that significant reductions in cost and size of the phased array have been achieved whilst maintaining comparable performance.

This indicates that the MRDMS-based phase shifter provides a better solution due to its smaller size. It also validates the fact that improvements in phase shifters lead to remarkable positive effects on phased arrays.

Not only in phased arrays, the proposed phase shifters could also be used in other antenna designs to introduce reconfigurability. In the work presented in Section 5.4, the MRDMS-based phase shifters were used to feed a 2-element phased array, and the phased array was used as a source to feed a PRS antenna. With the reconfigurable PRS structure, the PRS antenna fed by a fixed patch radiator can steer its beam, however the steering range is quite small from $-5°$ to $5°$. The fixed patch radiator was then replaced by the 2-element phased array to introduce more reconfigurability, realizing a widened steering angle from $-15°$ to $15°$. The two examples of the antenna employing MRDMS-based phase shifters show that the proposed phase shifter can serve as a good candidate in microstrip phased arrays due to its low cost, low profile, simple structure, simple control method, and design flexibility.

Chapter 6

Conclusions and Future Work

6.1 Conclusions

In this thesis, a novel type of low-cost phase shifter was proposed and then improved for phased array antennas. Phase shifters are key devices and are responsible for the high cost of phased arrays. Therefore, reducing the cost and size of phase shifters as well as their control circuits is of significance. In this work, firstly, we studied some basics of phased array antennas and reviewed different types of available phase shifters, to get a clear understanding of the requirements of phase shifters to be used in phased arrays. Then, a reconfigurable defected microstrip structure (RDMS) phase-shifting unit was proposed and used to design controllable stepwise phase shifters. Subsequently, an updated phase-shifting unit called modified RDMS (MRDMS) was advocated for its smaller profile, lower cost, and superior performance. Insights of the progress have been studied and a complete design scheme of the MRDMS-based phase shifters was concluded. After that, the obtained phase shifters were used to feed a 4-element phased array to validate their practicability in phased array antennas. Moreover, we have also employed the phase shifters in other antenna applications. A phased array fed partially reflective surface

(PRS) antenna was proposed and the phase shifters were used to provide phase shifts for the phased array source. More detailed conclusions are summarized as below.

The proposed RDMS and MRDMS phase shifters are all based on microstrip lines. The phase-shifting unit is made by etching a rectangle slot on a segment of microstrip line, and loading the slot with PIN diodes and capacitors. By switching the PIN diodes between the On- and Off-states, a phase shift is introduced. The RDMS and MRDMS phase-shifting units are actually switched-line phase shifters. When the units work in the On- and Off-states, the current paths have changed. This type of phase shifters provides true time delay, which is preferred in phased arrays for it can suppress beam squint. The capability of the RDMS and MRDMS units to provide phase shifts is mainly determined by two dimensions: the width and length of the slot (W_{slot}, L_{slot}). Generally, the value of a phase shift introduced by a RDMS or MRDMS unit increases with the slot dimensions W_{slot} and L_{slot}. However, the improvement comes with a sacrifice of the IL, since a larger slot leads to more reflection.

Subsequently, we cascaded several RDMS or MRDMS units separated from each other by a uniform space d to pursue increased phase shift. These cascaded structures are called RDMS or MRDMS groups. The simulation and experimental analysis of the groups lead to the following conclusions. Firstly, the phase shift value around $n\phi$ can be obtained by cascading n units with each unit providing a phase shift of ϕ. Secondly, the IL of the RDMS or MRDMS group is smaller than that of the single RDMS or MRDMS unit employed in the group. Thirdly, the separation distance d is the key parameter that significantly affects the IL and has a moderate effect on the phase shift value. These characteristics are beneficial and are attributed to the fact that the group employing several RDMS or MRDMS units is a slow-wave structure. The equivalent circuit of a group cascading several RDMS or MRDMS units is a transmission line with periodically loaded L/C circuits. By controlling the working states of the PIN diodes, the propagation constant β and phase velocity V_p can be changed, thus resulting in different time delays for the signals to pass through the circuit. A slow wave circuit (RDMS and MRDMS group) introduces less reflection than the abrupt discontinuity (RDMS and MRDMS unit).

The RDMS and MRDMS groups were then used in phase shifter designs. Stepwise phase shifters were realized by using a single group or cascading more groups and controlling them separately using biasing pads with L/C low-pass filters. A complete design procedure and some design considerations were summarized in Section 4.4.2 and validated by experiments. Several samples were fabricated and tested. The tested results agreed well with the simulated results. Different phase shifters that have phase-shifting ranges from 10° to 180° with various step sizes of 5°, 22.5°, and 45° were obtained.

Finally, the proposed phase shifters were used in phased array antennas. Feed networks were constructed by connecting Wilkinson power dividers with the RDMS and MRDMS phase shifters respectively. The RDMS- and MRDMS-based feed networks were employed to feed a linear patch array. Both the resultant phased arrays can switch their beam to −15°, 0°, and 15°, with an average gain of 10 dBi. However, the size and cost of a phased array employing the MRDMS phase shifters is only half of that of a phased array employing the RDMS phase shifters. The updated version of the phase shifter reduces the cost and size dramatically. Compared to other comparable phase shifters based on defected ground structure, the proposed phase shifter has the advantages of being low cost, low profile, easy to control, simple to fabricate, and easy to integrate into microstrip systems.

Moreover, the proposed phase shifters were also used in other applications other than traditional phased arrays. A reconfigurable PRS antenna employing a phased array excitation was proposed to achieve steerable beams with high gain. MRDMS-based phase shifters were specifically designed to provide phase shifts for the phased array excitation. The obtained antenna can switch its beam to nine directions (summarized in Table 5.2) with the gain above 11.7 dBi. This work further validated the practicality of the proposed MRDMS-based phase shifters in antennas.

On one hand, the proposed MRDMS phase shifters have several advantages, including the low cost, low loss, compact size, easy to fabricate and integrated with microstrip systems. On the other hand, they also have a drawback of low power handling ability. The low power handling capability is attributed to the employed PIN diode and slotted structure. However, it can be improved by replacing the current employed diodes with new types of diodes that have high power handling capability [152].

6.2 Future Work

The phase shifters presented in this dissertation have some possible extensions. Future work will focus on further improving the proposed phase shifters and using them in various antenna applications.

One possible extension of the phase shifter is to further reduce its size and cost. Section 4.2.2 gives the explanation of the fact that the reduced width of the phase-shifting unit does not degrade performance. The comparisons between the RDMS- and MRDMS-based phase shifters presented in Section 4.4.3 show that the size of the phase shifter was reduced by more than 80%. Moreover, the number of the lumped elements in this phase shifters was halved, resulting in lower cost. The achieved size reduction is prominent, but further reductions can be expected. For example, if we chose a narrower metal stub g_2 without changing any other parameters of a MRDMS unit shown in Fig. 4.1(b), the phase-shifting value could be increased. In other words, the length of the phase shifter required to provide a specific phase-shifting value can be reduced. This might lead to a higher IL, but it can be compensated by optimizing the matching circuit. In addition, our current design ultilizes two PIN diodes in a MRDMS unit. In the future, we could use only one PIN diode to reconfigure the phase-shifting unit. The principle of this work is to seek a simple, low cost solution to provide phase shift.

Another extension is to enhance the power handling capability of the proposed phase shifters. In current designs, the employed PIN diodes limited the power handling ability of the phase shifters. To address this problem, the employed PIN diodes can be replaced by high power diodes introduced in [].

Future work will also concentrate on the applications of the phase shifters' in phased arrays. Large-scale phased arrays will be built using the proposed phase shifters. An attention will be focused on the performance and cost of the phased array rather than the phase shifters. Specifically, in future work, the bias network used to control a great number of the phase shifters advocated in this thesis will be designed, and the phase shifters allocated in the feed network will be optimized separately to achieve the best matching.

Moreover, the MRDMS-based phase shifter can be used in reconfigurable antennas. Since the proposed phase shifters are based on microstrip lines, which are low cost and easy to realize, many antenna systems and microwave circuits employing microstrip lines can utilize the MRDMS phase-shifting units to introduce some reconfigurability. Controllable phase shifts provided by the MRDMS units can help antennas to achieve reconfigurable radiation patterns, polarizations, or frequency bands.

Appendix A

Symbols

F_a	Array factor
k	Wavenumber
λ	Wavelength
d	Separation distance between array elements
ϵ	Dielectric constant
δ	Loss tangent
D	Directivity
$\overline{\triangle^2}$	Variance of the beam pointing deviation
A	Wave amplitude
β	Propagation constant
ω	Radian frequency
Z	Characteristic impedance
$\triangle\phi$	Phase shift value
γ	Gyromagnetic constant
μ	Permeability
M	Magnetic moment

V	Volt
Ω	Ohm

Appendix B

Abbreviations

ABF	Analog Beamforming
BFN	Beamforming Network
dB	Decibels
DBF	Analog Beamforming
DC	Direct Current
DGS	Defected Ground Structure
DMS	Defected Microstrip Structure
IF	Intermediate Frequency
LTCC	Low-Temperature Co-fired Ceramic
MRDMS	Modified Reconfigurable Defected Microstrip Structure
MEMS	Micro-electronic-mechanical System
PDMS	Polydimethylsiloxane
PRS	Partially Reflective Surface
RDMS	Reconfigurable Defected Microstrip Structure
RF	Radio Frequency
SINR	Signal to Interference Noise Ratio

SLL	Sidelobe Level
TRS	Transmission and Receiving Module

Bibliography

[1] V. Dyadyuk, X. Huang, L. Stokes, J. Pathikulangara, A. R. Weily, N. Nikolic, J. D. Bunton, and Y. J. Guo, *Adaptive antenna arrays for Ad-Hoc Millimeter-Wave Wireless Communications*, E. M. Khatib, Ed. Adcanced Trends in Wireless Communications, 2011.

[2] O. Bazan and M. Jaseemuddin, "A survey on MAC protocols for wireless Adhoc networks with beamforming antennas," *IEEE Communications Surveys Tutorials*, vol. 14, no. 2, pp. 216–239, Feb. 2012.

[3] L. C. Godara, "Applications of antenna arrays to mobile communications, Part I: Performance improvement, feasibility, and system considerations," *Proceedings of the IEEE*, vol. 85, no. 7, pp. 1029–1030, Jul. 1997.

[4] ——, "Applications of antenna arrays to mobile communications, Part II. beamforming and direction-of-arrival considerations," *Proceedings of the IEEE*, vol. 85, no. 7, pp. 1031–1060, Jul. 1997.

[5] W. Liu and S. Weiss, *Wideband Beamforming: Concepts and Techniques*, ser. Wireless Communications and Mobile Computing. Wiley, 2010. [Online]. Available: https://books.google.com.au/books?id=ezI-pv_CDAMC

[6] R. C. Hansen, *Microwave Scanning Antenna.* New York: Academic, 1964.

[7] R. S. Elliot, "Beamwidth and directivity of large scanning arrays," *Microwave Journal*, vol. 6, no. 1, pp. 53–60, Dec. 1963.

[8] J. L. Allen, "The theory of array antenna," MASSACHUSETTS INST OF TECH LEXINGTON LINCOLN LAB, Tech. Rep., Jul. 1963.

[9] A. A. Oliner and G. H. Knittel, *Phase-Array Antennas.* Norwood: MA: Artech House, 1972.

[10] R. C. Hansen, *Significant Phased Array Papers.* Norwood: MA: Artech House, 1973.

[11] E. Brookner, *Practical Phase-Array Antenna Systems.* Norwood: MA: Artech House, 1991.

[12] D. Parker and D. C. Zimmermann, "Phased arrays - Part I: theory and architectures," vol. 50, no. 3, pp. 678–687, Mar. 2002.

[13] ——, "Phased arrays-Part II: implementations, applications, and future trends," *IEEE Transactions on Microwave Theory and Techniques*, vol. 50, no. 3, pp. 688–698, Mar. 2002.

[14] "Special issue on innovative phased array antennas based on non-regular lattices and overlapped subarrays," *IEEE Trans. Antennas Propag.*, vol. 60, no. 6, pp. 3078–3078, 2012.

[15] "Special issue on phased-array technology," *IEEE Trans. Microw. Theory Techn.*, vol. 60, no. 12, pp. 4231–4231, 2012.

[16] R. C. Hansen, *Phased Array Antenna.* Wiley, 1908.

[17] R. J. Mailloux, *Phased Array Antenna Handbook.* Bostion: Artech House, 2006.

[18] R. S. Elliott, *Antenna Thoery and Design.* Englewood Cliffs: NI: Prentice-Hall, 1981.

[19] E. T. Bayliss, "Design of monopulse antenna difference patterns with low sidelobes," *Bell System Technical Journal*, vol. 47, no. 5, pp. 623–650, 1968. [Online]. Available: http://dx.doi.org/10.1002/j.1538-7305.1968.tb00056.x

[20] G. Zeng, S. Li, Y. Zhang, and S. L, "Low side lobe pattern synthesis using projection method with genetic algorithm for truncated cone conformal phased arrays," *Journal of Systems Engineering and Electronics*, vol. 25, no. 4, pp. 554–559, Aug. 2014.

[21] A. B. Smolders and H. J. Visser, "Low side-lobe circularly-polarized phased arrays using a random sequential rotation technique," *IEEE Transactions on Antennas and Propagation*, vol. 62, no. 12, pp. 6476–6481, Dec. 2014.

[22] D. F. Guan, C. Ding, Z. P. Qian, Y. S. Zhang, W. Q. Cao, and E. Dutkiewicz, "An siw-based large-scale corporate-feed array antenna," *IEEE Transactions on Antennas and Propagation*, vol. 63, no. 7, pp. 2969–2976, Jul. 2015.

[23] B. A. Kopp, M. Borkowski, and G. Jerinic, "Transmit/receive modules," *IEEE Transactions on Microwave Theory and Techniques*, vol. 50, no. 3, pp. 827–834, Mar. 2002.

[24] B. Lu, S. X. Gong, S. Zhang, Y. Guan, and J. Ling, "Optimum spatial arrangement of array elements for suppression of grating-lobes of radar cross section," *IEEE Antennas and Wireless Propagation Letters*, vol. 9, pp. 114–117, 2010.

[25] P. V. Brennan, A. Narayanan, and R. Benjamin, "Grating lobe control in randomised, sparsely populated mimo radar arrays," *IET Radar, Sonar Navigation*, vol. 6, no. 7, pp. 587–594, Aug. 2012.

[26] A. Mizutani, K. Sakakibara, N. Kikuma, and H. Hirayama, "Grating lobe suppression of narrow-wall slotted hollow waveguide millimeter-wave planar antenna for arbitrarily linear polarization," *IEEE Transactions on Antennas and Propagation*, vol. 55, no. 2, pp. 313–320, Feb. 2007.

[27] C. Huang, Z. Zhao, Q. Feng, and X. Luo, "Suppression of grating lobes from a corrugated 2 x 2 slot antenna array with element spacing beyond a wavelength," *IET Microwaves, Antennas Propagation*, vol. 5, no. 13, pp. 1607–1612, Oct. 2011.

[28] J. Ruze, "The effect of aperture errors on the antenna radiation pattern," *Il Nuovo Cimento (1943-1954)*, vol. 9, no. 3, pp. 364–380, 1952. [Online]. Available: http://dx.doi.org/10.1007/BF02903409

[29] R. Elliott, "Mechanical and electrical tolerances for two-dimensional scanning antenna arrays," *IRE Transactions on Antennas and Propagation*, vol. 6, no. 1, pp. 114–120, Jan. 1958.

[30] B. D. Steinberg, *Principles of Aperture and Array Systems Design*. New York: Wiley, 1976.

[31] J. K. Hsiao, "Array sidelobes, error tolerance, gain, and beamwidth," Naval Research Laboratory, Tech. Rep., Sep. 1984.

[32] ——, "Design of error tolerance of a phased array," *Electronics Letters*, vol. 21, no. 19, pp. 834–836, Sep. 1985.

[33] R. Sahmel and R. Manasse, "Spatial statistics of instrument-limited angular measurement errors in phased array radars," *IEEE Transactions on Antennas and Propagation*, vol. 21, no. 4, pp. 524–532, Jul. 1973.

[34] W. Jiang, Y. Guo, T. Liu, W. Shen, and W. Cao, “Comparison of random phasing methods for reducing beam pointing errors in phased array,” *IEEE Transactions on Antennas and Propagation*, vol. 51, no. 4, pp. 782–787, Apr. 2003.

[35] J. Shen and L. W. Pearson, “The phase error and beam-pointing error in coupled oscillator beam-steering arrays,” *IEEE Transactions on Antennas and Propagation*, vol. 53, no. 1, pp. 386–393, Jan. 2005.

[36] M. I. Sholnik, *”Non-uniform arrays” in Antenna Theory*, R. E. Collin and F. J. Zucker, Eds. New York: McGraw-Hill, 1969.

[37] W. T. Patton, *”Array feeds” in Practical Phased-Array Antenna Systems*, E. Brookner, Ed. MA: Artech House, 1991.

[38] E. Holzman and A. K. Agrawal, “A comparison of active phased array, corporate beamforming architectures,” in *Phased Array System and Technology, IEEE International Symposium on*, Oct. 1996, pp. 429–434.

[39] J. S. Ajioka and J. L. McFarland, *”Beamforming feeds,” in Antenna Handbook, Thoery, Applications and Design*, Y. T. Lo and S. W. Lee, Eds. New York: Van Nostrand, 1998.

[40] W. H. Kummer, *Microwave Scanning Antennas.* New York: Academic, 1966, ch. Feeding and phase scanning.

[41] Y. Miura, J. Hirokawa, M. Ando, Y. Shibuya, and G. Yoshida, “Double-layer full-corporate-feed hollow-waveguide slot array antenna in the 60-GHz band,” *IEEE Transactions on Antennas and Propagation*, vol. 59, no. 8, pp. 2844–2851, Aug. 2011.

[42] A. U. Zaman and P. S. Kildal, "Wide-band slot antenna arrays with single-layer corporate-feed network in ridge gap waveguide technology," *IEEE Transactions on Antennas and Propagation*, vol. 62, no. 6, pp. 2992–3001, Jun. 2014.

[43] M. Sano, J. Hirokawa, and M. Ando, "Single-layer corporate-feed slot array in the 60-GHz band using hollow rectangular coaxial lines," *IEEE Transactions on Antennas and Propagation*, vol. 62, no. 10, pp. 5068–5076, Oct. 2014.

[44] T. Tomura, Y. Miura, M. Zhang, J. Hirokawa, and M. Ando, "A 45° linearly polarized hollow-waveguide corporate-feed slot array antenna in the 60-GHz band," *IEEE Transactions on Antennas and Propagation*, vol. 60, no. 8, pp. 3640–3646, Aug. 2012.

[45] F. F. Manzillo, M. Ettorre, M. Casaletti, N. Capet, and R. Sauleau, "Active impedance of infinite parallel-fed continuous transverse stub arrays," *IEEE Transactions on Antennas and Propagation*, vol. 63, no. 7, pp. 3291–3297, Jul. 2015.

[46] K. Wincza and S. Gruszczynski, "Microstrip antenna arrays fed by a series-parallel slot-coupled feeding network," *IEEE Antennas and Wireless Propagation Letters*, vol. 10, pp. 991–994, 2011.

[47] A. Vallecchi and G. B. Gentili, "Design of dual-polarized series-fed microstrip arrays with low losses and high polarization purity," *IEEE Transactions on Antennas and Propagation*, vol. 53, no. 5, pp. 1791–1798, May 2005.

[48] I. Slomian, I. Piekarz, K. Wincza, and S. Gruszczynski, "Microstrip antenna array with series feeding network designed with the use of slot-coupled three-way power divider," *IEEE Antennas and Wireless Propagation Letters*, vol. 11, pp. 667–670, 2012.

[49] H. Legay and L. Shafai, "Planar resonant series-fed arrays," *IEE Proceedings - Microwaves, Antennas and Propagation*, vol. 144, no. 2, pp. 67–72, Apr. 1997.

[50] T. Yuan, N. Yuan, and L. W. Li, "A novel series-fed taper antenna array design," *IEEE Antennas and Wireless Propagation Letters*, vol. 7, pp. 362–365, 2008.

[51] A. Lopez, "Monopulse networks for series feeding an array antenna," *IEEE Transactions on Antennas and Propagation*, vol. 16, no. 4, pp. 436–440, Jul. 1968.

[52] Y. B. Jung, I. Yeom, and C. W. Jung, "Centre-fed series array antenna for K-/Ka-band electromagnetic sensors," *IET Microwaves, Antennas Propagation*, vol. 6, no. 5, pp. 588–593, Apr. 2012.

[53] K. Wincza and S. Gruszczynski, "Microstrip antenna arrays fed by a series-parallel slot-coupled feeding network," *IEEE Antennas and Wireless Propagation Letters*, vol. 10, pp. 991–994, 2011.

[54] T. Munekata, M. Yamamoto, and T. Nojima, "A wideband 16-element antenna array using leaf-shaped bowtie antenna and series-parallel feed networks," in *Electromagnetics (iWEM), 2014 IEEE International Workshop on*, Aug. 2014, pp. 80–81.

[55] Y. Zhang, A. Chen, S. Cao, and D. Su, "Design of a circularly polarized 8×8 patch antenna array using a new series-parallel feed," in *Microwave, Antenna, Propagation and EMC Technologies for Wireless Communications, 2009 3rd IEEE International Symposium on*, Oct. 2009, pp. 411–414.

[56] M. Stoneback, M. Stoneback, and Y. Kuga, "Feasibility study of a wirelessly controlled and powered space-fed phased array antenna," *IEEE Transactions on Antennas and Propagation*, vol. 61, no. 12, pp. 5984–5991, Dec. 2013.

[57] R. J. Mailloux, "Space-fed subarrays using displaced feed," *Electronics Letters*, vol. 38, no. 21, pp. 1241–1243, Oct. 2002.

[58] M. Narasimhan, "Corrugated conical horn as a space feed for phased-array illumination," *IEEE Transactions on Antennas and Propagation*, vol. 22, no. 5, pp. 720–722, Sep. 1974.

[59] R. J. Mailloux, "Operating modes and dynamic range of active space-fed arrays with digital beamforming," *IEEE Transactions on Antennas and Propagation*, vol. 54, no. 11, pp. 3347–3355, Nov. 2006.

[60] P. Onno and A. Plitkins, "Miniature multi-kilowatt PIN diode mic digital phase shifters," in *Microwave Symposium Digest, 1971 IEEE GMTT International*, May 1971, pp. 22–23.

[61] L. Dunleavy, "GaAs MMICs perform in phase shifters," *Microwaves*, vol. 23, pp. 49–49, Apr. 1984.

[62] ——, *Microwave Semicnonductor Engineering.* New York: Van Nostrand: Reinhold Co., 1982.

[63] M. A. Morton, J. P. Comeau, J. D. Cressler, M. Mitchell, and J. Papapolymerou, "5 bit, silicon-based, X-band phase shifter using a hybrid π/t high-pass/low-pass topology," *IET Microwaves, Antennas Propagation*, vol. 2, no. 1, pp. 19–22, Feb. 2008.

[64] M. A. Morton and J. Papapolymerou, "A packaged MEMS-based 5-bit X-Band high-pass/low-pass phase shifter," *IEEE Transactions on Microwave Theory and Techniques*, vol. 56, no. 9, pp. 2025–2031, Sep. 2008.

[65] G. S. Shin, J. S. Kim, H. M. Oh, S. Choi, C. W. Byeon, J. H. Son, J. H. Lee, and C. Y. Kim, “Low insertion loss, compact 4-bit phase shifter in 65 nm CMOS for 5G applications,” *IEEE Microwave and Wireless Components Letters*, vol. 26, no. 1, pp. 37–39, Jan. 2016.

[66] M. A. Morton, J. P. Comeau, J. D. Cressler, M. Mitchell, and J. Papapolymerou, “Sources of phase error and design considerations for silicon-based monolithic high-pass/low-pass microwave phase shifters,” *IEEE Transactions on Microwave Theory and Techniques*, vol. 54, no. 12, pp. 4032–4040, Dec. 2006.

[67] R. V. Garver, “Broad-band diode phase shifters,” *IEEE Transactions on Microwave Theory and Techniques*, vol. 20, no. 5, pp. 314–323, May 1972.

[68] F. E. van Vliet and A. de Boer, “Fully-integrated core chip for X-band phased array T/R modules,” in *Microwave Symposium Digest, 2004 IEEE MTT-S International*, vol. 3, Jun. 2004, pp. 1753–1756 Vol.3.

[69] A. I. Khalil, M. Mahfoudi, F. Traut, M. Shifrin, and J. Chavez, “A X-band 4-bit MEMS phase shifter,” in *IEEE Compound Semiconductor Integrated Circuit Symposium, 2005. CSIC ’05.*, Oct. 2005, pp. 4 pp.–.

[70] G. e. a. Clark, “X- and Ku-band T/R, TTD and PA MIMICs,” Proc. GOMACTech, Tech. Rep. 131-133, Apr. 2005.

[71] S. R. Kumar, M. S. Leong, and P. S. Kooi, “Single fet loaded-line phase shifter configuration,” *Electronics Letters*, vol. 34, no. 4, pp. 379–381, Feb. 1998.

[72] R. Ramadoss, A. Sundaram, and L. M. Feldner, “Rf MEMS phase shifters based on PCB MEMS technology,” *Electronics Letters*, vol. 41, no. 11, pp. 654–656, May 2005.

[73] Y. J. Ko, J. Y. Park, and J. U. Bu, "Integrated 3-bit RF MEMS phase shifter with constant phase shift for active phased array antennas in satellite broadcasting systems," in *TRANSDUCERS, Solid-State Sensors, Actuators and Microsystems, 12th International Conference on, 2003*, vol. 2, Jun. 2003, pp. 1788–1791 vol.2.

[74] A. S. Abdellatif, A. A. Aziz, R. R. Mansour, and S. Safavi-Naeini, "Low-loss compact MEMS phase shifter for phased array antennas," *Electronics Letters*, vol. 51, no. 15, pp. 1142–1144, 2015.

[75] S. Kagita, A. Basu, and S. K. Koul, "Modeling of LTCC-ferrite tunable inductors and development of an L-band phase shifter," *IEEE Transactions on Magnetics*, vol. 51, no. 10, pp. 1–9, Oct. 2015.

[76] M. Kim, J. G. Yang, and K. Yang, "Switched transmission-line type Q-band 4-bit MMIC phase shifter using InGaAs pin diodes," *Electronics Letters*, vol. 46, no. 3, pp. 225–226, Feb. 2010.

[77] J. W. Lee and S. Y. Kim, "60 GHz switched-line-type phase shifter using body-floating switches in 0.13 um cmos technology," *Electronics Letters*, vol. 48, no. 7, pp. 376–378, Mar. 2012.

[78] S. Gong, H. Shen, and N. S. Barker, "A 60-GHz 2-bit switched-line phase shifter using sp4t RF-MEMS switches," *IEEE Transactions on Microwave Theory and Techniques*, vol. 59, no. 4, pp. 894–900, Apr. 2011.

[79] S. Dey and S. K. Koul, "Reliability analysis of Ku-band 5-bit phase shifters using MEMS SP4T and SPDT switches," *IEEE Transactions on Microwave Theory and Techniques*, vol. 63, no. 12, pp. 3997–4012, Dec. 2015.

[80] S. Lucyszyn, *Advanced RF MEMS*. Cambridge, MA, USA: Cambridge Univ. Press, 2010.

[81] N. Kingsley and J. Papapolymerou, “Organic ”wafer-scale” packaged miniature 4-bit RF MEMS phase shifter,” *IEEE Transactions on Microwave Theory and Techniques*, vol. 54, no. 3, pp. 1229–1236, Mar. 2006.

[82] D. Kholodnyak, E. Serebryakova, I. Vendik, and O. Vendik, “Broadband digital phase shifter based on switchable right- and left-handed transmission line sections,” *IEEE Microwave and Wireless Components Letters*, vol. 16, no. 5, pp. 258–260, May 2006.

[83] A. M. Abbosh, “Compact tunable reflection phase shifters using short section of coupled lines,” *IEEE Transactions on Microwave Theory and Techniques*, vol. 60, no. 8, pp. 2465–2472, Aug. 2012.

[84] C. S. Lin, S. F. Chang, C. C. Chang, and Y. H. Shu, “Design of a reflection-type phase shifter with wide relative phase shift and constant insertion loss,” *IEEE Transactions on Microwave Theory and Techniques*, vol. 55, no. 9, pp. 1862–1868, Sep. 2007.

[85] J. C. Wu, T. Y. Chin, S. F. Chang, and C. C. Chang, “2.45-GHz cmos reflection-type phase-shifter MMICs with minimal loss variation over quadrants of phase-shift range,” *IEEE Transactions on Microwave Theory and Techniques*, vol. 56, no. 10, pp. 2180–2189, Oct. 2008.

[86] F. Burdin, Z. Iskandar, F. Podevin, and P. Ferrari, “Design of compact reflection-type phase shifters with high figure-of-merit,” *IEEE Transactions on Microwave Theory and Techniques*, vol. 63, no. 6, pp. 1883–1893, Jun. 2015.

[87] H. R. Fang, X. Tang, K. Mouthaan, and R. Guinvarc’h, “180° and 90° reflection-type phase shifters using over-coupled lange couplers,” *IEEE Transactions on Microwave Theory and Techniques*, vol. 60, no. 11, pp. 3440–3448, Nov. 2012.

[88] D. C. Judy, J. X. Qiu, J. S. Pulskamp, R. G. Polcawich, and R. Kaul, "Reflection-type continuously-tunable phase shifter using PZT thin-film capacitors," *Electronics Letters*, vol. 45, no. 3, pp. 171–173, Jan. 2009.

[89] C. S. Lin, S. F. Chang, and W. C. Hsiao, "A full-360° reflection-type phase shifter with constant insertion loss," *IEEE Microwave and Wireless Components Letters*, vol. 18, no. 2, pp. 106–108, Feb. 2008.

[90] S. H. Choi, Y. M. Lee, and M. Kim, "60 GHz reflection-type phase shifter using 0.13 um cmos body-floating switches," *Electronics Letters*, vol. 47, no. 12, pp. 701–703, Jun. 2011.

[91] O. D. Gurbuz and G. M. Rebeiz, "A 1.6–2.3-GHz RF MEMS reconfigurable quadrature coupler and its application to a 360° reflective-type phase shifter," *IEEE Transactions on Microwave Theory and Techniques*, vol. 63, no. 2, pp. 414–421, Feb. 2015.

[92] J. Li, R. Shu, and Q. J. Gu, "10 GHz CMOS hybrid reflective-type phase shifter with enhanced phase shifting range," *Electronics Letters*, vol. 51, no. 23, pp. 1935–1937, 2015.

[93] R. N. Hardin, E. J. Downey, and J. Munushian, "Electronically-variable phase shifters utilizing variable capacitance diodes," in *Proc. IRE*, vol. 45, May 1960, pp. 944–945.

[94] X. Shi, Z. Wang, X. Tang, T. Tang, H. Gong, Q. Zhou, W. Bo, Y. Zhang, Z. Duan, Y. Wei, Y. Gong, and J. Feng, "Study on wideband sheet beam traveling wave tube based on staggered double vane slow wave structure," *IEEE Transactions on Plasma Science*, vol. 42, no. 12, pp. 3996–4003, Dec. 2014.

[95] S. K. Datta, V. B. Naidu, P. R. R. Rao, L. Kumar, and B. Basu, “Equivalent circuit analysis of a ring-bar slow-wave structure for high-power traveling-wave tubes,” *IEEE Transactions on Electron Devices*, vol. 56, no. 12, pp. 3184–3190, Dec. 2009.

[96] C. Chua and S. Aditya, “A 3-D U-shaped meander-line slow-wave structure for traveling-wave-tube applications,” *IEEE Transactions on Electron Devices*, vol. 60, no. 3, pp. 1251–1256, Mar. 2013.

[97] G. Guo, Y. Wei, M. Zhang, G. Travish, L. Yue, J. Xu, H. Yin, M. Huang, Y. Gong, and W. Wang, “Novel folded frame slow-wave structure for millimeter-wave traveling-wave tube,” *IEEE Transactions on Electron Devices*, vol. 60, no. 11, pp. 3895–3900, Nov. 2013.

[98] W. S. Chang and C. Y. Chang, “A high slow-wave factor microstrip structure with simple design formulas and its application to microwave circuit design,” *IEEE Transactions on Microwave Theory and Techniques*, vol. 60, no. 11, pp. 3376–3383, Nov. 2012.

[99] R. Romanofsky, “Slow-wave phase shifters, based on thin ferroelectric films, for reflectarray antennas,” NASA Glenn Research Centre, Cleveland, OH, United States, Tech. Rep., 2006.

[100] A. S. Nagra and R. A. York, “Distributed analog phase shifters with low insertion loss,” *IEEE Transactions on Microwave Theory and Techniques*, vol. 47, no. 9, pp. 1705–1711, Sep. 1999.

[101] E. G. Erker, A. S. Nagra, Y. Liu, P. Periaswamy, T. R. Taylor, J. Speck, and R. A. York, “Monolithic ka-band phase shifter using voltage tunable BaSrTiO3 parallel plate capacitors,” *IEEE Microwave and Guided Wave Letters*, vol. 10, no. 1, pp. 10–12, Jan. 2000.

[102] B. Lakshminarayanan and T. M. Weller, “Design and modeling of 4-bit slow-wave MEMS phase shifters,” *IEEE Transactions on Microwave Theory and Techniques*, vol. 54, no. 1, pp. 120–127, Jan. 2006.

[103] K. V. Caekenberghe and T. Vaha-Heikkila, “An analog RF MEMS slotline true-time-delay phase shifter,” *IEEE Transactions on Microwave Theory and Techniques*, vol. 56, no. 9, pp. 2151–2159, Sep. 2008.

[104] V. Janardhana, J. S. Roy, S. Pamidighantam, and R. G. Kulkarni, “Analysis of surface micro machined RF MEMS phase shifters,” *IEEE Aerospace and Electronic Systems Magazine*, vol. 23, no. 5, pp. 32–35, May 2008.

[105] A. L. Franc, O. H. Karabey, G. Rehder, E. Pistono, R. Jakoby, and P. Ferrari, “Compact and broadband millimeter-wave electrically tunable phase shifter combining slow-wave effect with liquid crystal technology,” *IEEE Transactions on Microwave Theory and Techniques*, vol. 61, no. 11, pp. 3905–3915, Nov. 2013.

[106] B. Lakshminarayanan and T. M. Weller, “Optimization and implementation of impedance-matched true-time-delay phase shifters on quartz substrate,” *IEEE Transactions on Microwave Theory and Techniques*, vol. 55, no. 2, pp. 335–342, Feb. 2007.

[107] G. F. Dionne, D. E. Oates, D. H. Temme, and J. A. Weiss, “Superconductivity for improved microwave ferrite devices,” *Lincoln Laboratory Journal*, vol. 9, no. 1, pp. 19–31, 1996.

[108] R. Romanofsky, “Array phase shifters: Theory and technology,” NASA Glenn Research Centre, Cleveland, OH, United States, Tech. Rep., Oct. 2007.

[109] A. Beyer, "Microwave and millimeter wave phase shifters dielectric and ferrite phase shifters," *International Journal of Microwave and Millimeter-Wave Computer-Aided Engineering*, vol. 3, no. 1, pp. 98–99, 1993.

[110] L. R. Whicker, "Review of ferrite phase shifter technology," in *Microwave Symposium, 1973 IEEE G-MTT International*, Jun. 1973, pp. 95–97.

[111] B. Lax and J. Pehowich, "Application of perturbation theory to toroidal ferrite phase shifters," *IEEE Transactions on Microwave Theory and Techniques*, vol. 39, no. 12, pp. 2198–2203, Dec. 1991.

[112] A. Abuelmaatti, J. Zafar, I. Khairuddin, A. A. P. Gibson, A. Haigh, and I. Morgan, "Variable toroidal ferrite phase shifter," *IET Microwaves, Antennas Propagation*, vol. 3, no. 2, pp. 242–249, Mar. 2009.

[113] Y. Xu, "Microwave ferrite toroidal phase shifter in grooved waveguide with reduced sizes," *IEEE Transactions on Microwave Theory and Techniques*, vol. 36, no. 6, pp. 1095–1097, Jun. 1988.

[114] C. R. Boyd, "Comments on the design and manufacture of dual-mode reciprocal latching ferrite phase shifters," *IEEE Transactions on Microwave Theory and Techniques*, vol. 22, no. 6, pp. 593–601, Jun. 1974.

[115] ——, "A dual-mode latching reciprocal ferrite phase shifter," *IEEE Transactions on Microwave Theory and Techniques*, vol. 18, no. 12, pp. 1119–1124, Dec. 1970.

[116] W. E. Hord, C. R. Boyd, and D. Diaz, "A new type of fast switching dual-mode ferrite phase shifter," in *Microwave Symposium Digest, 1987 IEEE MTT-S International*, vol. 2, May 1987, pp. 985–988.

[117] C. R. Boyd, "A latching ferrite rotary-field phase shifter," in *Microwave Symposium Digest, 1995., IEEE MTT-S International*, May 1995, pp. 103–106 vol.1.

[118] ——, "Ferrite rotary-field phase shifters: A survey of current technology and applications," in *Microwave Conference/Brazil, 1993., SBMO International*, vol. 1, Aug. 1993, pp. 305–310.

[119] W. E. Hord, "Average power capacity of rotary-field ferrite phase shifters," *IEEE Transactions on Microwave Theory and Techniques*, vol. 40, no. 12, pp. 2387–2391, Dec. 1992.

[120] A. Nafe and A. Shamim, "An integrable siw phase shifter in a partially magnetized ferrite ltcc package," *IEEE Transactions on Microwave Theory and Techniques*, vol. 63, no. 7, pp. 2264–2274, Jul. 2015.

[121] F. A. Ghaffar and A. Shamim, "A partially magnetized ferrite LTCC-based siw phase shifter for phased array applications," *IEEE Transactions on Magnetics*, vol. 51, no. 6, pp. 1–8, Jun. 2015.

[122] X. Yang, J. Wu, Y. Gao, T. Nan, Z. Zhou, S. Beguhn, M. Liu, and N. X. Sun, "Compact and low loss phase shifter with low bias field using partially magnetized ferrite," *IEEE Transactions on Magnetics*, vol. 49, no. 7, pp. 3882–3885, Jul. 2013.

[123] X. Yang, Y. Gao, J. Wu, Z. Zhou, S. Beguhn, T. Nan, and N. X. Sun, "Voltage tunable multiferroic phase shifter with YIG/PMN-PT heterostructure," *IEEE Microwave and Wireless Components Letters*, vol. 24, no. 3, pp. 191–193, Mar. 2014.

[124] J. J. Green and F. Sandy, "Microwave characterization of partially magnetized ferrites," *IEEE Trans. Microw. Theory Tech.*, vol. MTT-22, no. 6, pp. 641–645, Jun. 1974.

[125] C. Engineer Microsemi, *The PIN Diode Circuit Designers Handbook*, Powermite, Ed. 580 Pleasnt Street, Watertown, MA: Engineer Microsemi , Corp., 1992.

[126] MA-COM Technology Solutions, "Datasheet of MA4FCP300."

[127] ATC Technoligies, Inc., "Datasheet of ATC 600L Series Ultra-Low ESR, High Q, NPO RF, and Microwave Capacitors."

[128] M. Kozak and M. Karaman, "Digital phased array beamforming using single-bit delta-sigma conversion with non-uniform oversampling," *IEEE Transactions on Ultrasonics, Ferroelectrics, and Frequency Control*, vol. 48, no. 4, pp. 922–931, Jul. 2001.

[129] S. Kim and Y. E. Wang, "Two-dimensional planar array for digital beamforming and direction-of-arrival estimations," *IEEE Transactions on Vehicular Technology*, vol. 58, no. 7, pp. 3137–3144, Sep. 2009.

[130] K. Schuler and W. Wiesbeck, "Tapering of multitransmit digital beamforming arrays," *IEEE Transactions on Antennas and Propagation*, vol. 56, no. 7, pp. 2125–2127, Jul. 2008.

[131] J. Zhang, W. Wu, and D. G. Fang, "Single RF channel digital beamforming multibeam antenna array based on time sequence phase weighting," *IEEE Antennas and Wireless Propagation Letters*, vol. 10, pp. 514–516, 2011.

[132] D. S. Goshi, Y. Wang, and T. Itoh, "A compact digital beamforming smile array for mobile communications," *IEEE Transactions on Microwave Theory and Techniques*, vol. 52, no. 12, pp. 2732–2738, Dec. 2004.

[133] R. Zhang, Y. C. Liang, C. C. Chai, and S. Cui, "Optimal beamforming for two-way multi-antenna relay channel with analogue network coding," *IEEE Journal on Selected Areas in Communications*, vol. 27, no. 5, pp. 699–712, Jun. 2009.

[134] J. Via, I. Santamaria, V. Elvira, and R. Eickhoff, "A general criterion for analog Tx-Rx beamforming under ofdm transmissions," *IEEE Transactions on Signal Processing*, vol. 58, no. 4, pp. 2155–2167, Apr. 2010.

[135] S. Denno and T. Ohira, "Modified constant modulus algorithm for digital signal processing adaptive antennas with microwave analog beamforming," *IEEE Transactions on Antennas and Propagation*, vol. 50, no. 6, pp. 850–857, Jun. 2002.

[136] V. Venkateswaran and A. J. van der Veen, "Analog beamforming in mimo communications with phase shift networks and online channel estimation," *IEEE Transactions on Signal Processing*, vol. 58, no. 8, pp. 4131–4143, Aug. 2010.

[137] W. Shen, W. Y. Yin, and X. W. Sun, "Compact substrate integrated waveguide (SIW) filter with defected ground structure," *IEEE Microwave and Wireless Components Letters*, vol. 21, no. 2, pp. 83–85, Feb. 2011.

[138] J. K. Lee and Y. S. Kim, "Ultra-wideband bandpass filter with improved upper stopband performance using defected ground structure," *IEEE Microwave and Wireless Components Letters*, vol. 20, no. 6, pp. 316–318, Jun. 2010.

[139] J. Yang and W. Wu, "Compact elliptic-function low-pass filter using defected ground structure," *IEEE Microwave and Wireless Components Letters*, vol. 18, no. 9, pp. 578–580, Sep. 2008.

[140] D. Ahn, J. S. Park, C. S. Kim, J. Kim, Y. Qian, and T. Itoh, "A design of the lowpass filter using the novel microstrip defected ground structure," *IEEE Transactions on Microwave Theory and Techniques*, vol. 49, no. 1, pp. 86–93, Jan. 2001.

[141] S. Han, C.-S. Kim, D. Ahn, and T. Itoh, "Phase shifter with high phase shifts using defected ground structures," *Electronics Letters*, vol. 41, no. 4, pp. 196–197, Feb. 2005.

[142] C. Shafai, S. Sharma, L. Shafai, and D. Chrusch, "Microstrip phase shifter using ground-plane reconfiguration," *Microwave Theory and Techniques, IEEE Transactions on*, vol. 52, no. 1, pp. 144–153, Jan. 2004.

[143] C. Shafai, S. Sharma, J. Yip, L. Shafai, and L. Shafai, "Microstrip delay line phase shifter by actuating integrated ground plane membranes," *Microwaves, Antennas Propagation, IET*, vol. 2, no. 2, pp. 163–170, Mar. 2008.

[144] S. Hage-Ali, Y. Orlic, N. Tiercelin, R. Sauleau, P. Pernod, V. Preobrazhensky, and P. Coquet, "A millimeter-wave elastomeric microstrip phase shifter," in *Microwave Symposium Digest (MTT), 2012 IEEE MTT-S International*, Jun. 2012, pp. 1–3.

[145] S. Zheng, W. Chan, K. Tang, and K. Man, "Broadband parallel stubs phase shifter using defected ground structure," in *Microwave Conference, 2008. APMC 2008. Asia-Pacific*, Dec. 2008, pp. 1–4.

[146] J. A. Tirado-Mendez, H. Jardon-Aguilar, F. Iturbide-Sanchez, I. Garcia-Ruiz, V. Molina-Lopez, and R. Acevo-Herrera, "A proposed defected microstrip structure (DMS) behavior for reducing rectangular patch antenna size," *Microwave and Optical Technology Letters*, vol. 43, no. 6, pp. 481–484, 2004. [Online]. Available: http://dx.doi.org/10.1002/mop.20508

[147] CST Computer Simulation Technology, "CST Microwave Studio 2013."

[148] E. Wilkinson, "An N-way hybrid power divider," *Microwave Theory and Techniques, IRE Transactions on*, vol. 8, no. 1, pp. 116–118, Jan. 1960.

[149] T. Debogovic and J. Perruisseau-Carrier, “Array-fed partially reflective surface antenna with independent scanning and beamwidth dynamic control,” *Antennas and Propagation, IEEE Transactions on*, vol. 62, no. 1, pp. 446–449, Jan. 2014.

[150] S. Ourir, A.and Burokur and A. de Lustrac, “Electronic beam steering of an active metamaterial-based directive subwavelength cavity,” in *Antennas and Propagation, 2007. EuCAP 2007. The Second European Conference on*, 2007, pp. 1–4.

[151] D. Jackson and N. Alexopoulos, “Gain enhancement methods for printed circuit antennas,” *Antennas and Propagation, IEEE Transactions on*, vol. 33, no. 9, pp. 976–987, Sep. 1985.

[152] H. Fan, J. Geng, X. Liang, R. Jin, and X. Zhou, “A three-way reconfigurable power divider/combiner,” *IEEE Transactions on Microwave Theory and Techniques*, vol. 63, no. 3, pp. 986–998, March 2015.